STRUCTURAL AND FUNCTIONAL INVESTIGATION OF HUMAN CHEMOKINES AND APPLICATIONS OF HUMAN CHEMOKINES IN BLOCKING HIV-1 ENTRY

A Dissertation

by

HONGJUN JIN

Submitted to the Office of Graduate Studies of
Texas A&M University
in partial fulfillment of the requirements for the degree of

DOCTOR OF PHILOSOPHY

December 2007

Major Subject: Biochemistry

STRUCTURAL AND FUNCTIONAL INVESTIGATION OF HUMAN CHEMOKINES AND APPLICATIONS OF HUMAN CHEMOKINES IN BLOCKING HIV-1 ENTRY

A Dissertation

by

HONGJUN JIN

Submitted to the Office of Graduate Studies of
Texas A&M University
in partial fulfillment of the requirements for the degree of

DOCTOR OF PHILOSOPHY

Approved by:

Chair of Committee, Patricia J. LiWang
Committee Members, Michael D. Manson
C. Nick Pace
Jerry Tsai
Head of Department, Gregory D. Reinhart

December 2007

Major Subject: Biochemistry

ABSTRACT

Structural and Functional Investigation of Human Chemokines and Applications of Human Chemokines in Blocking HIV-1 Entry.

(December 2007)

Hongjun Jin, B.Sc., Lanzhou University, Lanzhou, China;

B. M., Beijing University of Chinese Medicine, Beijing, China

Chair of Advisory Committee: Dr. Patricia J. LiWang

Chemokines are important mediators of leukocyte migration. Chemokines bind to G protein–coupled receptors (GPCR) and cause conformational changes that trigger intracellular signaling pathways involved in inflammation, injury healing, cancer, metastasis, and HIV infections. No direct structural information about any chemokine receptor is available, but the structure of chemokines has been well studied. Structural studies of chemokines coupled with cell-biological investigations may lead to a better understanding of the mechanisms of chemokine-receptor interactions. In this Ph.D. project, I studied the structural and functional relationship between chemokines and chemokine receptors using NMR, X-ray crystallography, and mutagenesis approaches, coupled with several different cell-biology assays. We found that the conserved "chemokine fold" can support different dimerization types in the chemokines family, although changing the dimers from CC- to CXC-type fold is not readily accomplished. I also used an engineered covalently-bound dimer of the MIP-1β mutant, MIP-1β-A10C,

to study the relationship between dimerization of chemokines and their interaction with the CCR5 receptor. My results suggest that MIP-1β dimer neither bind nor activate the CCR5 receptor. I also studied the biophysical properties of one N-terminal awkward mutant of P2-RANTES, which was originally selected by others from a phage display using CCR5-expressing cells. Although the NMR and X-ray crystal studies revealed that the wild type RANTES is a tight homodimer, analytical ultracentrifugation reveals that P2-RANTES is a monomer in solution, the 1.7 Å resolution X-ray crystal structure of P2-RANTES was found to be a packed tetramer. The mutated N-terminal residues play a very important role in the tetramerization in the X-ray crystal structure. Finally I used the HIV-1 env mediated cell-cell fusion assay to study the combination of chemokines or chemokine variants with anti-HIV peptides C37 or/and T-20. A surprisingly synergistic effect was found between P2-RANTES and C37 or T-20. This combination stratagem may lead to further useful drug combinations or drug delivery for more potent anti-HIV treatments.

DEDICATION

To

My family

ACKNOWLEDGEMENTS

I would like to thank my adviser Dr. Patricia LiWang for the support and the opportunity to work in her research group. For this, I will be eternally grateful. I thank Drs. Nick Pace, Michael Manson and Jerry Tsai for serving as members of my committee. To Dr. David Giedroc who was my former committee member. To my group members who taught me many things during the group meetings and helpful discussions.

I thank Dr. Marc Alizon for offering us the cell lines HeLa-ADA and HeLa-P5L. I thank Dr. James C. Hu for assistance with the λ repressor selection system. I thank Dr. Pingwei Li for help us calculating the X-crystal structure. I also thank Joshua Hamilton, Dr. Melissa A. McCornack for very helpful discussions. I thank Dr. Amanda Jacks for technical assistance. I thank Jake Dennis for the technical support and helpful discussions. I thank Carl Carruthers for looking through my thesis. I thank Dr. Lawrence J. Dangott and Sabrina N. Schmidtke from the Protein Chemistry Lab at Texas A&M University, Department of Biochemistry & Biophysics for the MALDI-TOF Mass experiments. I thank Dr. Karl Koshlap and Dr. Xiangming Kong for the technical support on the NMR experiments. I thank Dr. Roger Smith for the technical support of the FACS experiments.

TABLE OF CONTENTS

CHAPTER Page

LIST OF FIGURES

Page

Page

LIST OF TABLES

CHAPTER I

INTRODUCTION

Background

The word chemokine is an abridged version of chemotactic cytokine. All chemokines belong to the cytokine superfamily. Chemokines are widely involved in leukocyte traffic and are produced by leukocytes and cells either constitutively or after induction by cytokines. Based on the way chemokines are produced, they can be separated into two different types: homeostatic and homeorhetic chemokines (1-4)**.** Some chemokines control cells of the immune system during immune surveillance and are secreted without any stimulation of the cell that produce them. These are known as homeostatic chemokines. Other chemokines have roles in development: they promote angiogenesis (the growth of new blood vessels) or guide cells to tissues that provide specific signals critical for cellular maturation. These chemokines are known as homeorhetic chemokines.

The major role of chemokines is to guide the migration of leukocytes. In general, cell migration in response to chemokines includes several sequential steps involving adhesion molecules, glycosaminoglycans (GAGs), chemokines, and chemokine receptors (5,6). First, adhesion molecules on the endothelium interact with mucin receptors on the leukocyte, causing a rolling behavior of the leukocyte along the cell surface (7,8). Secondly, chemokines, secreted in response to signals such as proinfla-

---

This dissertation follows the style and format of *The Journal of Biological Chemistry*.

-mmatory cytokines, are thought to bind GAGs on the endothelial cell surface, forming a chemokine gradient that retains leukocytes at the inflammatory site (9). Thirdly, the chemokine gradient provides a direction for the cell's movement. Interaction of chemokines with their receptors on the leukocytes then triggers intracellular signals that result in the migration of leukocytes from the blood vessel into the tissues. Finally, firm adhesion and extravasation of leukocytes occur along the chemokine gradient (Figure 1-1).

Chemokine and chemokine receptors

Chemokines are normally small (7-14 kDa) structurally related proteins. Based on the arrangement of N-terminal cysteine residues, chemokines can be divided into two major subfamilies, named CC and CXC, depending on whether the first two cysteine residues are adjacent (CC), or have an amino acid between them (CXC). Two small groups, CX3C chemokines (10) and C chemokines (11) also have been identified. To date, approximately 50 human chemokines and 20 chemokine receptors have been discovered (1). There have been at least 28 members of the CC chemokine subgroup ligands (CCL)-1 to -28 reported in humans. CC chemokines induce cellular migration by binding to and activating CC chemokine receptors, ten of which have been discovered to date and named CCR1-10. These receptors are expressed on the surface of different cell types to allow these cells to be attracted by chemokines (6, 15). For example, CCL5 (or RANTES) attracts cells such as macrophages (monocytes), eosinophils, and basophils, which express the receptor CCR5, CCR1 and CCR3 respectively. CCL4 (or MIP-1β) attracts mainly macrophages (monocytes) that express the CCR5 receptor.

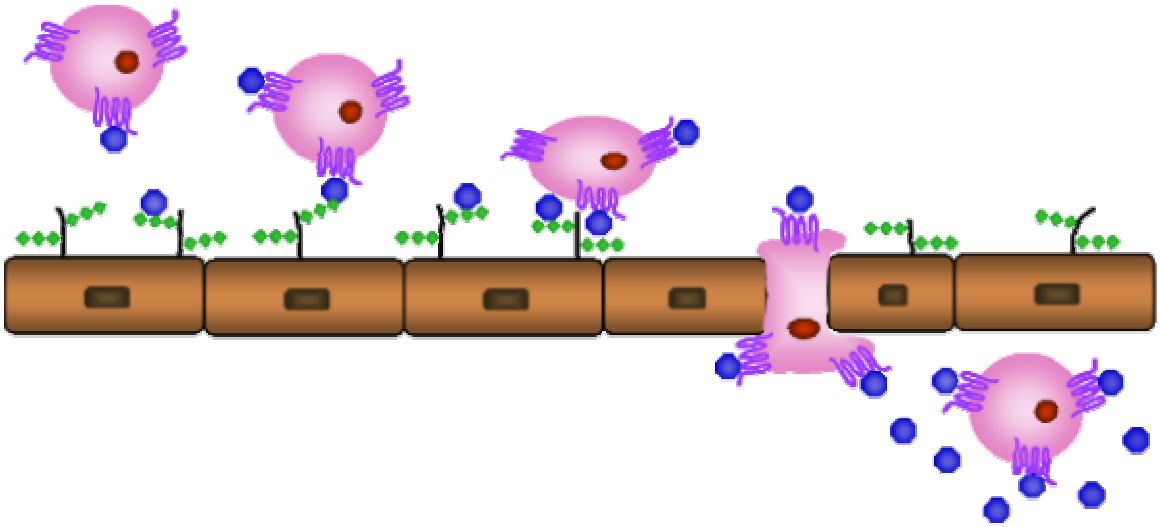

Figure 1-1: An overview of the biological action of chemokines. Chemokines (blue circles) form a concentration gradient by binding the glycosaminoglycans (small green diamonds) on the endothelium. Leukocytes (pink) detect the chemokines by binding them tightly using 7-transmembrane chemokine receptors (purple). The cells chemotax along the chemokine gradient, moving to the point of inflammation or infection.

In humans, 17 different CXC chemokines have been described (1). They are subdivided into two categories: those with a specific amino acid sequence of glutamic acid-leucine-arginine (ELR for short) immediately before the first cysteine of the CXC motif (ELR-positive), and those without an ELR motif (ELR-negative). ELR-positive CXC chemokines specifically induce the migration of neutrophils and interact with chemokine receptors CXCR1 and CXCR2. An example of an ELR-positive CXC chemokine is interleukin-8 (IL-8), which induces neutrophils to leave the bloodstream and enter into the surrounding tissue. Other CXC chemokines that lack the ELR motif, such as CXCL13, tend to be chemoattractants for lymphocytes. CXC chemokines bind to CXC chemokine receptors, of which seven have been discovered to date, designated CXCR1-7.

Two chemokines have been described for the C chemokine subgroup called XCL1 (lymphotactin-α) and XCL2 (lymphotactin-β) (6,15). These chemokines attract T- cell precursors to the thymus through interaction with the receptor XCR1. The only CX3C chemokine discovered to date is called fractalkine (or CX3CL1) (6,15). It is both secreted and tethered to the surface of the cell that expresses it, thereby serving both as a chemoattractant and as an adhesion molecule through interaction with the CX3CR1 receptor.

Tertiary structure and quaternary structure of chemokines

Sequence homology of chemokines is highly variable, ranging from less than 20% to over 90%, but all share very similar tertiary structures. Structures of many chemokines have been solved by NMR and X-ray crystallography, including: IL-8 (12,13), MIP-

1β (14), RANTES (15,16), MCP-1 (17,18), eotaxin (19), CX3CL1 (20), PF-4 (21), IP-10/CXCL10 (22), MCP-2 (23), and vMIP-II (24). These structures reveal that all chemokines adopt a remarkably conserved tertiary structure consisting of a disordered N terminus of 6–10 amino acids that functions as a key signaling domain in all chemokines characterized to date. This region is followed by a long loop (the N-loop) that ends in a 3_{10} helix and invariably contains important binding determinants, a three-stranded β-sheet, and a C-terminal helix. Disulfide bonds stabilize the overall topology (25).

Oligomerization of chemokines

Many chemokines form dimers and higher-order oligomers alone in solution or upon binding to GAGs (26-29). The dimers fall into two very different classes. CC chemokine dimers have a completely different organization than CXC chemokine dimers (14,25). The N-terminal residues of the CC chemokine MIP-1β are involved in the dimer interface, with residues Pro8 and Phe13 making several critical dimer contacts (Figure 1-2). The C-terminal helix from each monomeric subunit of MIP-1β points away from the other and makes no contact with the other subunit. On the other hand, the dimer of the CXC chemokine IL-8 consists of monomeric subunits that interact with each other along the first β strand, from residue 23-30, rather than acting on the other side of the molecule at the N-terminus (Figure 1-2). In contrast with the MIP-1β dimer, the C-terminal helix of IL-8 makes several critical dimer contacts with the other monomeric subunit. The overall shape of the dimer of the CC chemokine MIP-1β is elongated and cylindrical, but the dimer of the CXC chemokine IL-8 is compact and globular. Subsequenct chemokine structures have exhibited these same structural properties, with rare exceptions (18,30):

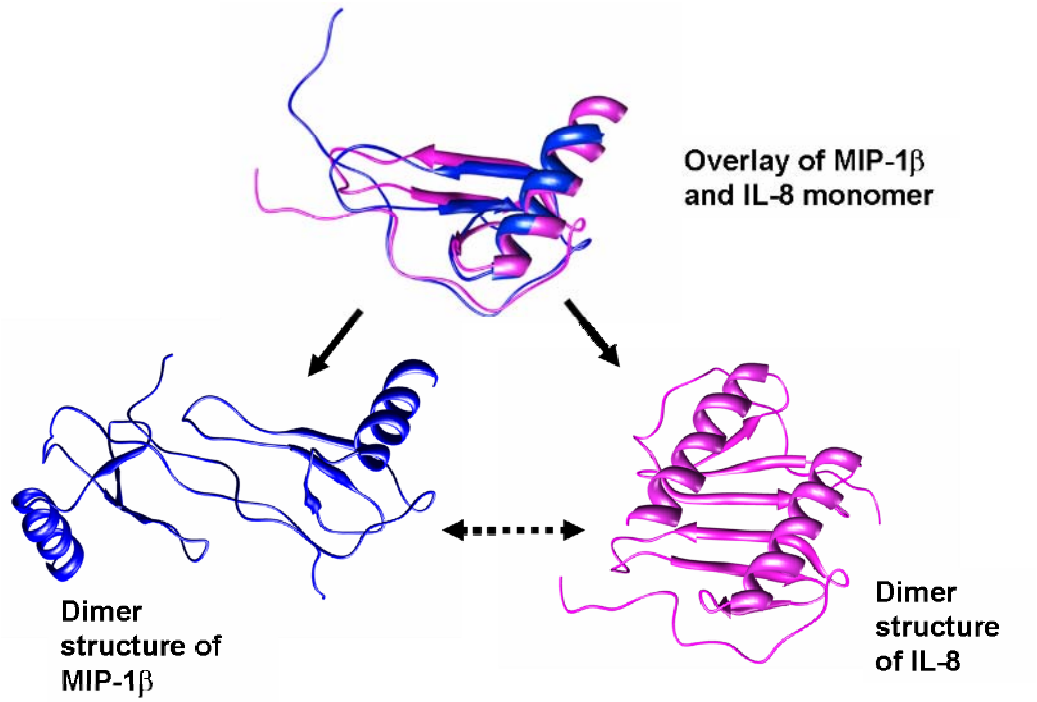

Figure 1-2: CC chemokines and CXC chemokines share similar "chemokine fold" momoneric structure, but have distinct dimer structures. Top: Overlay of the ribbon diagrams of a monomeric subunit of MIP-1β (purple) and IL-8 (magenta). Bottom Left: The N-terminal residues of MIP-1β are involved in the dimer interface, with residues Pro8, Phe13, and the 40's loop making critical dimer contacts. Bottom Right: The IL-8 dimer consists of monomeric subunits that interact with each other along the first β strand (β1) from residues 23 to 30. In contrast with the MIP-1β dimer, the C-terminal helix of IL-8 makes several critical dimer contacts with the other monomeric subunit. The PDB coordinates used for this Figure are 1hum (MIP-1β) and 1il8 (IL-8).

although not all chemokines are dimers, each CC chemokine that dimerizes shares the dimer arrangement of MIP-1β (15,17,18,31). Likewise, the CXC chemokines that dimerize share the dimer structure of IL-8 (32-34). Therefore, the chemokine monomeric fold clearly supports two different dimer structures (Figure 1-2).

Given that chemokines from all subfamilies share a common monomeric fold regardless of quaternary structure and that this monomer can naturally form two different types of dimers, there are likely to be changes in their sequences that will allow changes in quaternary structure. In chapter II of my thesis, I described the use of site-directed mutagenesis (structure based design) and random mutagenesis to study the interactions responsible for chemokine dimer formation.

A few chemokines are known to form tetrameric structures. Although the structure of MCP-1 was initially solved as a dimer in solution by NMR, subsequent crystallographic studies revealed the presence of both dimers and tetramers in two different crystal forms (18). Earlier studies of PF-4 showed a similar tetrameric architecture as the dominant form of the protein in solution (21). In the case of IP-10, two different tetramers were observed by crystallography, one similar to the MCP-1 and PF-4 tetramers and the other consisting of a novel 12-stranded β-sheet structure (22). Other chemokines, such as RANTES, MIP-1α, and MIP-1β, aggregate into even higher- order oligomers (35). For this reason, structures of these chemokines were solved at low pH, which destabilizes the aggregated form but leaves the CC dimer intact. Therefore, the dimers are likely the fundamental oligomeric subunits of the higher-order aggregates.

Tetramers are likely to be the next level of organization, and the higher-order structures are likely organized assemblies rather than random precipitates.

Although the dimerization and oligomerization of chemokines have been attractive for structural studies, some functional studies revealed that chemokines interact with receptors as monomers. This finding was demonstrated with structure-based design of mutants that are obligate monomers. For example, Clark-Lewis et al. made a synthetic variant of IL-8 containing a methyl group on the amide of Leu25, which inhibits hydrogen bonding between the central β-strands of opposing subunits in the dimer. The mutant does not dimerize; nevertheless, the receptor binding affinity of the variant and its ability to induce cell migration and release *in vitro* are equivalent to the wild-type protein (36,37). Of note, during my Ph. D. studies, based on the bioinformatics design by Dr. Jerry Tsai's group in our department, I also made a mutant on IL-8 in which two residues (R26 and V27) in the middle of the β strands are deleted. This mutant was found to be a folded monomer in solution (data not shown). Although we have not checked the biological function of this mutant, it at least stands as an alternative way to make an obligate monomer mutant for IL-8. A similar chemical modification of Thr8 in RANTES produced a monomeric variant with *in vitro* activity equivalent to the wild-type protein (9).

Two different strategies were used with MCP-1 and MIP-1β to make monomers. In the recombinant forms of these chemokines, substitution at Pro8, a residue that flanks the dimer interface and is present in many CC chemokines, results in variants that do not

dimerize (38,39). Like IL-8 and RANTES, these mutants also displayed *in vitro* binding and chemotaxis ability equivalent to their wild-type counterparts. This suggests that the chemokine monomer is the active form of the protein. But these "trapped" monomers do not exclude the possibility that a dimer chemokine could still bind to the receptor. Since several studies have produced controdictory results about this possibility (38,40-43), a "trapped" dimer would be useful to answer this question. In my research project (Chapter III), a trapped dimer was made by a single substitution at the dimer interface. We studied the function of this dimer in CCR5 receptor activation and binding. Our results clearly show that the dimer does not bind or to activate CCR5. Our studies clarify this matter and directly answer the question that normal physiological experiments have had difficulty answering.

Binding and activation of the chemokine receptor by chemokines

In pioneering studies on IL-8 using domain-swapping approaches, it was shown that there are two major sites of interaction between a chemokine and its chemokine receptor (42). The "two-site model" was quickly supported by many other chemokine-chemokine receptor studies and became a general model for chemokine binding and activation (43, 44). Briefly, in this model there are two spatially separate sites on the receptor, one in its extracellular domain, the other in its transmembrane domain. These are engaged by two separate sites on the chemokine: the first on the surface of the core region and the second located in the flexible N-terminal region. The first interaction shows high affinity and specificity and is responsible for the correct "addressing" of a chemokine to its receptor. It is also responsible for orienting the chemokine in such a way as to favor the second

interaction, which is responsible for the "message" function; namely induction of the conformational changes in the receptor that lead to signal transduction.

Receptor-binding sites on chemokines

A large number of studies have defined receptor-binding sites on chemokines. By generating N-terminal truncation mutants, studies demonstrated the crucial role of the N-terminus in both binding and signaling. For example for the CXC chemokine IL-8, an N-terminal deletion mutant had a greater than 10,000-fold loss of binding affinity for neutrophils and was completely inactive biologically (44). Later studies also showed that specific residues in the N-loop (Y13, Phe17, Phe21) were important for receptor binding and specificity, but that the C-terminal helix was not (45). For the CC chemokines MIP-1α, RANTES, MCP-1 and MIP-1β, similar results were discovered by the LiWang group and other colleagues (46-49). Of all these epitopes, it seems that the aromatic residues on the 13th position (F13 or Y13) contribute most to receptor binding. For example, in MIP-1β, when Phe13 is mutated to Ala, the affinity for CCR5 is reduced by a factor of ~1000 compared to the WT protein. However, in contrast to the high affinity contributed by the IL-8 N-terminus, deletion of N-terminal amino acids in a variant referred to as MIP(9) produced only a small reduction in binding, but activation was completely lost (50). This indicates that the N-terminus of CC chemokines may not be important for binding, but rather for activation. Similar results were reported for RANTES and MCP-1(46-49). All other receptor-binding epitopes involve basic Arg or Lys amino acids on the surface of the core protein MIP-1β (R18, K19, R22, R46, K48),

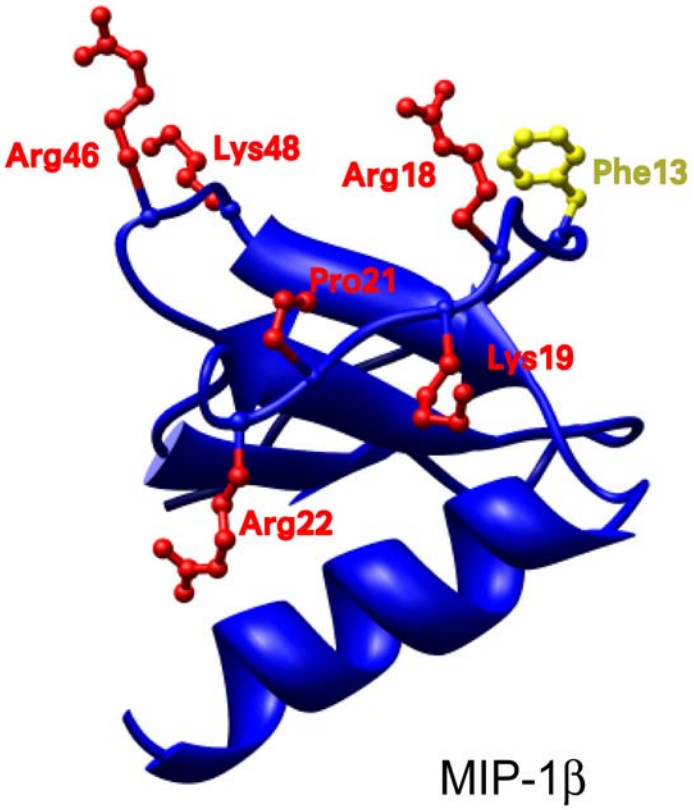

Figure 1-3: The residues of MIP-1β that make critical contacts with CCR5. NMR studies for each mutation confirmed that there is no tertiary structural variation. The monomeric form of the protein is shown. Phe13 (yellow) is the most critical residue for binding CCR5. The other residues (red) show at least a 10-fold reduction in binding when mutated (39, 47, 50).

and these are not confined to the N-loop but are more broadly distributed over the whole surface of the chemokine (Figure 1-3). Very similar results were reported for RANTES and MCP-1 (46-49).

Chemokine-binding sites on receptors

Much less is known about chemokine-binding sites on receptors because of the difficulties in determining structures for 7-transmembrane receptors. Several studies using receptor chimeras and truncation and point mutants have implicated a role for the receptor N-termini in chemokine binding (48,51-55). Additionally, several NMR structural studies have been conducted using N-terminal peptides from receptors (56-60). It has been observed that affinities between the receptor peptides and chemokines are much weaker (i.e., millimolar to high micromolar) than the cellular binding assay (i.e. nanomolar). Although we do not know exactly how the receptor interacts with chemokines, NMR studies complementing the mutagenesis studies indeed reveal that receptor binding occurs on the face of the chemokine that was implicated by mutagenesis. For example, in one of these studies, the solution structure of a complex between IL-8 and the CXCR1 N-terminal peptides shows the receptor peptide lying in an extended form along a hydrophobic cleft of the chemokine (60). Although most of the contacts are hydrophobic, three negatively charged residues in the peptide interact with basic residues on the IL-8 surface. This structure is consistent with the data from mutagenesis studies.

Many of the chemokine receptors are predicted to have tyrosine sulfation sites at their N-termini that play an important role in chemokine binding (61-64). The sequence contains of tyrosine residues flanked by aspartic acid residues, such as $D_{25}Y_{26}D_{27}Y_{28}$ in CCR2b and D_2Y_3, $Y_{10}D_{11}$ in CCR5. Tyrosine sulfation has been positively demonstrated for CCR5, CCR2b, CX3CR1, and CXCR4, and was found to enhance chemokine binding and HIV entry (61-64). These motifs create highly acidic patches on the receptors that presumably interact with complementary basic residues on chemokines.

Besides the biomedical mutagenesis and NMR studies, there are also several receptor-modeling studies. These modeling studies were generated a crude model of a chemokine interacting with its receptor based on the only known GPCR structure: bovine rhodopsin (65-68). The key features to note are the interaction of the receptor N-terminus with the chemokine and the positioning of the chemokine N-terminal signaling domain towards the receptor, although the contacts between the signaling domain and the receptor are largely unknown. Based on several small molecule modeling studies, along with the receptor mutagenesis studies, it is commonly accepted that the N-terminal signaling domain inserts into the helices TM2 and TM3 (69-72). However, in a recent study, the N-terminus of MIP-1α was labeled with benzophenone, a photoaffinity cross-linking agent, and used to covalently label CCR1 (73). After enzymatic and chemical cleavage of the complex, autoradiography of a polyacrylamide gel showed that the MIP-1α N-terminus interacts with the second extracellular loop between transmembrane helix 4 and 5, within a region spanning residues 178–194. A summary of studies of CCR5

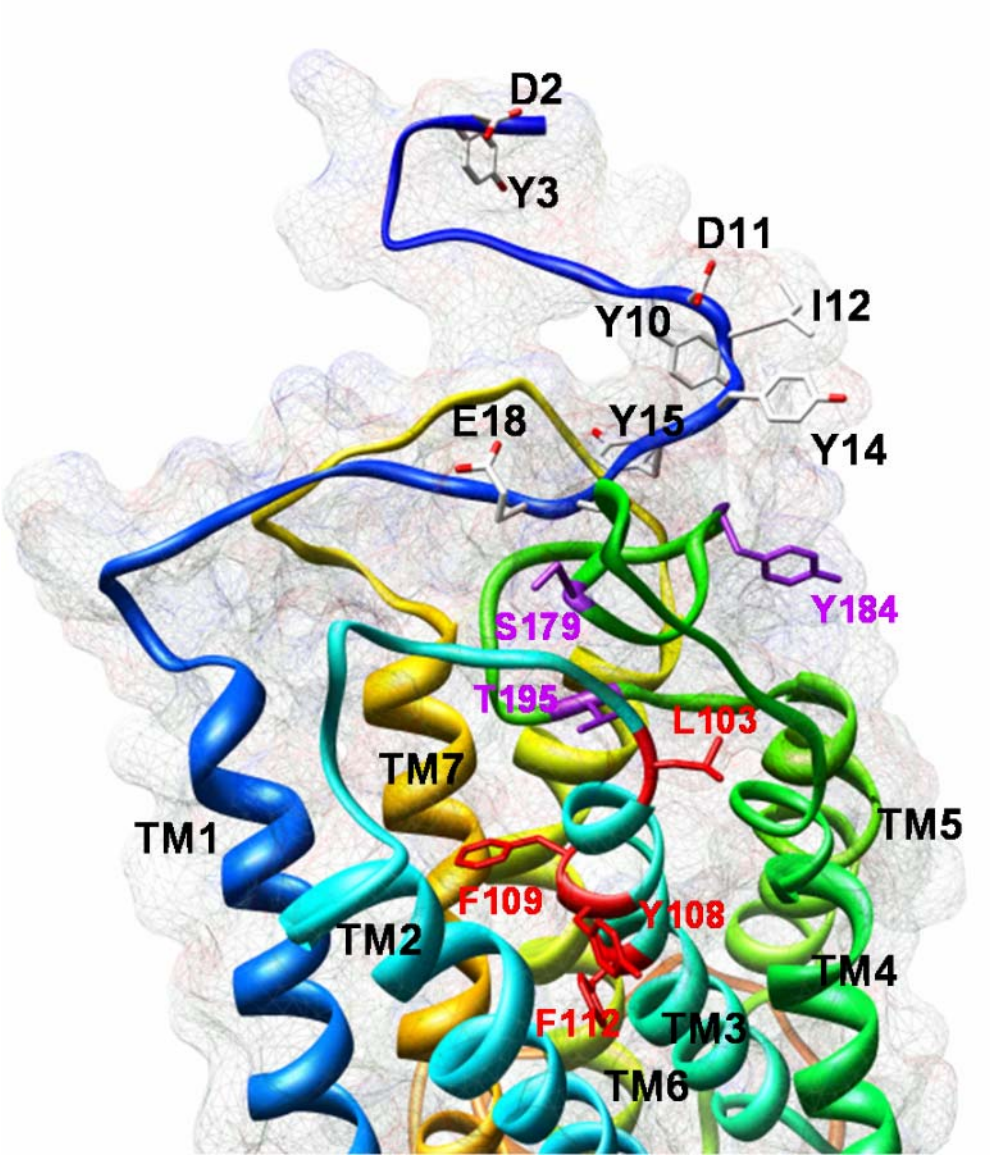

Figure 1-4: Schematic diagram of CCR5 residues implicated in chemokine binding by previous publications (67,68). The N-terminal residues: D2, Y3, Y10, D11, I12, Y14, Y15 and E18 (gray stick model) play an important role in chemokine binding. The second extracellular loop (ECL2, green) is also reported to bind to chemokines through hydrophobic interactions. Several residues on TM3 (Y108, F109 and F112 (red stick model)) were reported to be critical for activation by small agonists. Residues on ECL2 (S179, Y184, and T195, purple stick model) are correlated with the coreceptor function in R5-tropic HIV entry. The PDB file (1opw) of modeling structure of human CCR5 was published by Liu et al. (66).

binding and activation sites are highlighted on the modeling structure of CCR5 in Figure 1-4.

Chemokine and HIV entry

Chemokines and their receptors have attracted particular interest because of their role in HIV/AIDS. Figure 1-5 shows a simplified diagram of HIV fusion to a host cell. First, the HIV-1 env protein gp120 makes contact with the cell surface receptor CD4, causing a structural rearrangement that exposes the viral env protein gp41. The gp120/CD4 complex then contacts with the cellular co-receptor (either CCR5 or CXCR4) (74-76). Meanwhile, because of the exposure of gp41, an N-terminal fusion peptide (FP, aromatic residue rich region) of gp41 inserts into the host cell membrane, eventually pulling the membrane surface of the virus close to the membrane surface of the protein by folding the N-peptide (HR1, or NHR) back onto the C-peptide (HR2, or CHR, Figure 1-5) to form a "trimer of hairpins" (77). The CCR5 receptor is the major route for primary HIV infection in humans, while HIV strains that bind to CXCR4 appear later in the progression toward AIDS (78). Therefore, the chemokine ligands for these receptors, including MIP-1β, MIP-1α, RANTES, and SDF-1, are able to inhibit HIV infection, likely both by sterically blocking the receptor and by causing receptor internalization (74-76,79-84).

There are several key areas that remain to be explored in investigating the inhibition of HIV entry by chemokines. For example, does the quaternary state or GAG-binding ability modulate the effectiveness of chemokines in inhibition? What characteristics of

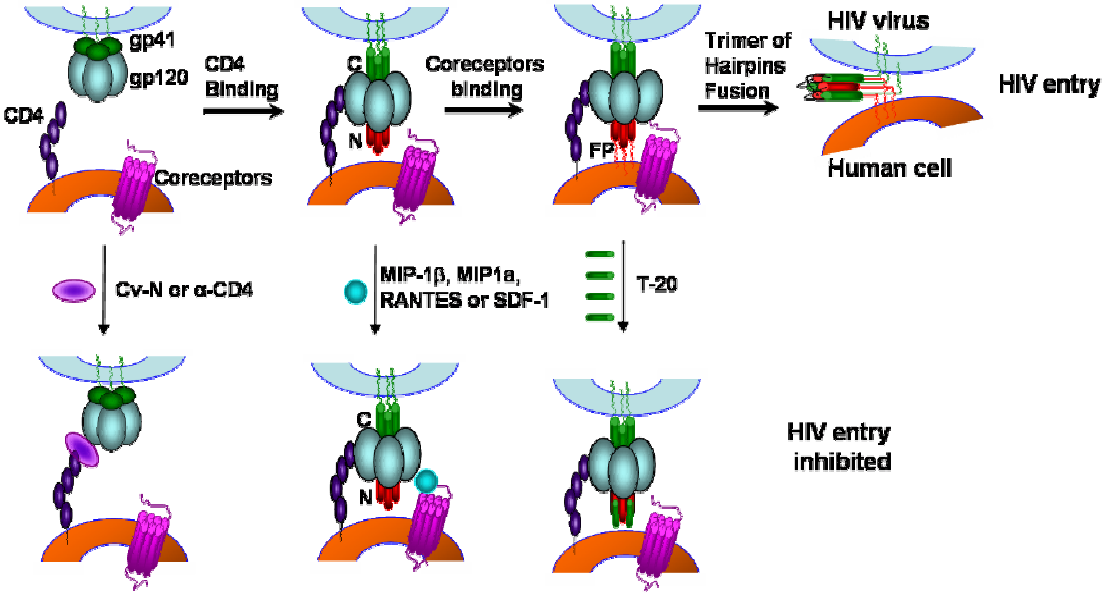

Figure 1-5: A simplified diagram of the multiple steps for HIV fusion to human cell. There are three sequential steps for HIV entry: CD4 binding (attachment), coreceptor (CCR5 or CXCR4) binding, and trimer of hairpins fusion. To block HIV entry, three general stratagems can be used: blocking CD4-gp120 interaction (Cv-N or CD4 antibodies), blocking gp120-chemokine receptors interaction (MIP-1β, MIP-1α, RANTES or SDF-1) or blocking gp41 trimer of helix bundle formation (T-20 or C37).

the chemokine allow maximal potency in HIV inhibition? Can chemokines be used as delivery vehicles for known therapeutics to improve their efficacy? In this Ph.D. project, I tried to answer these questions based on the current knowledge from structural and cell biology studies, but not all of these can be answered in my Ph.D. studies. The continuing studies in the P.LiWang lab will keep investigating all these interesting questions.

Modified chemokines as HIV inhibitors

Since the discovery that certain chemokines were "AIDS-suppressive factors" (82), many variants of MIP-1β, MIP-1α and RANTES were made, some to elucidate details of the mechanism of action of these proteins (35,39,47,50,85,86) and some to design agents with therapeutic potential (87,88). In the latter category, the vast majority of work has been carried out on the CC chemokine RANTES. In particular, a chemically modified form of RANTES called AOP-RANTES, which has a hydrophobic attachment at its N-terminus (Figure 1-6), was shown to be very effective at inhibiting HIV infection. The mechanism of action was shown to involve both sterica blocking of HIV entry and induced endocytosis of the CCR5 receptor (89-92). Other work has shown that receptor endocytosis is an important target of this type of HIV inhibitor (79,93), although receptor blockage is also a significant component of inhibition (93).

Recent work with modified RANTES has resulted in the synthesis of other hydrophobic N-terminal modifications to the chemokine, NNY- RANTES (94) and PSC-RANTES (87,93) (Figure 1-6). These hydrophobic N- terminally modified chemokines show stronger anti-HIV activity because they accelarate removal of CCR5 from the surface of the cell and thereby reduce viral access to cell surface binding sites (92,95-98).

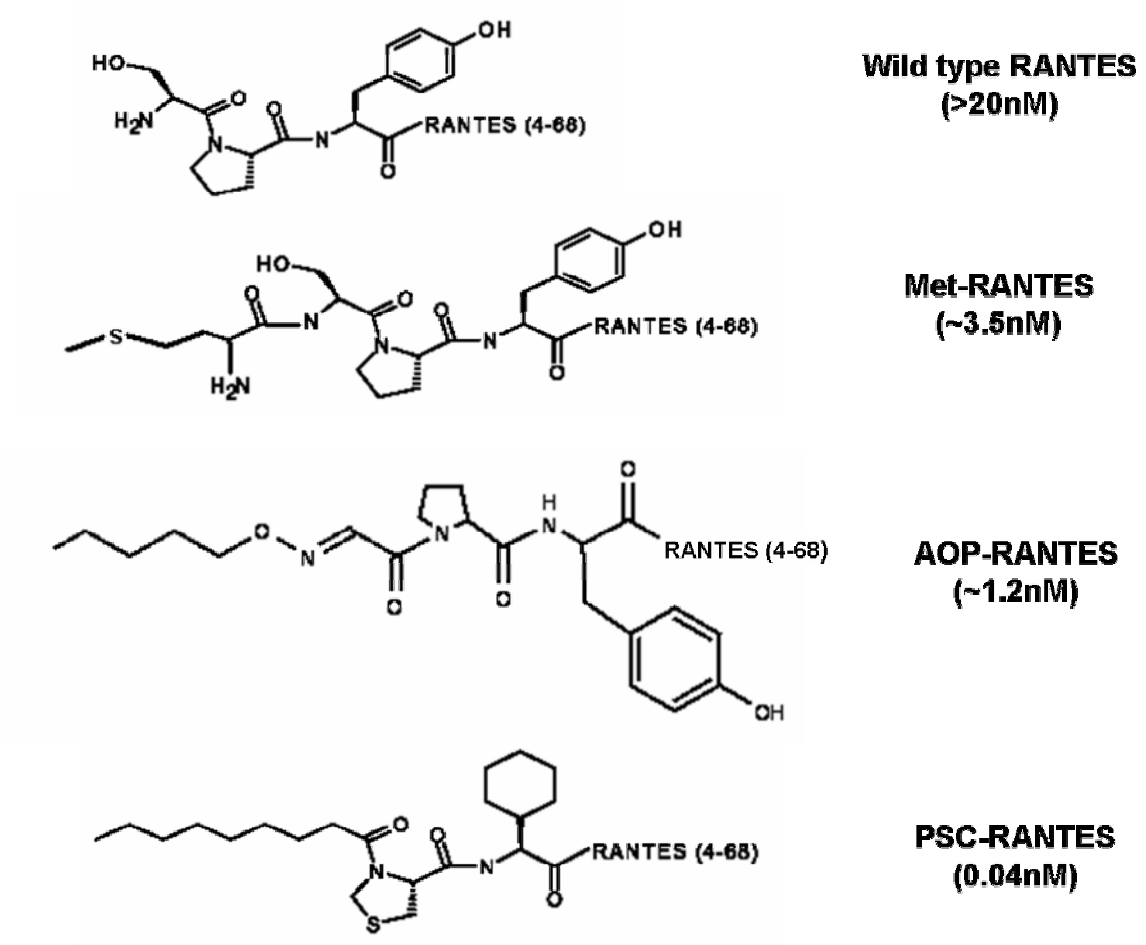

Figure 1-6: Diagram of N-terminal modifications of RANTES that result in increased anti-HIV potency. The numbers in parentheses are the IC50s from the R5-tropic cell-cell fusion assays (38,95,99).

Instead of using organic synthesis to modify the N-termini of chemokines, Hartley et al. used mutagenesis to screen potent anti-HIV chemokines through a phage display technique (100). The phage-displayed library of randomly mutated and N- terminally extended variants was screened by direct exposure to live CCR5-expressing cells. One of the modified six-site mutants, P2-RANTES (FSPLSSQSSA-RANTES (aa10-68)), was characterized as a super agonist of CCR5 and a potential inducer of receptor internalization. P2-RANTES exhibits not only significantly increased affinity for CCR5 but also enhanced receptor selectivity, retaining only trace levels of signaling activity via CCR1 and CCR3. Prior to my research, no structural information was available for this chemokine variant. In my Ph.D. studies, I overexpressed, refolded and purified P2-RANTES from *E. coli*. A detailed description of its structure is in chapter IV of this thesis.

HIV fusion inhibition

In recent years, some of the most promising progress in anti-HIV drug development has been abtained with the anti-HIV entry inhibitors. As shown in Figure 1-5, in order to block HIV entry, three general stratagems can be used: to inhibit CD4-gp120 interaction; to block gp120/41 chemokine receptor (CCR5 or/and CXCR4) interaction; or to prevent gp41 six-helix bundle formation.

Inhibitors that block the formation of the six-helix bundle represent the newest generation of anti-HIV drugs. The six-helix bundle structure of gp41 is comprised of N and C-terminal helical heptad repeats (101-103). The peptides corresponding to the HIV envelope protein gp41 N-terminal region (HR1) normally are called N-peptides and the

peptides corresponding to the HIV envelope protein gp41 C-terminal region (HR2) normally are called C-peptides (Figure 1-7). C-peptides and N-peptides are potent inhibitors of HIV entry. Their mechanism of inhibition involves binding in a helical conformation to the central coiled-coil of gp41 (101-103) to block formation of the trimer of hairpin that pulls the viral membrane close to the cell membrane. T-20 (also known as DP-178), which corresponds to the C-terminal residues of gp41, was recently approved by the FDA. Other C-peptides, such as C34, C36, C37, are also reported to have strong anti-HIV activity (101,104). C37, derived from the C-terminus of gp41, covering all sequence of C34, in particularly has been reported to have strong anti-HIV entry activity, and this peptide can be easily produced through overexpression in *E. coli.*

T-20 and C34 have proven useful in the modeling structural features of gp41, thereby revealing their potential to interfere with the pre-heparin formation by binding to the hydrophobic groove on the N terminal heptad repeat of gp41 (105). Although T-20 has been very successful, clinical trails revealed that the dose required is much higher *in vivo* than *in vitro* (106,107). The reasons for this higher dosage includes swift proteolysis and clearance of the unstructured peptide and non specific binding of T-20 binds to unrelated cell membranes or lipids (77,104,108,109) .We have hypothesized that if this small peptide can be carried by some delivery system, its specificity will increase.

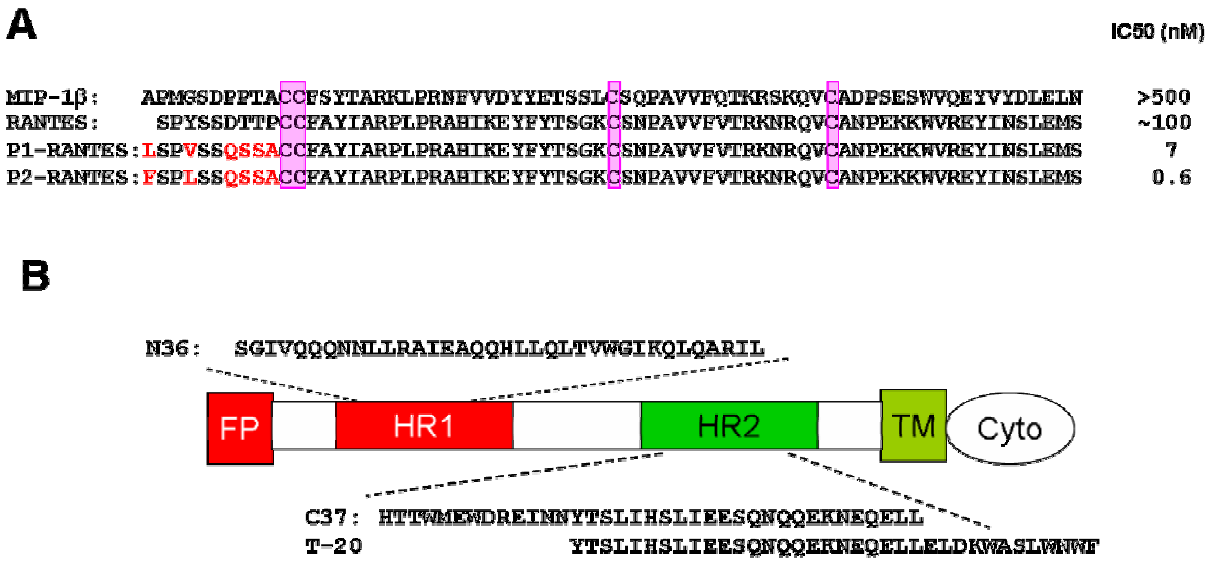

Figure 1-7: Amino acid sequences of HIV fusion inhibitors. A). CC chemokines MIP-1β, RANTES, P1-RANTES and P2-RANTES. The conserved Cys motifs are highlighted in purple. The six-site mutated residues of P1-RANTES and P2-RANTES are showing in red. The right column shows the actual IC_{50}s measured from the R5 tropic cell-cell fusion assay (100); B). C-peptides derived from HIV gp41. FP: fusion peptide, HR1: helix region 1 (N-terminus of gp41), HR2: helical region 2 (C-terminus of gp41), TM: transmembrane region, Cyto: cytoplasmic domains of gp41.

Design of chemokines with improved HIV-1 inhibition characteristics

The better structural understanding we have of interactions between chemokines and chemokine receptors, the better we will be able to design chemokine variants that inhibit HIV entry through both coreceptors interactions and fusion process. For example, it will be very interesting to use chemokines as delivery vehicles for known HIV inhibitors such as T-20 or C37.

Genetic studies revealed that Caucasian individuals bearing mutant alleles of the CCR5 chemokine receptor gene CCR5-Δ32 mutation (110,111) are resistant to certain strains of HIV. These people are resistant to infection with R5 HIV because the defect in CCR5 decreases HIV binding to this coreceptor, reducing its ability to infect target cells. Similarly, CCR5 internalization are likely to be important aspects of the ability of chemokines to inhibit HIV (79,89,91,93).

In designing anti-HIV stratagems, we sought to develop a way to harness the ability of chemokines to bind to CCR5 with clinically proven peptide T-20. Our hypothesis was that T-20 (or other C-peptides, such as C34 and C37) could be administered at much lower doses if it were combined with CCR5 or CXCR4-binding chemokines (Figure 1-8).

I combined several CCR5-binding chemokines with C-peptides using a cell-cell fusion assay, which is a standard *in vitro* test of HIV fusion. The results indicate that there is a strong synergistic effect between these CC chemokines and the C-peptides. The strongest synergy was found between P2-RANTES and the C37 peptide. Our collaborator tested this combination using the PBMC HIV infection assay, and a dramatic synergistic effect was achieved. These results indicate that blocking two

activities (CCR5 binding and interrupting of gp41 prehairpin state form) can be combined for potent HIV therapeutic effect. Further details are described in chapter V of this thesis.

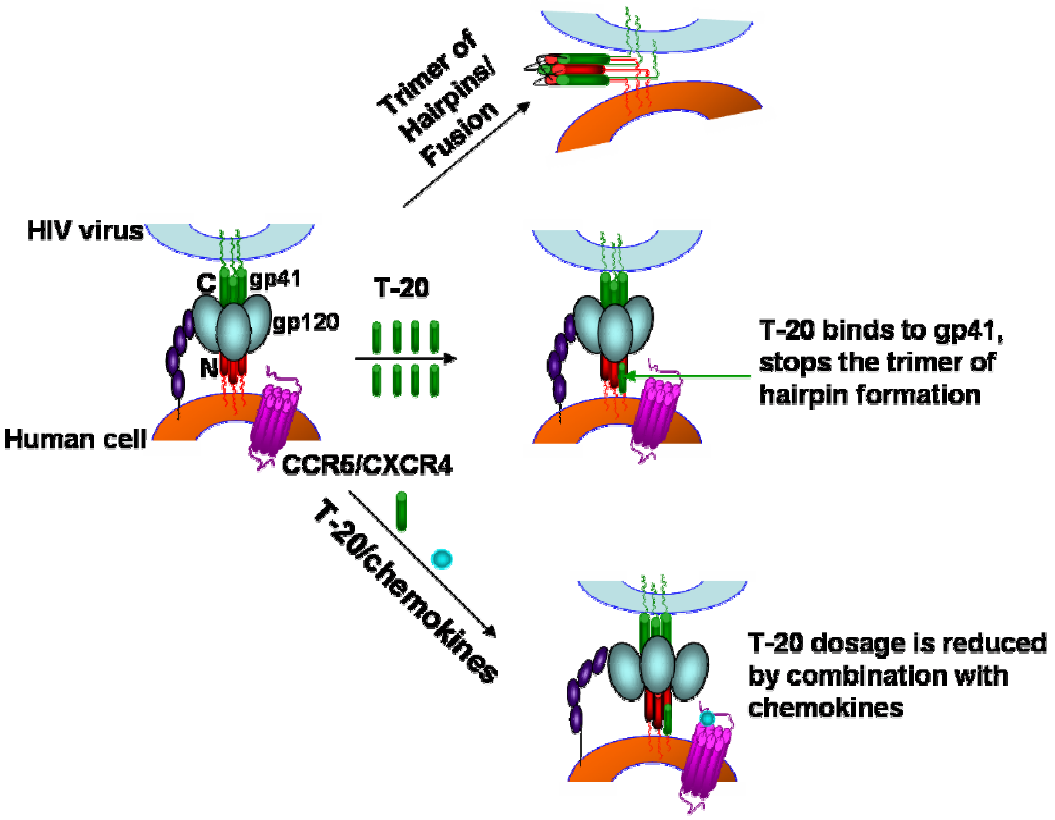

Figure 1-8: Model of HIV fusion and the proposed combination effect. Top: Model of HIV fusion to the host cell. Middle: The effect of T-20 in inhibiting fusion. Bottom: Proposed synergy of chemokines with T-20 to effectively inhibit HIV-1 entry.

CHAPTER II

INVESTIGATION OF CC AND CXC CHEMOKINE QUATERNARY STATE MUTANTS*

Introduction

Chemokines (chemotactic cytokines) are a group of small (7-14 kDa) structurally related proteins that regulate cell trafficking of various types of leukocytes through interactions with a subset of seven-transmembrane, G protein-coupled receptors. About 50 chemokines have now been identified in humans (3,112). Based on the arrangement of N-terminal cysteine residues, chemokines can be divided into two major subfamilies, CC and CXC, depending on whether the first two cysteine residues are adjacent (CC), or have an amino acid between them (CXC). Two small groups, CX_3C chemokines (10) and C chemokines (11) also have been identified. Due to their role in inflammation, chemokines also play a role in many diseases, including atherosclerosis and allergy (3,113). In addition, the HIV co-receptor, CCR5, is actually a chemokine receptor and is the natural receptor for the CC chemokines MIP-1α, MIP-1β and RANTES, making these chemokines natural HIV-blocking proteins (74,114).

All chemokines have been shown to have a common monomeric fold, the core of which is an antiparallel β sheet comprised of three β strands, followed by a C-terminal

---

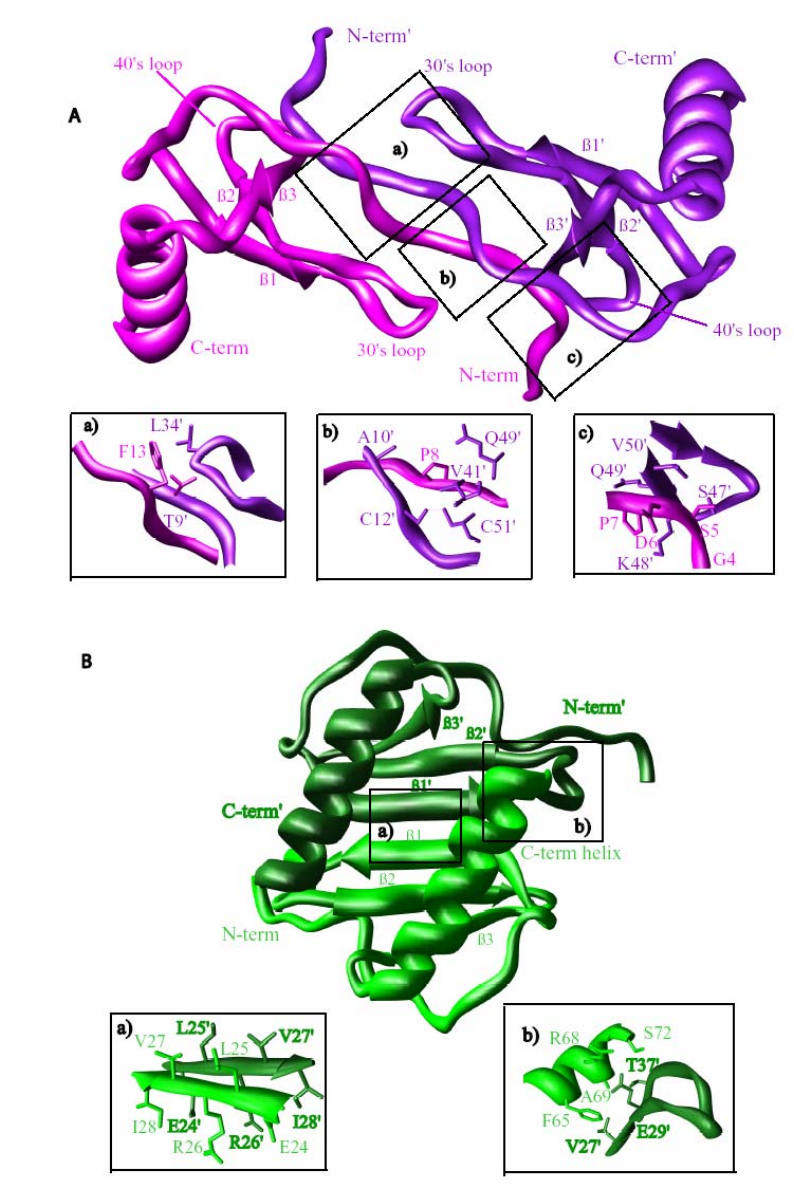

Figure 2-1: Ribbon diagram of the dimer structure of MIP-1β and IL-8. A) The MIP-1β dimer and close-ups of selected regions of dimer contact. The N-terminal residues of MIP-1β are involved in the dimer interface, with residues Pro8 (a), Phe13 (b) and the 40's loop (c) making several critical dimer contacts. The C-terminal helix from each monomeric subunit of MIP-1β points away from the other and makes no contact with the other subunit. B) The IL-8 dimer and close-ups of two regions that make intersubunit contact. The dimer consists of monomeric subunits that interact with each other along the first β strand (β1) from residue 23-30 (a). In contrast with the MIP-1β dimer, the C-terminal helix of IL-8 makes several critical dimer interactions with the other monomeric subunit (b). PDB coordinates used for this figures are 1hum (MIP-1β) and 1il8 (IL-8).

α-helix. Many chemokines also form dimers. However, CC chemokine dimers have a completely different organization than CXC chemokine dimers (14,25). The N-terminal residues of the CC chemokine MIP-1β are involved in the dimer interface, with residues Pro8 and Phe13 making several critical dimer contacts (Figure 2-1). The C-terminal helix from each monomeric subunit of MIP-1β points away from the other and makes no contact with the other subunit. On the other hand, the dimer of the CXC chemokine IL-8 consists of monomeric subunits that interact with each other along the first β strand, from residue 23-30, rather than acting on the other side of the molecule at the N-terminus (Figure 2-1B). In contrast with the MIP-1β dimer, the C-terminal helix of IL-8 makes several critical dimer interactions with other monomeric subunit. The overall shape of the dimer of the CC chemokine MIP-1β is elongated and cylindrical, but the dimer of the CXC chemokine IL-8 is compact and globular. Later structures of chemokines have also exhibited these structural properties with rare exceptions (18,30): although not all chemokines are dimers, each CC chemokine that dimerizes shares the dimer arrangement of MIP-1β (15,17,18,31). Likewise, the CXC chemokines that dimerize share the dimer structure of IL-8 (32-34). Therefore, the chemokine monomeric fold clearly supports two different dimer structures. Moreover, functional work suggests a biological role for both the dimeric and the monomeric form of the chemokine (9,29,37-39,115).

Given that chemokines from all subfamilies share a common monomeric fold regardless of quaternary structure and that this monomer can naturally form two different types of dimer, the hypothesis is made that there are likely to be changes in

sequences that will allow changes in quaternary structure, perhaps including allowing one stable dimer type to be turned into the other dimer type. Since MIP-1β and IL-8 can be considered to be prototypical CC and CXC chemokines respectively, this hypothesis can be tested. We and others have reported several mutations in MIP-1β and IL-8 that allow formation of monomeric variants, although no attempts were made to determine if the new monomeric scaffold could support other mutations or form alternate dimer types (37-39,116).

The present studies report the use of rational mutagenesis (structure based design) and random mutagenesis, to allow insight into the interactions responsible for chemokine dimer formation. A combination of nuclear magnetic resonance (NMR) spectroscopy, analytical ultracentrifugation, and size exclusion chromatography were used to analyze more than 24 MIP-1β and IL-8 variants produced both rationally and by the randomization/selection process.

Experimental Procedures

Production of structure-based design variants

For changes at the termini of the proteins (to remove the N-terminal 8 residues from MIP-1β, to add C-terminal of IL-8 to MIP(9), to remove 6 residues from C-terminal of IL-8, or to add 9 amino acids of MIP-1β to N-terminal of IL-8) standard thermocycling reactions were carried out with primers encoding the proper change. To put the β1 strand of IL8 onto MIP-1β, PCR mutagenesis was carried out in a two-step reaction by using primers according to the β1 strand sequence of MIP(9)-IL-8 β1 combined with N-

terminal forward primer and C-terminal reverse primer for MIP(9). The PCR products were purified and digested with NcoI and BamH I restriction endonuclease, and cloned into the Nco I and BamH I site of vector pET-32a(+) (Novagen). To make the single site or multiple site mutations, mutagenesis on IL-8 were carried on using the QuikChange (Stratagene) method. All mutations were confirmed by DNA sequencing.

Plasmids and primers for the randomization library

The genes for WT MIP-1β, IL-8, MIP-START (starting point monomeric mutant of MIP-1β, designed in the present study) and IL-8-START (starting point monomeric mutant of IL-8, designed in the present study) were placed into the screening vector JH391 (117) using the BamH I and Sal I restriction sites. Phage stocks were initially obtained from the laboratory of Dr. James Hu and propagated as described (118). The phages used were phage λ KH54 and phage λ h80. Both of these phage stocks are deleted for the cI gene and differ only in the recognition of the receptors needed to gain initial access to the host cell. Oligonucleotide primers for mutagenesis were ordered from IDT (Coralville, IA), with bases to be randomized designated as "N" in the sequence. For randomization of regions within approximately twenty base pairs of the 5' or 3' termini, an overhang PCR was performed to create a library of mutants. For randomization of regions distant from the termini, two separate thermocycling reactions were used to accomplish randomization: Initially, two separate but complementary (except for the region of mutation) oligonucleotides were created. These primers were used with terminal oligonucleotide primers to create "half-gene products" that were then annealed together in another thermocycling reaction to create a "full-gene product"

randomized only in the desired region. The randomized gene product and the JH391 plasmid were subjected to restriction digestion by Sal I and BamH I restriction enzymes. The randomized inserts and JH391 plasmid were then ligated (10 ng of gene with 100 ng of vector).

Phage selection of random chemokine variants

A "cross-streak" test individually examines the success or failure of a particular λ fusion partner in conferring resistance to phage infection. First, phage λ KH54 is streaked horizontally across an LB agar plate. Next, streaks of cells from a single colony containing a construct to be tested are drawn orthogonal to the phage line. The vitality of the cells after they cross the phage line indicates the presence or absence of a functional λ repressor. A method to screen large numbers of random mutants has been described (119). Briefly, ligation mixtures containing the chemokine variants fused to the λ repressor in the JH391 vector were transformed using electroporation into AG1688 *E. coli* cells and then plated onto agar plates containing λ KH54 and h80 phage. A small portion of the transformation mixture was removed and plated under permissive conditions (no phage) to allow an assessment of the number of mutants screened. The plasmid from surviving colonies was purified and retransformed into AG1688 cells and the cells were challenged again with phage to ensure that all colonies harvested from the initial high-throughput plate were in fact resistant to phage based on the dimerization of λ repressor due to vector-encoded chemokine and not on artifacts of natural selection in the *E. coli* cells. The gene for a chemokine variant that continually demonstrated the ability to convey phage resistance was then shuttled into the pET expression system

(Novagen). (MIP-START and its related random mutants were placed into pET32a(+) at the Nde I-BamH I sites, and the expressed proteins do not have a histidine tag on the N-terminus; IL-8-START and its related random mutants were placed into pET15b at the Nde I-BamH I sites, and when expressed, these proteins have a 6 histidine tag on the N-termini to facilitate the purification.) Purified protein was examined by analytical ultracentrifugation, NMR, and/or size exclusion chromatography.

Construction of cI fusion mutants

To construct cI fusion mutants, the gene for cI-MIP-1β WT, cI-MIP-START, cI-IL-8 WT, cI-IL-8-START and two MIP-START mutations MIP_8S and MIP_8G and one of IL-8-START mutation IL-8_86 were amplified from the JH391 vector by using standard thermocycling reactions and ligated into pET15b (Novagen) Nde I-BamH I sites, the coded protein have the 6XHistag on the N-termini to facility the purification.

Protein expression and purification

For wild type proteins and MIP-1β variants and IL-8 variants from the mutagenesis, protein expression and purification followed a standard chemokine refolding and purification method published previously (39). For the cI fusion mutants, a slight variation on the procedure was used, in that the proteins were expressed in rich medium, and the protein inclusion body was taken up in 50 ml of 6M Guanidine chloride, 20 mM sodium phosphate buffer pH 7.2 containing 250 mM NaCl and 10 mM 2-mercaptoethanol and loaded onto a 5ml chelating column (Amersham Pharmacia Biotech) equilibrated with nickel sulfate and the guanidinium buffer. The protein was refolded on the column using a gradient to slowly decrease the amount of guanidine

chloride in 20 mM sodium phosphate buffer pH 7.5 containing 250 mM NaCl, then eluted with imidazole. The fractions containing refolded protein were pooled together and directly diluted 10 fold into 10% acetonitrile and 0.1% trifluoroacetic acid solution, and loaded onto an equilibrated C4 reversed phase column (Vydac, Hesperia, CA). The protein was eluted using an acetonitrile/0.1% TFA gradient. Fractions containing the proteins were quickly frozen in liquid nitrogen and lyophilized by the Labconco freeze dry system (Labconco Corporation) into dried powder. A small amount of the fractions of each run was collected and run on 12% SDS-PAGE to confirm the protein purity.

Size exclusion chromatography for cI fused chemokine mutants

The purified protein powder was first dissolved into 20 mM sodium phosphate buffer pH 2.5 containing 150 mM NaCl, and then the pH of the solution was adjusted to 7.2 with a small amount of 4M NaOH. The solution was centrifuged at 12000 rpm for 20 minutes to remove any possible precipitation. The dissolved refolded protein (~ 0.5ml) was loaded onto a Superdex G75 gel filtration column (Amersham Pharmacia Biotech) equilibrated with 20mM pH 7.2 sodium phosphate buffer containing 150 mM NaCl and the protein was eluted with this buffer (for cI-MIP-1β WT elution was carried out with 20 mM sodium phosphate buffer pH 7.2 containing 500 mM NaCl) and run using the Pharmacia Akta system. The gel filtration column was calibrated with several standard marker proteins (BioRad) in the same running buffer, and the molecular weight of cI-fused chemokines mutants were estimated using the calibrated standard curve. All sample elution was performed at 0.4ml/min, 1ml fractions were collected, and the protein content was analyzed by 12% SDS-PAGE.

Analytical ultracentrifugation (AUC)

Sedimentation equilibrium data were collected on a Beckmann XL-A analytical ultracentrifuge rotor An-60 Ti at 25˚C with multiple speeds and variable protein concentration to obtain the molecular weight or dimer dissociation constant of the proteins under study. The protein concentrations were determined by absorbance at 280 nm using the extinction coefficients estimated by the Expasy web server (http://us.expasy.org/). Samples were dissolved with 20 mM pH 7.2 (with the exception of IL-8-START , IL-8_86 and IL-8_A13 which were dissolved at pH 5.0 to maximize solubility) sodium phosphate buffer containing 150 mM NaCl (cI-MIP-1βWT was centrifuged in 500 mM NaCl due to its tendency to aggregate at lower salt concentrations). During each equilibrium experiment, samples were monitored by absorbance at 280 nm. For each mutant, AUC experiments were done at constant concentration with multiple speeds, or with runs at various concentrations with multiple speeds: 50μM IL-8-START, 50μM IL-8_A13 and 50μM IL-8_86 run at 26500 rpm and 37500 rpm; 45μM, 90μM and 180μM MIP-START run at 16000 rpm, 26500 rpm and 40000 rpm respectively; 30μM MIP-8S and 30μM MIP-68S run at 26500 rpm and 37500 rpm; 10μM cI-IL-8WT run at 16000 rpm, 26500 rpm; 10μM and 15μM cI-IL-8-START run at 16000 rpm and 20000 rpm respectively; 20μM cI-IL-8_86 run at 16000 rpm and 37500 rpm; 20μM cI-MIP-1βWT run at 16000 rpm and 26500 rpm; 10μM and 12μM cI-MIP-START run at 16000 rpm and 20000 rpm respectively; 30μM cI-MIP_8S and 20μM cI-MIP_8G run at 16000 rpm and 26500 rpm respectively. The solvent density (ρ) and partial specific volume of the protein($\bar{v}$) were calculated from the amino

acid composition using the program Sednterp (obtained from the Boston Biomedical Research Institute RASMB web site). The data were processed using the program Origin, which is useful for both detecting multiple equilibria and estimating the value of the equilibrium constants from the absorbance data (120). Each set of experimental data was fit to an ideal model or monomer–dimer equilibrium model using a nonlinear least squares fit. The data of cI-MIP-1β WT and cI-IL-8 WT fit best to the monomer-dimer equilibrium model. The dimer K_d (disassociation constant) values were calculated using a similar method as described by others (121,122). All other proteins fit best with a single ideal monomer model, from which was obtained the calculated molecular weight. For each mutant, the average molecular weight and standard deviation were calculated from multiple experiments.

Nuclear Magnetic Resonance

NMR spectra were acquired at 25 °C on a Varian Unity Plus 500 MHz spectrometer equipped with an *xyz* gradient penta probe. ^{15}N-^{1}H HSQC (heteronuclear single quantum coherence) spectra were collected with 512* points in the proton dimension and 128* points in the nitrogen dimension. A spectral width of 6000 was used in the ^{1}H dimension and 1500.68 Hz for ^{15}N . The samples were placed in Shigemi tubes (Allison Park, PA) and the spectra referenced relative to DSS (2,2-dimethyl-2-silapentane-5-sulfonate) (123). The data were processed using the program nmrPipe (124) and analyzed using the program PIPP (125). For MIP-1β mutants, the samples were dissolved in 10% D2O with 20mM sodium phosphate, pH 7.2, 100mM NaCl; for IL-8 mutants, samples were dissolved in 10% D2O solvent with 20 mM sodium phosphate, pH 5, 100 mM NaCl.

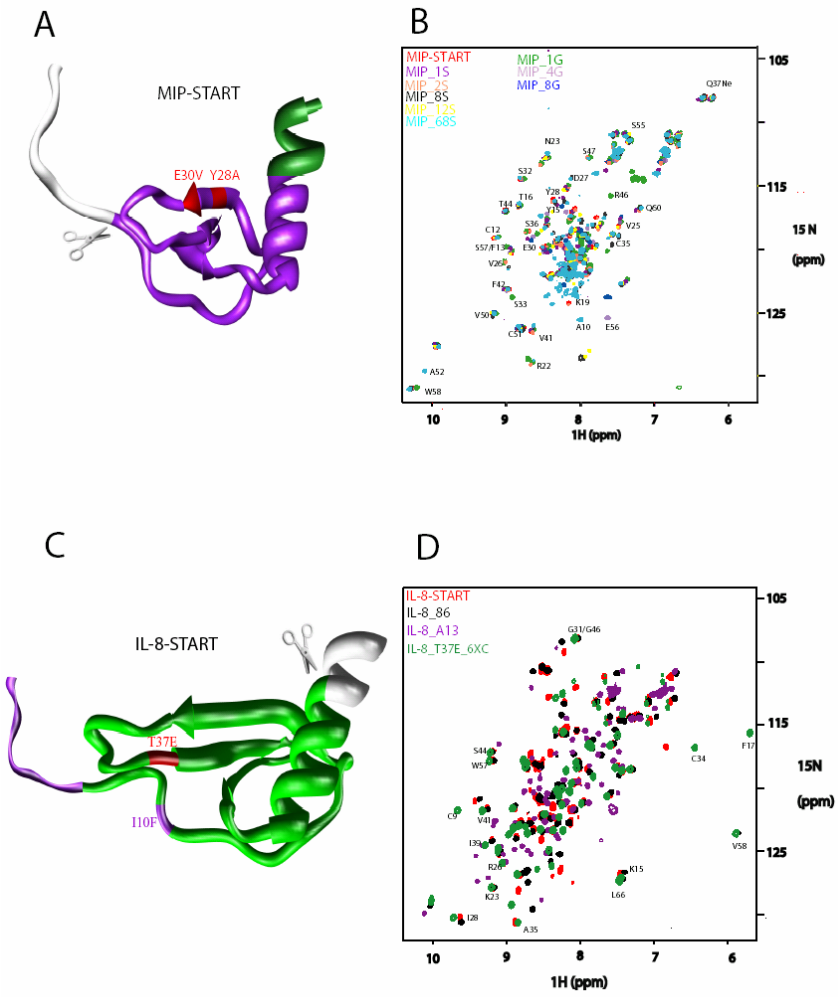

Figure 2-2: A) Ribbon diagram of a model of the designed variant MIP-START. In addition to truncation of the first 8 residues, two amino acids in the β1 strand were mutated (Y28, E30; red) and 4 residues from the C-terminal helix were replaced with 8 residues from IL-8, lengthening the helix by one turn (green). PDB coordinates used for this figure are 1hum. B) Overlay of the NMR ^{15}N - ^{1}H HSQC spectra of MIP-START and all eight folded random variants. The labeled assignments of MIP-START are inferred from similarity to previously published mutants (50,126). Each variant is represented with different color: MIP-START (red), MIP_1S (purple), MIP_2S (orange), MIP_8S (black), MIP_12S (yellow), MIP_68S (light blue), MIP_1G (green), MIP_4G (lavender) and MIP_8G (dark blue). C) Ribbon diagram of a model of the designed variant IL-8-START. IL-8-START lacks the last 6 residues of the C-terminus, and also has a T37E mutation (purple). The first 9 residues of N-terminal MIP-1β were added onto IL-8–START, as well as the Phe13 from MIP-1β (purple). PDB coordinates used for this Figure are 1IL8. D) The ^{15}N - ^{1}H HSQC spectra of two folded IL-8 mutants IL-8_86 (black), IL-8_A13 (purple) and IL-8_T37E_6XC (green) overlaid with the spectrum of IL-8-START (red). The labeled assignments of peaks are from IL-8_T37E_6XC (unpublished data).

Results

Structure-based mutagenesis of chemokines to alter quaternary state

In a first step toward altering the CC and CXC chemokine dimer, rational mutagenesis was employed to both disrupt the natural dimer and to favor formation of the dimer of the other subfamily. It has been shown that removing the N-terminal residues of MIP-1β results in a folded, monomeric protein (50), so all MIP-1β variants reported here lack the first 8 amino acids. Since the β1 strand region is critical for IL-8-type dimer formation, residues 26-31 in MIP-1β were replaced with the analogous resides in IL-8. However, rather than resulting in an IL-8-type dimer, the resulting protein was unfolded (data not shown). The structure of MIP-1β reveals that several β1 residues participate in important intramolecular contacts, so a more conservative set of changes were made in which only Y28 and E30 were mutated to residues analogous to their IL-8 counterparts (Y28A and E30V, respectively). This resulted in a folded, monomeric protein (data not shown). Since the β1 variation did not lead to an IL-8-type dimer, the other major area of IL-8 dimerization was added to MIP-1β. As shown in Figure 2-1B, the IL-8 C-terminal helix makes critical dimer contacts and the helix is longer than that of MIP-1β. Therefore, in addition to the N-terminal truncation and alteration of the β1 strand, the four C-terminal residues of the MIP-1β helix were replaced by eight residues of IL-8 helix, lengthening the helix by one turn. The resulting protein is diagrammed in Figure 2-2A and the NMR spectrum is shown in Figure 2-2B.

While the extensively altered MIP-1β variant was successfully produced as a folded protein, it was found to be a monomer, with no affinity for either dimer type.

In our study of the quaternary state of IL-8, we first focused on mutations in the β1 strand, since this region forms the center of the dimer interface (Figure 2-1B). Mutations were made to the β1 strand (L25A/V27E), resulting in a weakened dimer that was in equilibrium with the monomeric form. This suggests that the β1 strand provides dimer stability through both backbone interactions and side chain interactions (data not shown). A more successful strategy for making purely monomeric IL-8 was to remove the critical dimer contacts made by the C-terminal helix. This was accomplished by employing the double strategy of shortening the helix by 6 residues (first suggested to weaken the dimer by Rajarathnam et al. (127)) and simultaneously mutating Thr37, a residue in the 30's loop that contacts the helix from the other subunit (shown to be involved in the dimer (128)) (Figure 2-1B). These mutations resulted in a folded, wholly monomeric variant of IL-8 (Figure 2-2D).

To attempt to form a MIP-1β-type dimer with monomeric IL-8, the N-terminus of this IL-8 variant was replaced with the N-terminus of MIP-1β. The vast majority of MIP-1β dimer contacts are made by its N-terminal region, particularly residues Pro8 and Phe13 (Figure 2-1A), so the IL-8 variant replaces residues1-7 with the first 9 residues from MIP-1β, and also includes Phe13 from MIP-1β (while retaining the structurally necessary N-terminal CXC of the original IL-8). However, despite the extensive mutation to this protein, analytical ultracentrifugation shows it to be a monomer

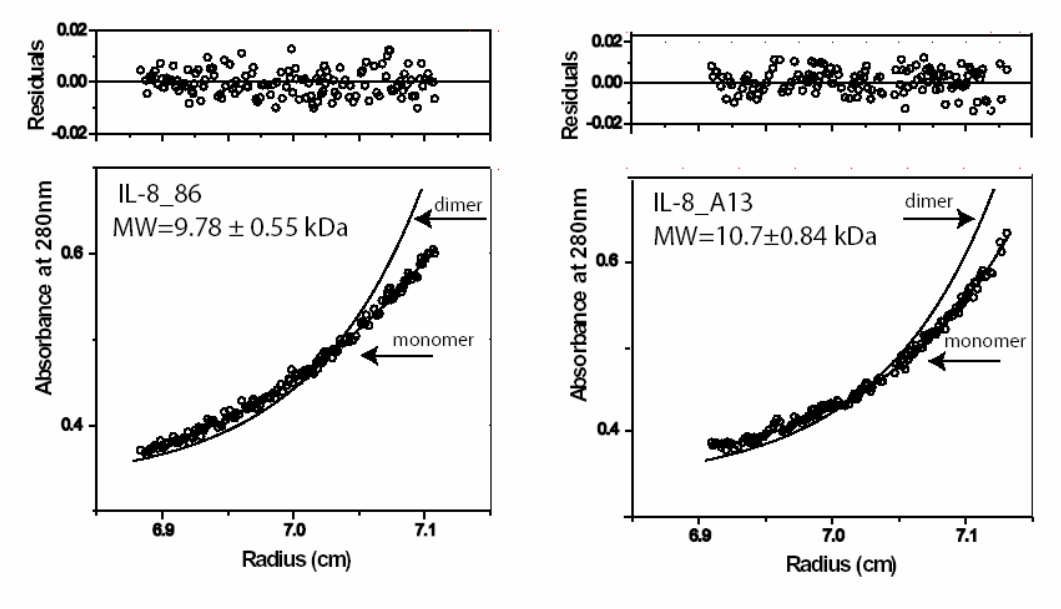

Figure 2-3: Analytical ultracentrifugation data of IL-8_86 (left) and IL-8_A13 (right). For each panel, the lower plot shows the raw data and the best fit to a specific model. The upper plot shows residuals from fitting the model. The estimated molecular weight includes the N-terminal histidine tag. The number shown in table 2-3 differs slightly because it shows the average value obtained from multiple runs. The line denoted "dimer" is for comparison and indicates a curve that would be obtained for a monomer-dimer equilibrium.

(Figure 2-3). This mutant was termed "IL-8-START" for the random mutagenesis described below.

Random mutagenesis and dimer selection

Since structure-based mutagenesis provided many sequences that remained folded but were monomeric, it was decided to randomly mutate a monomeric starting point from each protein to determine whether alternate dimers could be formed or whether even more monomeric variants were possible. The final MIP-1β variant described above was designated MIP-START for the purposes of random selection (Figure 2-2A describe the full set of mutations to make MIP- START). Since this variant lacks the first eight residues of the N-terminus, no mutation is likely to cause reversion back to a wild-type MIP-1β dimer. Therefore, any dimers produced by randomization would likely be either similar to IL-8 or an equally interesting alternate arrangement. As described above, MIP-START already contains some elements of the IL-8 dimer structure that might, upon further mutation, help promote the formation of the IL-8-type dimer. Similarly, the IL-8 variant ultimately described above was designated IL-8-START (Figure 2-2C describe the full set of mutations to make IL-8-START) and was chosen as the beginning chemokine variant for randomization. Since IL-8-START lacks the last 6 residues of the C-terminus, randomization is unlikely to cause reversion back to a wild-type IL-8 dimer because it is unlikely that the shortened C-terminal helix can reach the other subunit to make dimer contacts. Therefore, any dimers produced by randomization would likely be either structurally similar to MIP-1β or an interesting alternate arrangement.

The λ phage selection system

Several strains of bacteria are susceptible to infection by λ phage, which eventually causes host bacterial cell death by cell lysis. However, cells are able to survive infection by phage if the λ repressor is present in the cell. The dimerization of the C-terminus of the λ repressor facilitates the N-terminus of the λ repressor binding to the phage operator. Importantly for the current work, it has been shown that fusions of unrelated proteins to the N-terminus of the λ repressor can confer phage resistance if the fusion partner facilitates dimerization of the λ repressor (129,130). Thus, replacing the C-terminus of the λ repressor with a selected polypeptide chain, allowing the fusion repressor to propagate within the host cell, and then infecting with λ phage, allows a simple life-or-death assay for dimerization. If the bacterial cells survive a challenge with the λ phage infection, this indicates that the selected polypeptide chain dimerizes, and confers resistance to the phage; if the bacterial cell dies upon challenge with the λ phage, this indicates that the selected polypeptide chain is monomeric or does not dimerize the λ repressor in a suitable conformation to bind DNA.

Randomized libraries of constructs containing chemokine variants were transformed into electrocompetent AG1688 *E. coli* cells, as described in Methods. In order to obtain an accurate count of how many possible colonies were analyzed by the selection process, a small portion (1%) of the transformation mixture was separated and plated on LB agar plates that did not contain phage. By counting the number of colonies that appear on the non-infected plate, extrapolation of the number of colonies screened on the phage-

exposed plate was possible. In this manner, the number of different variants from a randomized pool that had been screened could be estimated. With this high-throughput system, it is possible to screen up to 180,000 random variants on one plate. On average, approximately 50,000 mutants can be screened on one phage-coated plate. In order to eliminate false positives, the plasmids from all positives obtained from the selection procedure were purified and re-transformed into AG1688 cells, and re-tested using the low-throughput cross-streak method. Only the constructs that allowed cell survival in both types of screen were considered true positives and studied further.

As controls for the screen, the genes for wild type MIP-1β, MIP-START, wild type IL-8 and IL-8-START were placed into the JH391 vector to make a fusion with the N-terminus of the λ repressor (cI), and transformed into AG1688 *E. coli* cells. Three constructs performed as expected: cI fusions of MIP-START and IL-8-START (both determined to be monomers), showed clear signs of cell death at the phage-bacteria interface, and cells containing the IL-8 construct, which should dimerize, showed complete vitality. Wild type MIP-1β-containing cells did not survive despite the fact that this chemokine has been shown to form a tight dimer (50). The orientation of the dimer or the lack of stability to proteolysis of MIP-1β in the bacterial cell perhaps caused the cell to be susceptible to phage lysis. Further work on this construct is reported below. Nevertheless, since the IL-8 positive control and both monomeric chemokine variants performed as expected (such that at least for the MIP-START-toward-IL-8 direction the starting and ending points performed as expected), the screening procedure proceeded.

Randomization with the goal of moving from MIP-1β toward the IL-8 dimer

The structure of the IL-8 dimer reveals two major regions of dimer interaction (Figure 2-1B). The most obvious dimer interface region is the antiparallel β–sheet formed by the β1 strands of each IL-8 monomer. In addition, significant dimer contacts are made in IL-8 by the C-terminal helix in contact with the 30's loop of the other subunit. Our work and work by others shows that the IL-8 dimer is at least partially retained even with significant changes in the side chains of the β1 strand amino acids, indicating a significant component of stability is provided simply by the backbone interactions (37,128). In an attempt to mutate the MIP-1β monomeric variant MIP-START toward the IL-8-type dimer, MIP-START was mutated at the C-terminus and 30's loop region, and also in the β1 strand. The resulting mutants were screened as described above.

In the 30's loop region of MIP-START Thr31, Ser32, Pro38 and Ala39 were randomly mutated. (Cys35 and surrounding amino acids were not mutated due to the structural importance of Cys35 in forming a disulfide bridge. Pro38 is not part of the turn of the loop so this residue was considered structurally safe to mutate.) A total of 500,000 colonies were screened, and 3 mutants survived, passing both the high throughput screen and the cross streak phage screen (Table 2-1). However, two of these variants were found to contain stop codons in the mutated region. It has been found that some small peptides do allow survival in this selection system without necessarily being

Table 2-1: The amino acid sequences of the rational (designed) mutants and the phage system-selected chemokine random variants.

MIP-1β WT:	APMGSDPPTACCFSYTARKLPRNFVVDYYETSS--LCSQPAVVFQTKRSKQVCADPSESWVQEYVYDLELN----	F
MIP(9):	--------TACCFSYTARKLPRNFVVDYYETSS--LCSQPAVVFQTKRSKQVCADPSESWVQEYVYDIELN----	F
MIP(9)-IL8β1:	--------TACCFSYTARKLPRNFV***KELRVI***SS--LCSQPAVVFQTKRSKQVCADPSESWVQEYVYDIELN----	U
MIP(9)Y28AV30E:	--------TACCFSYTARKLPRNFVVD***A***Y***E***TSS--LCSQPAVVFQTKRSKQVCADPSESWVQEYVYDIELN----	F
MIP-START:	--------TACCFSYTARKLPRNFVVD***A***Y***E***TSS--LCSQPAVVFQTKRSKQVCADPSESWVQEYVYDF***LKRAENS***	F
MIP_1S:	--------TACCFSYTARKLPRNFVVD***A***Y***E***TSS--LCSQPAVVFQTKRSKQVCADPSESWVQEYVYDF***SKRRENP***	F
MIP_2S:	--------TACCFSYTARKLPRNFVVD***A***Y***E***TSS--LCSQPAVVFQTKRSKQVCADPSESWVQEYVYDF***TKRNENI***	F
MIP_7S:	--------TACCFSYTARKLPRNFVVD***A***Y***E***TSS--LCSQPAVVFQTKRSKQVCADPSESWVQEYVYDF***LKRWENK***	U
MIP_8S:	--------TACCFSYTARKLPRNFVVD***A***Y***E***TSS--LCSQPAVVFQTKRSKQVCADPSESWVQEYVYDF***SKRIENR***	F
MIP_12S:	--------TACCFSYTARKLPRNFVVD***A***Y***E***TSS--LCSQPAVVFQTKRSKQVCADPSESWVQEYVYDF***LKRLENT***	F
MIP_61S:	--------TACCFSYTARKLPRNFVVD***A***Y***E***TSS--LCSQPAVVFQTKRSKQVCADPSESWVQEYVYDF***GKRREN***-	U
MIP_68S:	--------TACCFSYTARKLPRNFVVD***A***Y***E***TSS--LCSQPAVVFQTKRSKQVCADPSESWVQEYVYDF***EKR***----	F
MIP_1G:	--------TACCFSYTARKLPRNFVVD***A***Y***E***TSS--LCSQPAVVFQTKRSKQVCADPSESWVQEYVYDF***RKRYENS***	F
MIP_4G:	--------TACCFSYTARKLPRNFVVD***A***Y***E***TSS--LCSQPAVVFQTKRSKQVCADPSESWVQEYVYDF***YKRKENY***	F
MIP_8G:	--------TACCFSYTARKLPRNFVVD***A***Y***E***TSS--LCSQPAVVFQTKRSKQVCADPSESWVQEYVYDF***AKRRENV***	F
IL-8 WT:	---SAKELRCQCIKTVSKPFHPKEIKELRVIESGPHCANTEIIVKLSDGRELCLDPKENWVQRVVEKFLKRAENS	F
IL-8-L25AV27E:	---SAKELRCQCIKTVSKPFHPKEIKE***A***R***E***IESGPHCANTEIIVKLSDGRELCLDPKENWVQRVVEKFLKRAENS	F
IL-8-M3:	---SAKELRCQCIKTVSKPFHPKEIKELRVIESGPHCAN***E***EIIVKLSDGRELCLDPKENWVQRVVEKFLKR***E***EN***E***	F
IL-8-M5:	---SAKELRCQCIKTVSKPFHPKEIKE***A***R***E***IESGPHCAN***E***EIIVKLSDGRELCLDPKENWVQRVVEKFLKR***E***EN***E***	U
IL-8-T37E-6XC:	---SAKELRCQCIKTVSKPFHPKEIKELRVIESGPHCAN***E***EIIVKLSDGRELCLDPKENWVQRVVEKFL------	F
IL-8-START:	***APMGSDPPT***CQC***F***KTYSKPFHPKFIKELRVIESGPHCAN***E***EIIVKLSDGRELCLDPKENWVQRVVEKFL------	F
IL-8_A13:	***APMGVFHLQ***CQC***F***KTYSKPFHPKFIKELRVIE**PFGN**CAN***E***EIIVKLSDGRELCLDPKENWVQRVVEKFL------	F
IL-8_5:	***APMGAAPYR***CQC***F***KTYSKPFHPKFIKELRVIE**ALFI**CAN***E***EIIVKLSDGRELCLDPKENWVQRVVEKFL------	U
IL-8_9:	***APMGVNRRM***CQC***F***KTYSKPFHPKFIKELRVIE**HVLP**CAN***E***EIIVKLSDGRELCLDPKENWVQRVVEKFL------	U
IL-8_28:	***APMGVSLCH***CQC***F***KTYSKPFHPKFIKELRVIE**LLFD**CAN***E***EIIVKLSDGRELCLDPKENWVQRVVEKFL------	U
IL-8_36:	***APMGAEYCR***CQC***F***KTYSKPFHPKFIKELRVIE**ATII**CAN***E***EIIVKLSDGRELCLDPKENWVQRVVEKFL------	U
IL-8_47:	***APMGGQSSR***CQC***F***KTYSKPFHPKFIKELRVIE**SLLM**CAN***E***EIIVKLSDGRELCLDPKENWVQRVVEKFL------	U
IL-8_49:	***APMGDVHLY***CQC***F***KTYSKPFHPKFIKELRVIE**FYAV**CAN***E***EIIVKLSDGRELCLDPKENWVQRVVEKFL------	U
IL-8_63:	***APMGSDPPT***CQC***F***KTYSKPFHPKFIKELRVIE**VT**--CAN***E***EIIVKLSDGRELCLDPKENWVQRVVEKFL------	U
IL-8_68:	***APMGVVICL***CQC***F***KTYSKPFHPKFIKELRVIE**TPFP**CAN***E***EIIVKLSDGRELCLDPKENWVQRVVEKFL------	U
IL-8_86:	***APMGARLEG***CQC***F***KTYSKPFHPKFIKELRVIE**SDCR**CAN***E***EIIVKLSDGRELCLDPKENWVQRVVEKFL------	F
IL-8_B15:	***APMGVPLIF***CQC***F***KTYSKPFHPKFIKELRVIE**ILYL**CAN***E***EIIVKLSDGRELCLDPKENWVQRVVEKFL------	U

The residue numbers for the MIP-1β variants are based on the numbering of wild type MIP-1β; the residue numbers for the IL-8 variants are based on the numbers of wild type IL-8. Residues highlighted by italic are rationally designed mutant residues, while underlined residues signify changes selected by the λ repressor system. Below each alignment is the predicted secondary structure based on the wild type MIP-1β and IL-8 structure. F/U in the last column indicates whether the purified proteins studied by NMR are folded (F) or unfolded (U). There are 8 folded mutations from MIP-1β mutagenesis screen, and two folded mutations from the IL-8 mutagenesis screen.

folded dimeric proteins (131), so these positives were not studied further. The gene for the third positive mutant was subsequently subcloned into an expression vector and purified. However, the NMR spectrum of this protein revealed it to be an unfolded protein (Tables 2-1).

In the β1 strand region of MIP-START, Asp27, Ala28, Tyr29, Val30 and Thr31 were randomly mutated. 400,000 colonies were screened, of which 2 mutants survived the phage screening (Table 2-1). Again, both of these were found to have stop codons in this region. Therefore, none of these truncated proteins were subsequently purified.

In terms of selecting for full-length, folded protein, the most successful region of mutagenesis in MIP-START was the C-terminal helix (Table 2-1). In this region amino acids Leu66, Ala69 and Ser72 were randomly mutated, as these comprise the appropriate face of the helix for making dimer contacts. 730,000 colonies were screened, resulting in 11 mutants that survived the phage screens. One of these was shown to contain a frame shift mutation and was not studied further. The genes for the remaining 10 of these mutant chemokines were placed into an expression vector and subsequently purified. NMR studies indicated that 8 of these were nicely folded, while 2 proteins were unfolded (Table 2-1, Table 2-2 and Figure 2-2B).

Randomization with the goal of moving from IL-8 toward the MIP-1β dimer

The MIP-1β dimer is formed by contacts across the N-terminus and also by contacts between the N-terminal amino acids and both the 30's and the 40's loop (Figure 2-1A). In an attempt to form the CC chemokine MIP-1β-type dimer from IL-8, the 30's loop and the N-terminal regions on IL-8-START were mutated and screened using the high

Table 2-2: Results of the λ phage homodimer repressor selection system screen for random variants of MIP-1β and IL-8. MIP-START and IL-8-START are described in the text and in Figure 2-2.

Mutagenesis Region	MIP-1β variant MIP-START			IL-8 variant IL-8-START		
	C-term (L66/A69/S72)	β1-strand (D27/A28/ Y29/V30/T31)	30's loop (T31/S32/ P38/A39)	N-term (S2/D3/ P4/P5/T6)	30's Loop (S30/G31/ P32/ H33)	N-term and 30's loop (S2/D3/P4/P5/T6/ S30/G31/P32/H33)
Number of colonies screened	730,000	400,000	500,000	470, 000	1,200,000	2,700,000
Total positives from phage selection	11	2	3	3	2	11
Number of mutants containing stop codon, frame shift, or unable to be stably expressed	1	2	2	3	2	0
Number of purified proteins	10	0	1	0	0	11
Number of folded proteins	8	0	0	0	0	2
Number of unfolded proteins	2	0	1	0	0	9

throughput screening method. As mentioned, DNA from successful colonies in the high throughput screen was further tested with the cross streak method to remove false positives.

In the 30's loop region (Ser30, Gly31, Pro32 and His33), a total of 1,200,000 colonies were screened, of which 2 mutants passed both types of screening procedure. One of these genes contained a stop codon in the sequence, so was not studied further. Expression of the other gene was unsuccessful after repeated attempts at purification.

In the N-terminal region of IL-8-START (Ser2, Asp3, Pro4, Pro5 and Thr6), 470,000 colonies were screened, of which 3 mutants passed the screen. Each of these was sequenced and shown to contain a stop codon near the beginning of the gene, coding for a short peptide (as seen for some of the MIP-START screens). Therefore, none of these were subsequently expressed or purified.

Extensive screening was carried out by mutating IL-8-START simultaneously at both the N-terminus and the 30's loop (Ser2, Asp3, Pro4, Pro5, Thr6, Ser30, Gly31, Pro32 and His33). It was recognized that both Gly and Pro contribute structurally to the turn in IL-8, but since this region makes some of the few non-N-terminal dimer contacts in MIP-1β and since this loop in IL-8 is long enough to not require a tight turn, mutagenesis proceeded. 2,700,000 colonies were screened, resulting in 11 mutations that conferred survival in both types of phage selection. The genes for these were placed into expression vectors and the resulting protein purified. NMR studies indicated that only 2 of these proteins were folded while 9 proteins were unfolded. Each of these proteins was very difficult to work with, requiring multiple preparations and resulting in

very poor yields both in protein amounts and in final folded product, suggesting that this family of mutants results in generally unstable protein.

In total, 6,000,000 colonies were screened, resulting in 16 MIP-1β variants that conferred survival to phage, and 16 IL-8 variants that conferred survival to phage. Of these, the genes for 22 were placed into expression vectors, the protein purified, resulting in 8 folded MIP-1β mutants and 2 folded IL-8 mutants (Table 2-1, Figure 2-2B, Figure 2-2D); see below for analysis).

Analysis of the purified mutants from the screen of random variants

The designed MIP-START and IL-8-START were determined to be monomers by AUC (Table 2-3), and NMR was used to compare these starting monomers with the random variants. Nuclear magnetic resonance is a powerful method to investigate the structure of proteins and to detect residue-specific changes in structure. The ^{15}N-^{1}H HSQC (Heteronuclear Single Quantum Coherence) experiment provides a spectrum showing a single peak corresponding to each covalently bonded ^{15}N-^{1}H pair in the protein. The chemical shift position of a peak is dependent on the local molecular environment and as a result the HSQC spectrum for each protein is unique, providing a "fingerprint" of the protein.

In order to analyze the positive mutants from the selection, the MIP-1β variants described above were purified individually and their spectra were measured. These spectra were overlaid with that of MIP-START to determine the level of change from the original monomer starting point. Figure 2-2B shows the ^{15}N - ^{1}H HSQC spectrum of all eight folded variants overlaid with the starting monomer MIP-START. These

Table 2-3: The summary of molecular weight and dimerization state of IL-8 and MIP-1β mutants in this chapter.

Mutants	Monomer molecular weight (kDa)	AUC estimated molecular weight (kDa)*	AUC estimated dimer Kd (μM)**	Size exclusion chromatography estimated molecular weight (~kDa)	Conclusion: D: dimer M: monomer
IL-8 WT	8.36	Dimer	0.194	16	D[a,b]
IL-8-L25A_V27E	8.37	Dimer	151.5	16/8	D[a,b]
IL-8-T37E-6XC	7.67	N.D.	-	8	M[a,b]
IL-8-START	10.3	10.0±0.6	-	10	M[a,b,c]
IL-8 _A13	10.0	9.46±1.2	-	10	M[a,b,c]
IL-8 _86	9.95	9.31±0.5	-	10	M[a,b,c]
MIP-1β	7.80	Dimer	0.73[e]	N.D.	D[a,b,c]
MIP(9)Y28AV30E	7.01	N.D.	-	N.D.	M[c]
MIP-START	7.51	8.14±0.5	-	8	M[a,b,c]
MIP_1G	7.68	N.D.	N.D.	N.D.	M[c]
MIP_4G	7.73	N.D.	N.D.	N.D.	M[c]
MIP_8G	7.61	N.D.	N.D.	N.D.	M[c]
MIP_1S	7.62	N.D.	N.D.	N.D.	Mc
MIP_8S	7.63	6.59±0.6	-	N.D.	M[a,c]
MIP_12S	7.61	N.D.	N.D.	N.D.	M[c]
MIP-68S	7.17	10.1±0.4	-	N.D.	M[a,c]
cI-IL-8 WT	25.5	Dimer	1.0 (-0.4+0.6)	50	D[a,b]
cI-IL-8-START	25.2	28.9±2.5	-	25	M[a,b]
cI-IL-8_86	24.8	22.7±6.1	-	25	M[a,b]
cI-MIP-1β WT	24.9	Dimer	13.1(-4.7+3.6)	50	D[a,b]
cI-MIP-START	24.7	24.8±0.9	-	25	M[a,b]
cI-MIP_8S	24.8	25.8±0.1	-	25	M[a,b]
cI-MIP_8G	24.7	23.5±4.7	-	N.D.	M[a]

(a: Determined by analytical ultracentrifugation equilibrium experiments; b : Estimated by size exclusion chromatography; c: Estimated by NMR HSQC spectrum comparison with known protein; e. Laurence et al. 2000. * For each mutant, average and standard deviation are calculated from multiple experiments (constant concentration variable speed or variable concentration and speed: 50μM IL-8-START,50μM IL-8_A13 and 50μM IL-8_86 run on 26500rpm and 37500rpm; 45μM, 90μM and 180μM MIP-START run on 16000rpm, 26500rpm and 40000rpm respectively; 30μM MIP_8S and 30μM MIP-68S run on 26500rpm and 37500rpm ;10μM cI-IL-8 WT run on 16000rpm and 26500rpm;10μM and 15μM cI-IL-8-START run on 16000rpm and 20000rpm respectively;20μM cI-IL-8_86 run on 16000rpm and 37500rpm;20μM cI-MIP-1β WT run on 16000rpm and 26500rpm;10μM and 12μM cI-MIP-START run on 16000rpm and 20000rpm respectively;30μM cI-MIP_8S and 20μM cI-MIP_8G run on 16000rpm and 26500rpm respectively. Data from each individual experimental are best fit with a single ideal model using Origin program (Beckman Inc.) except IL-8 WT, MIP-1β WT, cI-IL-8 WT and cI-MIP-1β WT which are best fit with monomer-dimer association model and are indicated with "Dimer" in the table. ** Positive or negative number mean positive or negative 95% confidential intervals from the best fitting of weighted self association monomer-dimer model using Origin program (Beckman Inc.) . N.D.: Not done -: Data are not consistent with monomer-dimer self association model.)

random mutants are nicely folded, but the spectra are very similar to known monomer MIP-START, indicating a similar structure to the starting material without a major quaternary rearrangement. Therefore, a reasonable conclusion is that all selected MIP-1β mutants are still monomers.

The folded IL-8 mutants described above and in Table 2-1 were purified and their "fingerprint" ^{15}N - ^{1}H HSQC spectra were measured and compared to that of IL-8-START to determine the level of structural change from the starting monomer. Both IL-8_A13 and IL-8_86 were clearly folded, and showed some significant spectral variation from the starting monomer (Figure 2-2D). However, these variants were further studied by AUC (analytical ultracentrifugation) (Figure 2-3) which showed them to still be monomers, not dimers. Therefore neither of these mutants selected by the repressor fusion phage system appears to be a dimer.

Characterization of the repressor fused chemokines mutants in vitro

It was somewhat surprising that the chemokine mutants selected by the repressor fusion system appear to be monomers, not dimers, since the selection with cI-fused monomers should cause bacteria to die when challenged with phage. However, studies of the expressed and purified random variants were carried out on the chemokines alone, free of the fusion partner, while the selection system is based on the ability of the protein to dimerize when it is fused with the N-terminus of the λ repressor. Therefore, the positive variants might be dimers when fused to the λ repressor but monomers in the absence of the fusion partner. In order to test this possibility, some of the chemokine variants in fusion with the repressor were examined. Wild type MIP-1β, IL-8, and

several of variant chemokines shown in Table 2-1 were expressed and purified as fusions with the N-terminus of the λ repressor, creating the same protein that is used in the bacterial selection system to allow the cell to avoid phage lysis. These proteins were investigated by size exclusion chromatography and analytical ultracentrifugation in order to assess their quaternary state.

Both wild type MIP-1β and wild type IL-8, when fused to the N-terminus of the λ repressor, eluted as dimers on a Superdex G75 column (Figure 2-4) and behaved as dimers in the analytical ultracentrifuge (Table 2-3), as expected. In addition, the monomeric variants MIP-START and IL-8-START also behaved as expected when fused to the N-terminus of the λ repressor, behaving as monomers in analytical ultracentrifugation experiments and eluting from the G75 column as monomers (Table 2-3, Figure 2-4). However, two representative variants positively selected from the phage screen, MIP_8S and IL-8_86, exhibited properties indicative of monomers, not dimers when fused to the λ repressor (Figure 2-4, Table 2-3). This is consistent with the results (described above) of these variants expressed without the λ fusion partner, which also revealed fully monomeric protein. These results show that chemokine variants selected from the repressor based homodimer system do not appear to be dimers, in the presence or absence of fusion partner, at least under the current various *in vitro* conditions.

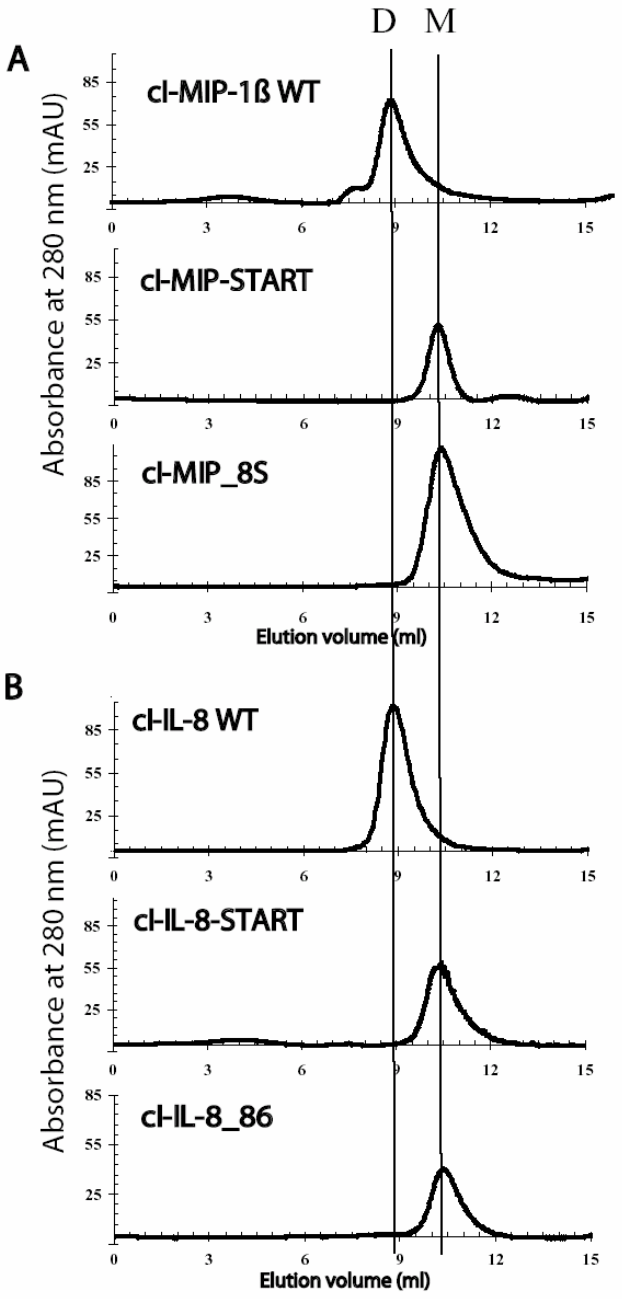

Figure 2-4: Size exclusion chromatography of the λ repressor (cI)-fused chemokine variants. The vertical axis represents the absorbance at 280 nm; the horizontal axis represents the elution volume (mL) of the samples analyzed. The vertical line denoted "D" indicates the elution position of a cI-fused chemokine dimer (MW 50 kDa) while the vertical line denoted "M" indicates the position of a cI-fused chemokine monomer (MW 25 kDa). A) cI fused MIP-1β and variants. B) cI fused IL-8 and variants.

Discussion

The twenty natural amino acids provide for a nearly unlimited number of possible protein sequences but the total number of protein folds expected to exist is relatively small, with many proteins falling into structurally similar families (132). Clearly, some folds are extremely abundant, including the chemokine fold. Currently there are about 50 identified chemokines and all determined structures show that these proteins share a very similar "chemokine fold" although very different quaternary structures have been observed. Interestingly, CC chemokines that dimerize show a typical MIP-1β type dimer and CXC chemokines that dimerize share a typical IL-8 type dimer (25,31). The exceptions to these generalizations are rare and occur in situations where solution studies support this trend, while the X-ray crystal structure appears to show atypical quaternary structure (17,18,133,134). Regardless, the chemokine monomeric unit can support at least two very different dimer types.

Recent evidence, including *in vivo* work, has demonstrated that the chemokine dimer is important for function, likely involved in binding cell surface sugars that allow localization of the chemokine prior to receptor binding (9,29,115,116). However, monomeric variants of several chemokines have been shown to be competent to bind and activate the cognate chemokine receptor (37-39), indicating that a monomer-dimer equilibrium is an important component of chemokine function.

In the current work, both structure-based "rational" mutagenesis and random mutagenesis were applied to two representative members of the chemokine family of proteins in order to investigate the robustness of the chemokine fold and the ability of

the chemokine to form an alternate dimer arrangement. Mutations to MIP-1β (representative of the CC subfamily) and to IL-8 (representative of the CXC subfamily), based on their known structures, were successful in disrupting the dimer of each protein to make a folded monomer. Others have reported changes to IL-8, particularly in the β1 strand region, with varying changes to the quaternary structure. Lowman et al. mutated residues 24 and 28 and found little change in the dimer dissociation constant, eventually opting to make multiple mutations to disrupt the intersubunit helix contact in order to form a monomer (128). More recently, other double mutations in the β1 strand were reported to result in monomers (116). In our hands, mutations to the β1 strand of IL-8 weakened the dimer, but to make a fully monomeric protein we opted to truncate the C-terminal α-helix. For either IL-8 or MIP-1β, further mutation to favor the dimer type of the other subfamily generally still resulted in a folded monomer rather than an alternate dimer, suggesting that the chemokine fold can be adopted by a wide variety of amino acid sequences, although the chemokine dimer is much more sensitive to specific amino acid arrangement.

A novel use of a λ repressor-based homodimer selection system to investigate chemokine dimerization was employed for large-scale dimer selection of randomly mutated MIP-1β and IL-8 variants. This work resulted in more sequence variation in monomers, but no dimer forms: the screened "positive" CC chemokine mutants, and, to a lesser extent, the CXC mutants, were observed by NMR to be similar to the starting monomeric variant.

The lack of success in forming dimers may have several causes. It is possible that the correct region of mutation that would lead to an alternate dimer in either chemokine was not chosen, or sufficient numbers of colonies in the selection system were not screened. Many of the selected variants were found to be expressed as inclusion bodies and refractory to refolding attempts, suggesting that despite tolerating a great deal of sequence variation, eventually stability of the protein becomes a problem in the selection. In addition, there is the possibility that the use of (human) chemokine fusion partners in the (bacterial) selection system did not allow proper folding in the cell and therefore compromised the selection process, despite the fact that the control fusion constructs were mostly successful upon challenge with phage. There is also the possibility that the chemokine dimer is difficult to form in the presence of a large fusion partner. CC chemokines dimerize at their N-terminus, which is also the location of the fusion partner in the selection system. While in theory, there is a long enough linker region to allow dimerization to occur, this may be energetically disfavored. Indeed, investigation of the wild type CC chemokine MIP-1β in fusion with the repressor shows a weaker dimer by analytical ultracentrifugation than the fusion of repressor with wild type CXC chemokine IL-8. Finally, of course, there is the possibility that no moderate amount of sequence variation will allow a switch of chemokine dimer type despite the unique characteristics of the family that make alternate dimers seem like a structural possibility.

CHAPTER III

THE HUMAN CC CHEMOKINE MIP-1β DIMER IS NOT COMPETENT TO BIND TO THE CCR5 RECEPTOR*

Introduction

Chemokines (chemotactic cytokines) are a group of small (7-14 kDa) structurally related proteins that regulate cell trafficking of various types of leukocytes through interactions with a subset of seven-transmembrane, G protein-coupled receptors (GPCRs) and cell surface glycosaminoglycans (GAGs). There are two major chemokine subfamilies, CC and CXC, named for the placement of conserved Cys residues near the N-terminus. The critical role played by chemokines in recruiting leukocytes and inhibiting HIV entry has led to a great deal of interest in their structural biology. Many chemokine structures have been solved, both by NMR and X-ray crystallography (12,14,15,17,19,25,32,133,135). These structures reveal that all chemokines share a common fold, composed of three β strands in a Greek key arrangement, followed by a C-terminal α-helix. Many chemokines form dimers with affinities generally in the high nanomolar or low micromolar range, leading several groups to study the biological role of the chemokine quaternary state. An early study in this area showed that the obligate

---

monomer of the CXC chemokine IL-8 did retain activity on neutrophils *in vitro* (37), and later work by our group and others showed that monomeric variants of the CC chemokines MIP-1β and MCP-1 were also able to bind and activate their respective receptors (38,39).

However, a growing body of evidence suggests a biological role for the dimer. An obligate dimer of the CXC chemokine IL-8 was shown to be able to bind its receptor (40-42) as was the CC chemokine MCP-1 (38,43) although in the latter case it is not clear whether the cross-linked dimers that were reported had a similar dimer structure to the wild type protein. More recently, it was shown that monomeric variants of some chemokines were unable to recruit leukocytes *in vivo*, despite having receptor activity *in vitro* (9). Further indication of the role of the chemokine dimer includes studies in which GAGs have been shown to mediate chemokine oligomerization (38), including playing a direct role in tightening the CC chemokine dimer (29).

Despite the accumulation of data regarding the role of quaternary state in chemokine function, and the clear evidence that at least some chemokine monomers are competent to activate cognate receptors *in vitro*, no direct evidence has yet been reported on whether a CC chemokine dimer can or can not bind to its receptor. In particular, it has never been shown definitively if a chemokine dimer is able to bind the CCR5 receptor or if the dimer has some role in receptor function, in part because it is not possible to observe the quaternary state of a chemokine in standard receptor experiments. Chemokine receptors have been shown to dimerize (136,137), leading to the possibility that multimerization of chemokine ligand on the receptor could lead to multimerization

of the receptor. This question is particularly intriguing since the two chemokine subfamilies have completely different dimer structures, leading to the possibility of different results for different subfamilies (138). In the present study, a covalent dimer of the CC chemokine MIP-1β was produced by a single amino acid substitution (MIP-1β-A10C). This variant was shown to be a non-dissociating dimer that forms a disulfide bond at the center of the dimer interface, and its structure is largely the same as the wild type protein. It has been determined that MIP-1β-A10C neither binds nor activates the MIP-1β receptor, CCR5. However, the receptor activity was recovered upon reduction of the intermolecular disulfide bond. To the best of our knowledge, results reported here represent the first direct evidence that the CC chemokine dimer does not bind to its receptor and thus offers new implications for chemokine-related drug development.

Experimental Procedures

Production and purification of MIP-1β variants

The genes for MIP-1β-A10C and A10S were produced using the Quikchange™ procedure (Stratagene, La Jolla, CA) in a variant of pET32-Xa/LIC (Novagen, Madison, WI). Mutations were confirmed through DNA sequencing. These MIP-1β variants protein were produced in *E. coli* strain BL21(DE3) and purified as follows. The cells were grown in 1 liter of minimal medium containing $^{15}NH_4Cl$ as the sole nitrogen source (when preparing protein for NMR assignment experiments, $^{13}C_6$-glucose was the sole carbon source). Protein production was induced by addition of IPTG to 1 mM in 37C culture for 7 hours, and the cells were harvested by centrifugation at 6,000 x g in an

F10S-6X500y rotor (Piramoon Technologies Inc.) for 30 minutes. The cells were resuspended in 30 mL of 500 mM NaCl, 20 mM Tris (pH 8), and 10 mM benzamidine and French pressed twice at 16,000 psi. After centrifugation for 30 minutes at 17,000 x g in an SS34 rotor (Sorvall Instruments), the pellet was resuspended in 10 mL of 5 M guanidinium chloride, 50 mM Tris (pH 8), 50 mM NaCl, 2mM EDTA, and 10 mM β-mercaptoethanol. The solution was stirred overnight and then centrifuged for 30 minutes at 17,000 x g to remove remaining insoluble pellet. To refold the uncut protein, the solution was dropped slowly into 100 mL of 50 mM Tris (pH 8), 50 mM NaCl, 2 mM EDTA, and 5 mM β-mercaptoethanol. The diluted protein solution was allowed to remain at room temperature for 2 h, and then was dialyzed at 4 °C in 20 mM Tris (pH 8) to remove guanidine chloride and BME. After dialysis, precipitated matter was removed by centrifugation for 30 minutes at 15,000 x g in an F14S-6X250y rotor (Piramoon Technologies Inc.) and the protein was purified on a C4 reversed phase chromatography column (Vydac, Hesperia, CA), and lyophilized by the Labconco freeze dry system (Labconco Corporation). The C4 column was found to effectively separate protein with correctly formed disulfide bonds from protein that was observed to be unfolded, presumably due to incorrect disulfide bond formation. To remove the fusion tag, the protein powder was solubilized into ~1mL of 20 mM sodium phosphate (pH 2.5) and the volume was increased to ~ 40 mL in 20 mM Tris (pH 8), 50mM NaCl, and 2 mM $CaCl_2$. Factor Xa (Novagen) was used for the proteolytic cleavage, which typically took 2 weeks at room temperature. SDS-PAGE was used to monitor the cutting reaction.

Finally, the cut MIP-1β variants were purified over a C4 reversed phase chromatography column and lyophilized.

Non-reducing SDS-PAGE

Equal amounts of MIP-1β variant samples (~10 μg) were resuspended in 10 μl of 20 mM Tris-HCl (pH 8.0) buffer and mixed with 10 μl of 2X loading sample buffer (20mM Tris-HCl, pH6.8, 4% SDS, 0.2% bromophenol blue, 20% glycerol) with or without 50 mM β-mercaptoethanol (reducing reagent), boiled, and electrophoresed on an 17% SDS-PAGE gel.

Analytical ultracentrifugation (AUC)

Sedimentation equilibrium experiments were carried out on a Beckmann XL-A analytical ultracentrifuge using rotor An-60 Ti at 25˚C. For MIP-1β-A10C under non-reducing conditions, the speeds used were 25,000, 38,000, and 45,000 rpm. Samples were composed of 10 μM protein in 20 mM pH 2.5 sodium phosphate buffer containing 150 mM NaCl. For MIP-1β-A10C under reducing conditions, the protein was dissolved into 200 μL of 20 mM pH 2.5 sodium phosphate buffer containing 150 mM NaCl to a concentration of 10μM. The pH was raised to 7.4 by addition of 2 μl of 1 M NaOH, the solution was made to 1 mM DTT, and incubated overnight. Then 2 μL of 50% phosphoric acid was added to lower the pH to 2.5 for AUC experiments. The rotor speeds for this reduced sample were 25000, 35000 and 45000 rpm. During each experiment, samples were monitored by absorbance at 280 nm. The solvent density (ρ) and partial specific volume of the protein ($\bar{v}$) were calculated from the amino acid

compositions using the program Sednterp (obtained from the Boston Biomedical Research Institute RASMB web site). The data were processed using the program Origin (Beckman) for detecting multiple equilibria and estimating the value of the equilibrium constants from the absorbance data (39,121). Each set of experimental data was fit to an ideal model or monomer–dimer equilibrium model using a nonlinear least squares fit.

Selective reduction of MIP-1β-A10C

In order to reduce the inter-molecular disulfide bond formed by the substitution of Cys for Ala in MIP-1β, the purified MIP-1β-A10C powder was dissolved in 20 mM phosphate buffer saline (pH7.4), 1mM DTT (dithiothreitol, Sigma) was added, and the solution was incubated at room temperature for 16 hours and then quenched by adding 1 M phosphoric acid to lower the pH to 2.5. Trifluoroacetic acid was added to 0.1%, acetonitrile was added to 10% and the reduced protein was purified on a C4 column and lyophilized into dried powder.

NMR spectroscopy

All NMR spectra were acquired at 25 $^{\circ}$C on a Varian INOVA 600 MHz spectrometers using protein samples at ~1 mM concentration in 20mM phosphate, 10mM NaCl buffer (pH 2.5). Chemical shifts were referenced to DSS by the method of Wishart et al. (123).

Backbone ^{13}C, ^{15}N, ^{1}H assignment of MIP-1β-A10C and reduced MIP-1β-A10C were assigned by using the triple resonance experiments HNCACB (139,140), CBCA(CO)NH (141) and HBHA(CO)NH (142). Side-chain assignment of MIP-1β-A10C were determined by using C(CO)NH-TOCSY (143,144),HC(CO)NH-TOCSY(145) (in H_2O) and HCCH-COSY(146) in D_2O. Proline assignment was aided by a home-written

proline-edited ^{13}C-HSQC experiment. Distance constraints were obtained from 3D ^{15}N and ^{13}C-edited NOESY and 4D ^{13}C/^{13}C-edited NOESY(147) experiments with a mixing time of 150 ms.

CCR5-expressing cell lines

A CHO-K1 cell line coexpressing CCR5, $G_{\alpha 16}$, and apoaequorin was a kind gift from Dr. Marc Parmentier from the Institute of Interdisciplinary Research of the Free University of Brussels (ULB) Medical School, Brussels, Belgium. This cell line was described previously (148) and is used for binding and functional assays. Briefly, cells were cultured in HAM's F12 medium supplemented with 10% fetal calf serum (Invitrogen Corporation), 100 units/mL penicillin, and 100 μ*g*/mL streptomycin (Invitrogen Corporation). Following selection with 400 μ*g*/mL G418 (Invitrogen Corporation) for 14 days, the population of mixed cell clones was used in binding and functional studies.

A TZM-bl HeLa cell line stably expressing large amount of human CCR5 was obtained from the NIH AIDS Research and Reference Reagent Program, Division of AIDS, NIAID, NIH: TZM-bl from Dr. John C Kappes, Dr. Xiaoyuan Wu and Tranzyme Inc. The details of this cell line were described previously (149,150).

Binding assays

CHO-K1 cells expressing wild-type CCR5 were collected from plates with Ca^{2+} and Mg^{2+}-free PBS supplemented with 5 mM EDTA, gently pelleted for 2 min at 1000*g*, and resuspended in binding buffer (50 mM Hepes (pH 7.4), 1 mM $CaCl_2$, 5 mM $MgCl_2$, and 0.5% BSA). Competition binding assays were performed in Minisorb tubes (Nunc),

using 0.08 nM radio-labeled [^{125}I]- MIP-1β (Amersham-Pharmacia Biotech, 2000 Ci/mmol) as a tracer, variable concentrations of MIP-1β or its mutants, and 40 000 cells in a final volume of 0.1 mL. The level of total binding was measured in the absence of competitor, and the level of nonspecific binding was measured with a 100-fold excess of unlabeled ligand. Samples were incubated for 90 min at 25 °C, and then the bound tracer was separated by filtration through GF/B filters presoaked in 0.5% PEEA. Filters were counted for 1 min in the Beckman Coulter Gamma LS 5000TA counter.

Binding assays utilizing HeLa cells were carried out in the TZM-bl cell line by fixing the cells onto the 24-well culture plate following the protocol mentioned previously (151). Briefly, TZM-bl cells were cultured in 75 cm^2 flask in DMEM medium with 10% FBS, 100 units of penicillin and 0.1mg/ml of streptomycin until 30% confluency. Then the cells are detached and seeded onto 24-well culture plate, at 10^5 cells per well, overnight. The next day, cells were washed twice in cold PBS and then were overlaid with 150 µl of the cold binding buffer. Cells were incubated for 2 hrs at 4 ºC with 0.05 nM ^{125}I-labeled human MIP-1β (Amersham-Pharmacia Biotech) in the presence of various concentrations of chemokine mutants. The reactions were stopped by washing wells four times with the cold binding buffer plus 0.5 M NaCl. Cells were lysed by the addition of 0.5 mL of 1% SDS. Lysates were transferred to a counting vial, and bound radioactivity was counted for 1 min in the Beckman Coulter Gamma LS 5000TA counter.

All determinations were performed in duplicate and repeated at least three times. Binding parameters (IC_{50}) were determined with KaleidaGraph version 3.6 (Synergy Software) using nonlinear regression applied to a one-site competition model.

Representative data is shown in Figure 3-5A and Figure 3-5B. The results are reported as fitted IC_{50} mean value ± S.D. nM.)

Functional assays

The functional response of CCR5-expressing cells to chemokines was analyzed by measuring the luminescence of aequorin as described previously (152). CHO-K1 cells (described above) were collected from plates with Ca^{2+} and Mg^{2+}-free DMEM (Invitrogen) supplemented with 5 mM EDTA, pelleted for 2 min at 1000*g*, resuspended in DMEM at a density of 5×10^6 cells/mL, and incubated for 2 h in the dark in the presence of 5 μM coelenterazine H (Promega). Cells were diluted 5-fold before being used. Agonists in 50 μL of DMEM were added to 50 μL of a cell suspension (50,000 cells), and luminescence was measured for 30 seconds in an Orion II microplate luminometer (Berthold Techniques, Germany). Determinations were performed in triplicate, and repeated at least three times. The receptor activation EC_{50} were determined with KaleidaGraph using nonlinear regression applied to a one-site ligand binding model. Representative data is shown in Figure 3-5A. The results are reported as fitted EC_{50} mean value ±S.D. nM.

Heparin sepharose chromatography of GAG binding studies

GAG binding capacity of chemokine mutants were studied by using the heparin Sepharose chromatography as mentioned in previous publications (153,154). Briefly, equal amounts of MIP-1β-A10C, MIP(9), MIP-1β-F13L and MIP-1β-L34W (approximately 10μg of lyophilized protein) was taken up in 0.5 mL of 50mM Tris (pH7.4) and injected onto a 1 mL Hi-Trap heparin column (Pharmacia) using the AKTA

FPLC system (GE Healthcare). The column was equilibrated with 5mL of the same buffer followed by a gradient of 0 to 1.0 M NaCl in 50 mM Tris (pH7.4) at a rate of 0.5 mL/min for 60 min. The elution profile was monitored by UV absorbance at 280nm. The salt concentration corresponding to the center of each eluted peak is a relative determinant of the GAG binding ability of that mutant.

Results

MIP-1β-A10C is a covalent non-dissociating dimer

In order to obtain an obligate MIP-1β dimer, a single substitution from Ala to Cys at the 10th position, which is in the center of dimer interface, was made (Figure 3-1A). To determine the oligomerization state of MIP-1β-A10C, SDS-PAGE experiments were carried out. In the presence of reducing reagent β-mercaptoethanol, MIP-1β-A10C migrates nearly identically to wild type MIP-1β on the gel. In the absence of β-mercaptoethanol, MIP-1β-A10C migrates more slowly than the wild type MIP-1β (Figure 3-1B) at a position indicative of a covalent dimer. To further confirm this, we carried out analytical ultracentrifugation equilibrium experiments on the purified protein. The ultracentrifugation data did not fit to either a dissociating dimer model or to a monomer model, but rather the best fit of the data was to a single species of 15.5 kDa (twice the size of the calculated the monomer molecular weight), indicating MIP-1β-A10C is indeed a non-dissociating covalent dimer (Figure 3-1C).

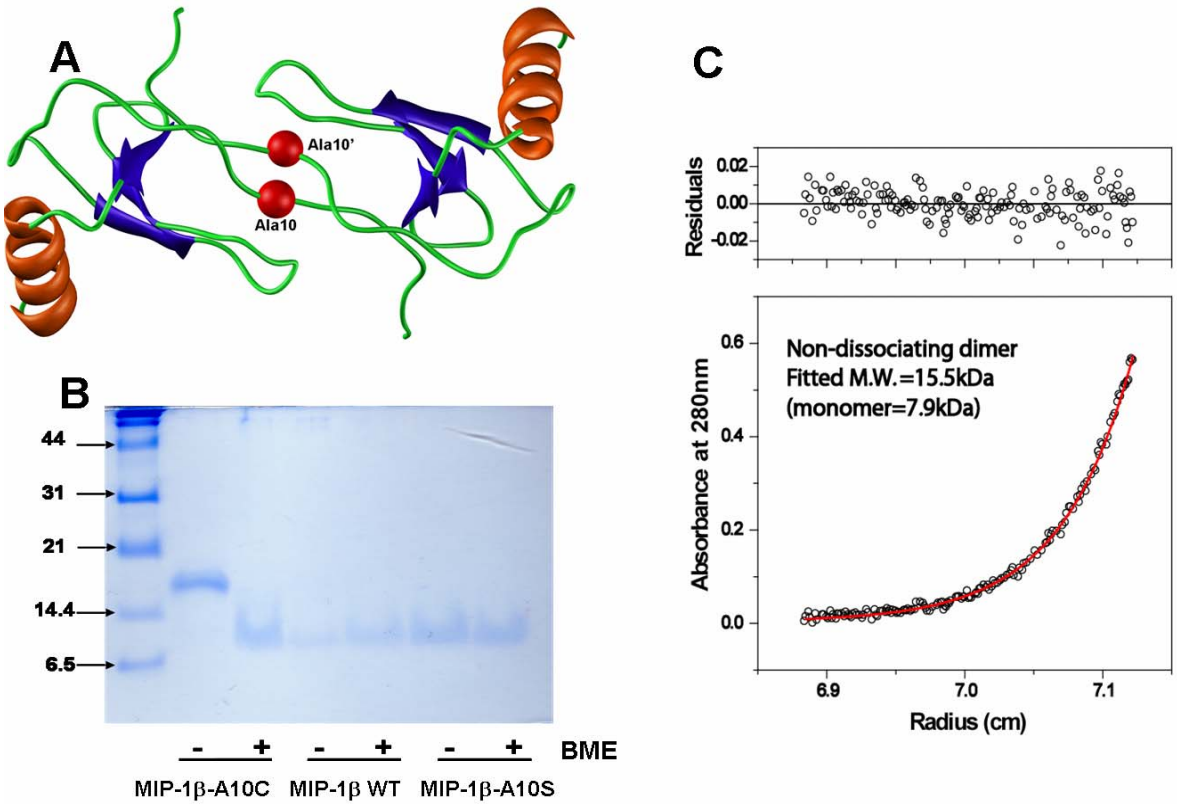

Figure 3-1: MIP-1β-A10C is a covalent dimer. A). The ribbon diagram of the homodimer structure of MIP-1β (PDB code: 1hum). Ala10 (red sphere) is in the center of the dimer interface. B). Results of non-reducing and reducing 17% SDS-PAGE. Lanes from left to right: molecular weight marker (units in kDa), MIP-1β-A10C without BME (β-mercaptoethanol); MIP-1β-A10C with BME; MIP-1β WT without BME; MIP-1β WT with BME; MIP-1β -A10S without BME; MIP-1β-A10S with BME. Only the sample MIP-1β-A10C without BME shows a molecular weight (~16 kDa) approximately twice that of the other samples (~8 kDa) indicating MIP-1β-A10C is a covalent dimer. C). Analytical ultracentrifugation equilibrium experiments show that MIP-1β-A10C behaves as a single species having the size of a MIP-1β dimer.

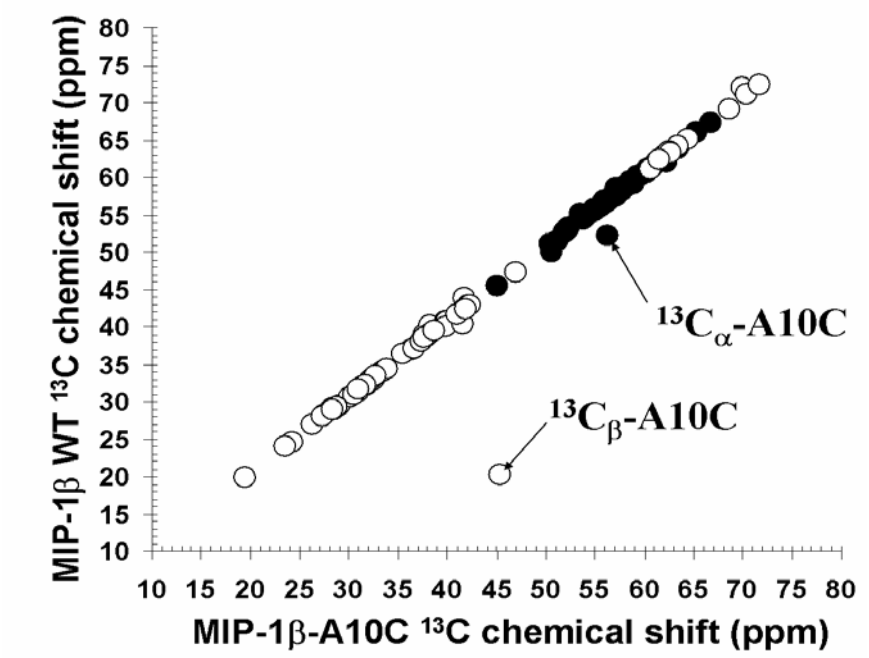

Figure 3-2: MIP-1β-A10C has a nearly identical structure to wild type MIP-1β. ^{13}C C_α (filled circles) and C_β (open circles) chemical shift plot of wild type MIP-1β versus MIP-1β-A10C. The chemical shift values of $^{13}C_\alpha$ and ^{13} C_β for most residues between the two proteins are essentially identical except at the site of mutation (Ala10 on MIP-1β, Cys10 on MIP-1β-A10C).

MIP-1β-A10C is similar in structure to the wild type MIP-1β dimer

The A10C mutation results in three contiguous cysteines (Cys10, Cys11, Cys12), each of which must form a correct disulfide bond to result in correctly folded protein. While Cys 10 is involved in an intermolecular crosslink, Cys11 and Cys12 form internal disulfide links (to Cys35 and Cys51 respectively) as a critical component of the wild type tertiary structure. A detailed NMR investigation was carried out to determine whether the structure of the covalent dimer MIP-1β-A10C is identical to that of the wild type MIP-1β dimer. Complete backbone (^{15}N, $^{1}H_N$, $^{13}C_\alpha$, $^{13}C_\beta$) chemical shifts were determined for MIP-1β-A10C, and compared to the wild type values. $^{13}C_\alpha$ and $^{13}C_\beta$ chemical shifts are sensitive to secondary structure and overall fold of the protein, and Figure 3-2 shows that these values are essentially identical between the two proteins except at the site of mutation. This indicates that the A10C variant has a typical chemokine fold that is likely very similar to wild type MIP-1β. Further, these data in addition to intramolecular NOE distance contacts (data not shown) indicate that the native disulfide bonds (Cys11-Cys35, Cys12-Cys51) have not been perturbed.

To determine if the interaction of the two monomeric subunits in MIP-1β-A10C is the same as in the wild type dimer, we carried out 3D ^{15}N and ^{13}C-edited NOESY and 4D $^{13}C/^{13}C$-edited NOESY experiments on MIP-1β-A10C. These data (Figure 3-3) show that the MIP-1β-A10C dimer makes almost all of the same inter-subunit contacts as the wild type dimer, including contacts between G4, S5, D6, and P7 to V50'; D6 to

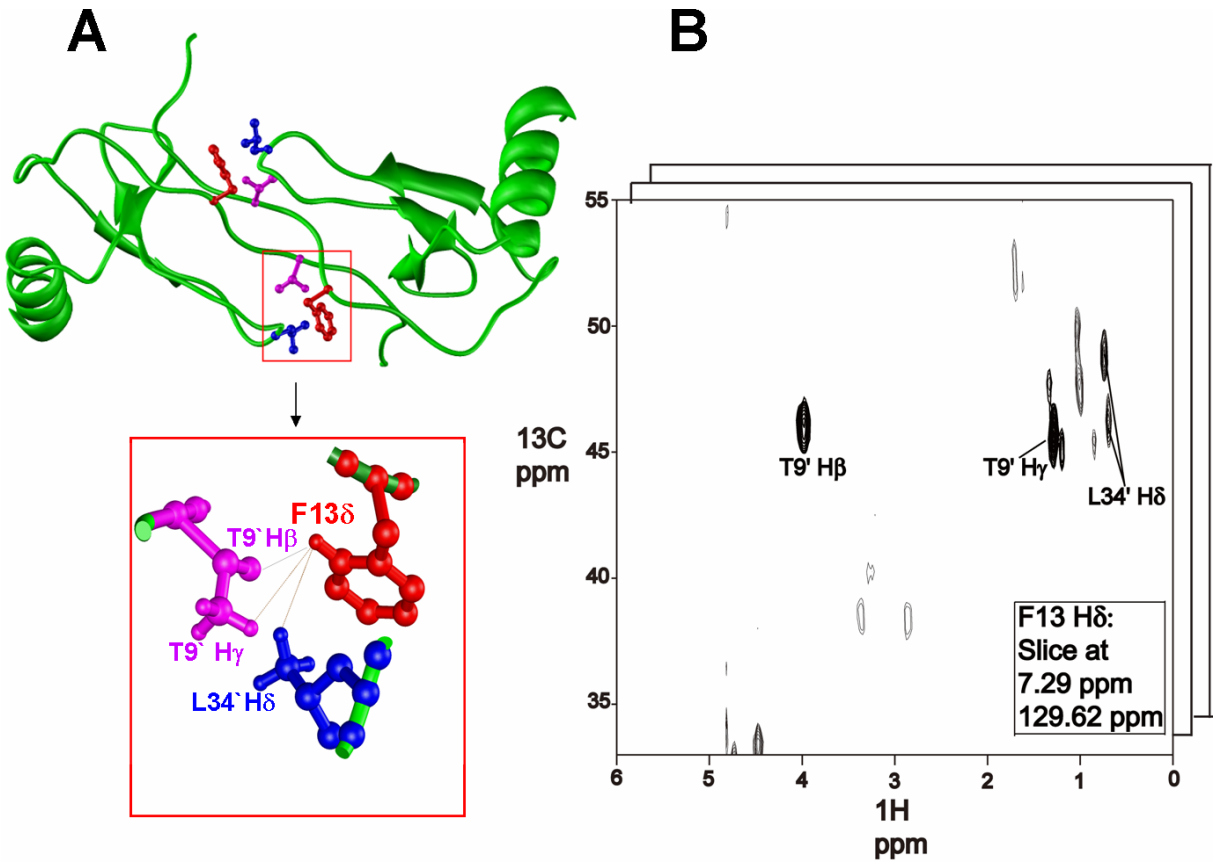

Figure 3-3: MIP-1β-A10C has identical dimer contacts as MIP-1β WT. A). Ribbon diagram of the wild type MIP-1β dimer structure shows the dimer interface and an enlarged picture close to the critical residue Phe13 (14). B). Selected slice from the 4D ^{13}C-edited NOESY of MIP-1β-A10C showing that this variant has wild type dimer intermolecular contacts. The intermolecular NOE peaks of MIP-1β-A10C indicate that Hδ of residue Phe13 makes contact across the dimer with Hβ and Hγ of Thr9' and Hδ of Leu34' in the structure of MIP-1β-A10C.

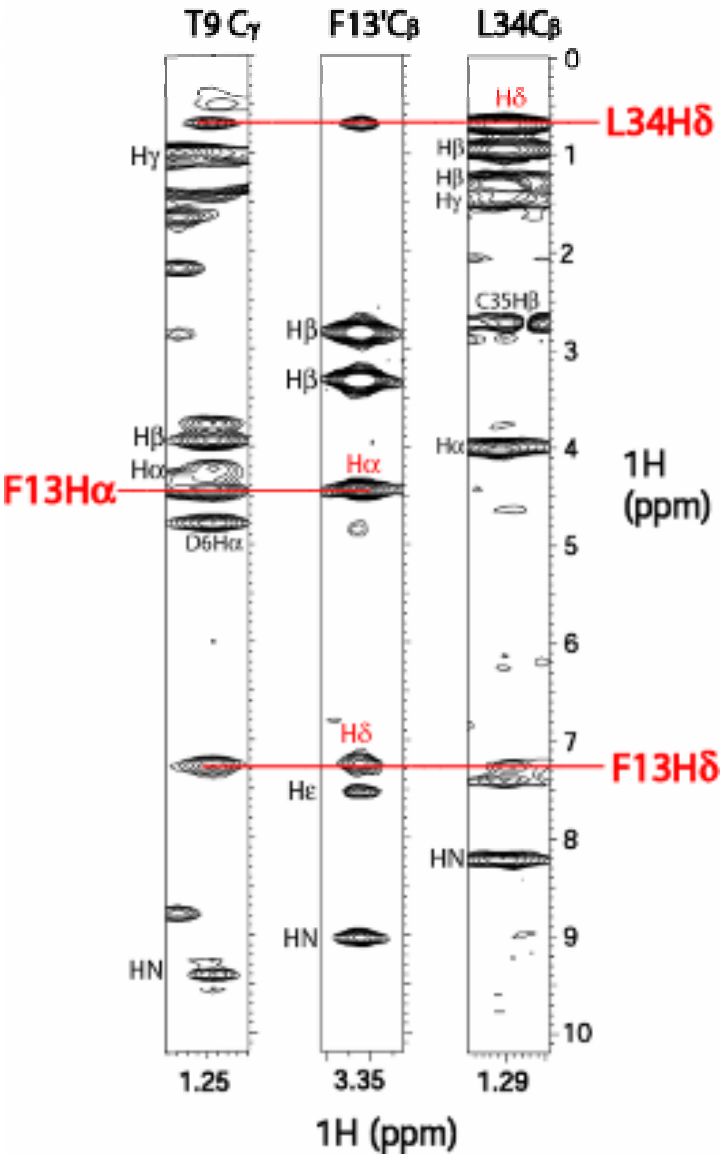

Figure 3-4: Selected dimer contacts that were observed in MIP-1β-A10C by 3D NOESY spectra.

C51'; P8, T9 to C12'; P8 to V41'; and numerous contacts (Figure 3-4) between Phe13 and T9' and Leu34', which can only be made across the dimer and not intra-molecularly (Table 3-1). Not every contact reported for the wild type dimer was able to be distinguished for MIP-1β-A10C, although in many cases NOE peaks may be present but were too overlapped or low intensity to be assigned unambiguously. For example, the description of the wild type MIP-1β dimer mentions contact between S47' and both G2 and S5 (14), but due to extensive overlap we could not unambiguously assign an NOE peak for these contacts. In addition, a few contacts are present in MIP-1β-A10C that indicate closer intersubunit contacts for certain atoms than were seen in the wild type dimer structure, including NOE contact between S5 and T16' Hγ, and between F13 Hα (as opposed to the side chain) and L34'. This could indicate an altered structure compared to the wild type protein or could be explained by spin diffusion during the NMR experiment. However, overall the structural results suggest that MIP-1β-A10C is nearly identical in structure to the wild type dimer, and so our functional results do indeed reflect the function of the chemokine dimer, and are not an artifact of altered conformation.

The MIP-1β-A10C dimer is not active on the receptor CCR5

Two measures of chemokine receptor function are typically carried out: activity assays and binding assays. The activity assays generally measure the release of intracellular calcium stores after productive engagement of the chemokine receptor by its ligand. Binding assays measure the level of chemokine binding to the receptor, regardless of whether an intracellular signal is able to be transmitted. To measure the

Table 3-1: Intermolecular NOE contacts observed for MIP-1β-A10C.

MIP-1β WT dimer contact		MIP-1βA10C intermolecular NOESY peaks
G4	K48	G4Ha-K48'Hd
	V50	G4Ha-V50'Hg
S5	T16'	S5Hb-T16'Hg2
	V50'	S5Ha-V50'Hg (both methyls) S5Hb-V50'Hg (both)
D6	T16'	D6Hb-T16'Ha, Hb, Hg2
	V50'	D6Ha-V50'Hg D6Hb-V50'Hg (both)
	C51'	D6Hb-C51'Hb
P7	V41'	P7Ha-V41'Hg
	Q49'	P7Ha-Q49'Hb P7Ha-Q49'Ha
	V50'	P7Ha-V50'Ha P7Ha-V50'Hg (both)
P8	C12'	P8Ha-C12'Ha P8Hb-C12'Ha,Hb
	T31'	P8Hb-T31'Ha P8Hb-T31'Hg2 P8Hd-T31'Ha
	V41'	P8Ha-V41'Hg (both) P8Hb-V41'Hg(both) P8Hd-V41'Hg(both)
T9	F13'	T9Ha-F13'Hd T9Hb-F13'Hd T9Hg2-F13'Ha T9Hg2-F13'Hd
F13	T9'	F13Hd-T9'Ha,Hb,Hg2
	L34'	F13Ha-L34'Hd (both) F13Hb-L34'Hd (both) F13Hd-L34'Hd (both)

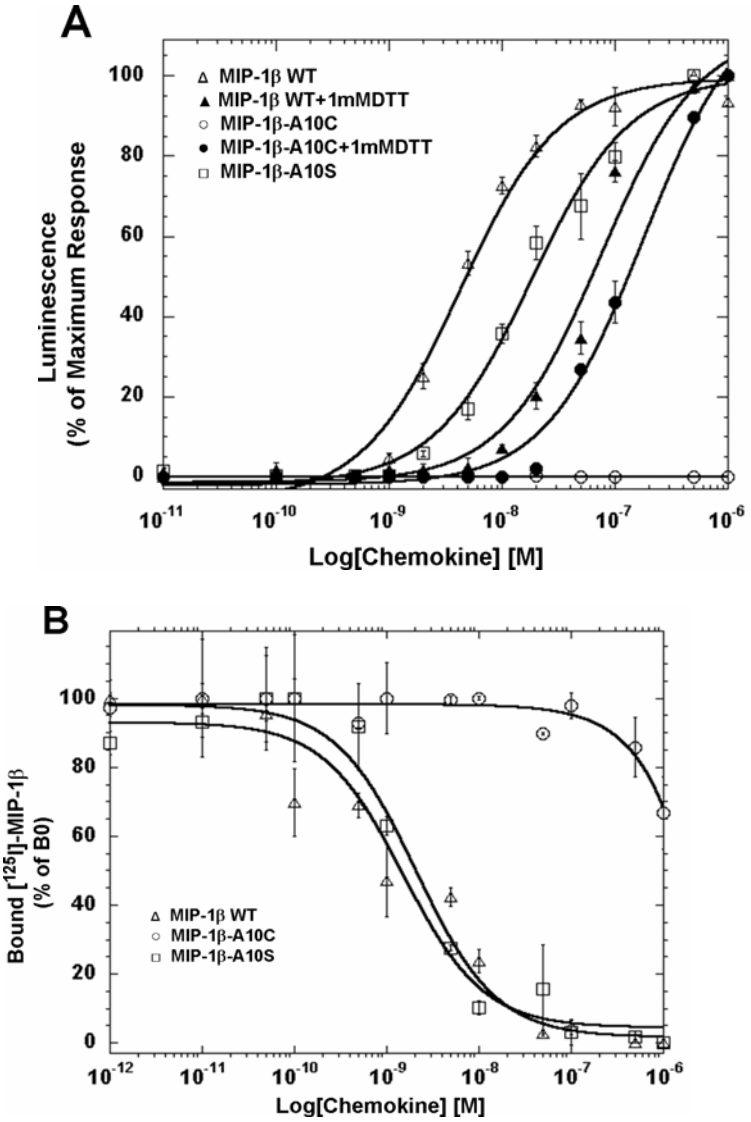

Figure 3-5: MIP-1β-A10C does not bind CCR5. A). CCR5 activity assays using CHO-K1 cells that stably express CCR5 on their surface. MIP-1β-A10C elicits no activity (open circles) until it is incubated overnight with 1mM DTT (filled circles) at which point EC_{50}=179±28 nM. Wild type MIP-1β in the presence (filled triangles) of 1mM DTT is moderately less active (76±16 nM) than wild type MIP-1β in the absence of DTT (open triangles; 11±2.6 nM). The variant MIP-1β-A10S (open squares) is nearly active as wild type MIP-1β (18±2.9 nM). B). CCR5 binding assay, using the same CHO-K1 cells with ^{125}I labeled MIP-1β as a tracer. MIP-1β-A10C does not show any significant binding to CCR5 even at micromolar concentrations (open circles). Wild type MIP-1β (open triangles) yields an IC_{50} = 1.5±0.6 nM and MIP-1β-A10S (open squares) yields an IC_{50} = 2.1±0.6 nM.

ability of MIP-1β-A10C to activate the CCR5 receptor, activity assays were carried out on CHO-K1 cells bearing human CCR5. As shown in Figure 3-5A, MIP-1β-A10C is unable to elicit a response even at micromolar concentrations. Similarly, binding assays reveal that MIP-1β-A10C is unable to bind CCR5 (Figure 3-5B). To demonstrate that mutation to the 10^{th} position is functionally tolerated and that the lack of activity in the A10C variant is due to the obligate dimer, the Ala10Ser mutation was made in MIP-1β. This variant was shown to be nearly fully active, as expected (Figure 3-5A, 3-5B). Since NMR analysis indicates that the obligate MIP-1β-A10C dimer has the same structure as wild type MIP-1β, our data suggest that the lack of ability to bind CCR5 is indeed because of the quaternary state of the molecule (i.e. the dimer) rather than due to any disruption caused by an amino acid change at the 10^{th} position.

Partial rescue of receptor activity by selective reduction of the intermolecular disulfide bond

To demonstrate that the dimer form of the chemokine is responsible for the loss of activity, MIP-1β-A10C was incubated in mild reducing conditions (1 mM DTT) to reduce the intermolecular disulfide bond, breaking the covalent bond between the monomeric subunits. Figure 3-5 shows that some activity on CCR5 is observed for the reduced mutant.

To demonstrate that mild treatment with DTT does indeed break the disulfide bond of the covalent dimer, analytical ultracentrifugation was carried out on MIP-1β-A10C in the presence of DTT. Under these conditions the best fit to the data was to a dissociating dimer with a Kd of 2.7μM, indicating that the covalent link had successfully been

reduced (data not showing). To eliminate the possibility that this treatment may also reduce the internal disulfide bonds of the protein, NMR experiments were carried out on the MIP-1β-A10C variant after treatment with DTT to determine whether these conditions disrupted the structure of the mutant. Carbon chemical shifts are not only powerful indicators of protein conformation, but have been shown to be diagnostic of the participation of cysteine in a disulfide bond (155). The chemical shift assignments for the backbone atoms of MIP-1β-A10C and reduced MIP-1β-A10C were obtained using a series of three-dimensional experiments (139,141) with ^{13}C, ^{15}N labeled protein. The chemical shift values of $^{13}C_{\beta}$ for Cys10, Cys11, Cys12, Cys35 and Cys51 for MIP-1β-A10C under oxidizing conditions were consistent with a fully disulfide crosslinked species, while under mild reducing conditions (1 mM DTT), the chemical shifts of MIP-1β-A10C were consistent with a reduced Cys 10, and oxidized Cys11, Cys12, Cys35 and Cys51 (Figure 3-6). This strongly indicates that under the mild reducing conditions used, the intermolecular crosslink is reduced, while the overall structure of the protein is intact and still contains the wild type disulfide bonds. Overall then, the results show that the rescue of activity upon reduction is due to the breaking of the dimer into monomeric units that are structurally intact. Therefore, the intermolecular disulfide bond of MIP-1β-A10C, and not any structural rearrangement, is the cause of the lack of receptor activity for the covalent dimer form of the mutant.

Since only a moderate level of rescue was observed for the MIP-1β-A10C variant in the presence of DTT, it is possible that variation in the 10th position does affect CCR5

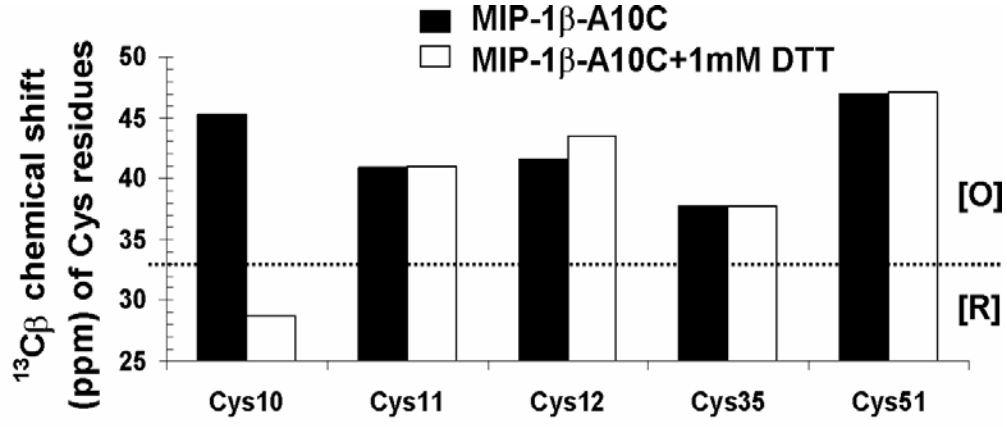

Figure 3-6: Only Cys10 is reduced in 1 mM DTT. The $^{13}C_\beta$ chemical shift values of Cys residues were obtained from standard assignment spectra on samples both in the presence and absence of 1 mM DTT. As reported by Sharma et al (155), if the chemical shift value $^{13}C_\beta$ of Cys residue is above about 33 ppm (cutoff line shown), the Cys is oxidized; if the chemical shift value is below the cutoff line, the Cys is reduced. NMR data collected from MIP-1β-A10C (black bar) and MIP-1β-A10C+1mM DTT (white bar) indicated that the mutated residue Cys10 is oxidized (along with the other four Cys residues). With 1 mM DTT, only the mutated residue Cys10 is reduced.

activity of MIP-1β, or it is possible that DTT negatively affects the outcome of the activity assay. Therefore, activity assays with wild type MIP-1β in the presence of DTT were also carried out, and showed a reduced activity for the wild type protein (Figure 3-5A, 3-5B). Since the above NMR data suggest that the structure of the chemokine remains intact in the presence of the reducing reagent, these experiments suggest that the presence of DTT is harmful to the CHO cells, even in the brief period of an activity assay. Results were more dramatic for binding assays in the presence of DTT, where the several hours required for the experiment resulted in visibly unhealthy cells and poor results. Therefore, binding results were not able to be obtained for the MIP-1β-A10C variant in the presence of DTT on CHO cells. Binding experiments on CCR5-expressing TZM-bl HeLa cells consistently suggested that reduced MIP-1β -A10C could compete for CCR5 binding, but again the date were very poor, possibly due to the presence of DTT, even though the cells appeared healthy (data not shown).

The covalent MIP-1β-A10C dimer retains glycosaminoglycan binding ability

Heparin Sepharose chromatography is a well-established technique used to assess the ability of a protein to bind to physiological glycosaminoglycans (GAGs) (153,154). Several chemokine mutants of varying quaternary state, including the monomeric variant MIP(9)(50), the weak dimers F13L(39) and L34W(29), and the covalent dimer MIP-1β-A10C, were tested for their ability to bind to a heparin sulfate column under identical conditions. Elution was carried out with a sodium chloride gradient. While monomeric variant MIP(9) and weakly dimerizing variants F13L, L34W elute earlier

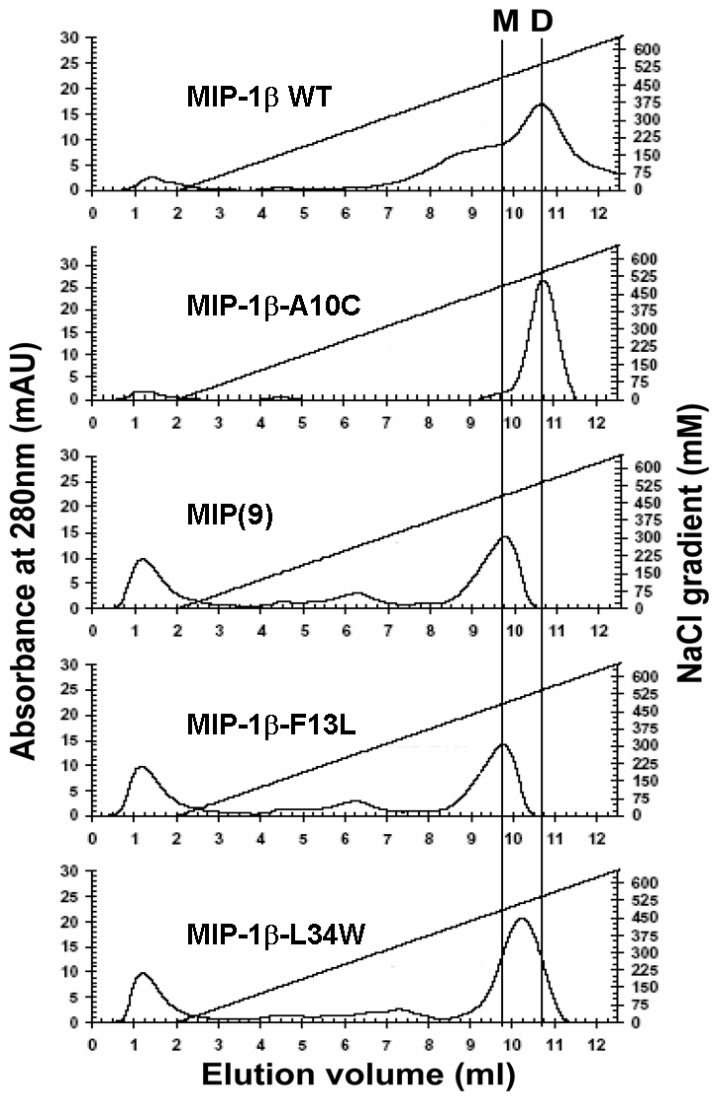

Figure 3-7: Heparin sepharose chromatography of several dimerization variants of MIP-1β. Equal amounts of MIP-1β-A10C, MIP(9), MIP-1β-F13L and MIP-1β-L34W were loaded onto a heparin sepharose column and eluted using NaCl gradients. The vertical line denoted with "D" indicates the elution position of the MIP-1β wild type dimer. The vertical line denoted with "M" indicates the elution position of wholly monomeric variant MIP(9).

than the wild type protein, the covalent dimer MIP-1β-A10C required at least as much salt as the wild type protein to elute from the column (Figure 3-7) indicating that the dimer form of the protein is competent to bind GAGs even though it has no receptor binding capacity.

Discussion

Structural studies show that many chemokines form dimers, and biophysical investigations have revealed that the dimer dissociation constant of chemokines is generally in the low micromolar range (25). While this dimer affinity suggests a predominant monomeric form of the protein at the nanomolar concentrations presumed to be present biologically, numerous studies have shown that the dimer K_d is very sensitive to solution conditions, so it is possible that dimers are present in significant concentrations *in vivo* (128,156). In support of the chemokine dimer as a biologically functional entity, it has been shown that chemokines mutated to remove the ability to dimerize do not function *in vivo*, despite these variants having the ability to bind and activate their cognate receptor *in vitro* (9). Overall, although a great deal has been reported about the receptor function of chemokine variants (39,47,128), little evidence has been accumulated regarding the specific role of the dimer in receptor binding or activation, because it is difficult to determine which protein species is actually making contact with the receptor: A "monomeric" variant may actually dimerize on the receptor, or, alternately, even a high affinity chemokine dimer may dissociate before binding the receptor.

The only way to definitively test the affinity of a dimer for the chemokine receptor is to covalently join two monomeric subunits in a way that maintains the structure of the wild type dimer. This has been reported for the CXC chemokine IL-8, where several strategies have been utilized to make a covalent dimer (40-42,157). In general, it was found that a covalent IL-8 dimer was able to bind both receptors CXCR1 and CXCR2, but with lower affinity than the wild type protein. Further work with peptides derived from the receptor CXCR1 indicate that the IL-8 monomer is the high affinity ligand for the receptor (41,158). However, the CXC chemokine dimer has a completely different structure than the CC chemokine dimer and has many receptor binding residues still on the surface of the protein. In contrast, the CC chemokine dimer buries residues that have been shown to be critical for receptor binding (39,47,159). This suggests that a receptor-bound CC dimer would make different contacts than a receptor bound CC chemokine monomer. Therefore, we have designed a trapped dimer of MIP-1β by replacing Ala10 at the center of the dimer interface with Cys, forming a disulfide bond between two monomeric subunits (Figure 3-1A). This protein is demonstrably a non-dissociating dimer, and shows almost all of the intermolecular interactions typical of the MIP-1β dimer. Assays of both CCR5 binding and CCR5 activity reveal that this covalent dimer is not competent to bind its receptor (Figure 3-5A and 3-5B). Therefore, we conclude that the MIP-1β dimer is not competent to bind or activate its receptor, and that this conclusion is very likely to be general for the CC chemokine subfamily.

What then is the biological role of the CC chemokine dimer? Evidence has accumulated that the ability of chemokines to bind cell surface glycosaminoglycans

(GAGs) is linked to the chemokine quaternary state. Some years ago it was shown that GAG binding causes aggregation of both CC and CXC chemokines (160). In more recent studies, it was demonstrated that the monomeric form of MIP-1β has a lower affinity for a variety of GAG disaccharides than the wild type (dimer) form (115). Further, the binding of GAGs by MIP-1β was shown to increase the chemokine dimer affinity (29). Similarly, the CXC chemokine SDF-1 was shown to dimerize with higher affinity under in the presence of several solutes, including GAGs (156). Although GAG-induced oligomerization may be a mechanism to reduce chemokine activity, the GAG binding surface and receptor binding surface of MIP-1β do overlap so lesser activity of chemokines in the presence of GAGs may also be a function of competition between GAG and receptor for chemokine binding (47).

These data support a model of chemokine action in which the chemokine is immobilized on the endothelial surface in the dimeric (or higher order oligomeric) form by binding to cell surface GAGs. The ability to dimerize is likely critical for GAG affinity, for chemokine gradient formation, or for the ability of the chemokine to be presented appropriately to the receptor on the surface of a chemotaxing leukocyte that is passing nearby. Dissociation of the chemokine oligomer into monomeric subunits likely occurs as part of the process of transferring the chemokine from the GAG to the receptor. This dissociation from the dimer (or oligomer) form to the monomer form is evidently necessary in order to bind and activate the cognate receptor, at least in the case of CC chemokines, as shown by the present work on the CC chemokine MIP-1β.

CHAPTER IV

BIOPHYSICAL STUDIES OF POTENT ANTI-HIV CHEMOKINE MUTANT PROTEIN P2-RANTES

Introduction

Chemokines bind to seven transmembrane-spanning G-protein-coupled receptors (GPCRs) and mediate leukocyte migration involved in a wide range of physiological phenomena including immunodefense, inflammatory, nerve cell derivation, would healing, cardiac angiogenesis, cancer development and are involved in blocking HIV infection (1,3,25,161,162). The CC chemokine, CCL5/RANTES (Regulated upon Activation Normal T cell Expressed and Secreted) can bind and activate receptors CCR1, CCR3, CCR4 and CCR5 (1,3,25). RANTES can mediate chemotaxis and activation of macrophages (or monocytes), eosinophils, basophils and T cells (162,163). Increased RANTES expression is related to a wide range of inflammatory disorders and pathologies (3,162,164). RANTES also inhibits HIV-1 entry and infection by competing with the virus for CCR5 binding (1,76,80,165).

It has been shown that the N-termini of RANTES are critical for receptor binding and activation. Alanine scanning mutagenesis revealed that the N-loop region is the determinant for binding the receptor and the N-terminal region is for receptor activation (46). For example, it has been found that Arg17 is necessary for RANTES binding to CCR1, Phe12 for binding to CCR3, and Pro2, Phe12 and Ile15 for binding to CCR5. Pro2, Asp6, Thr7 near the N-terminus are involved in activating CCR1; Pro2 and Try3

for CCR3; and Try3 and Asp6 for CCR5 (46). Several N-terminal truncated derivatives, extended mutants and N-termini modification mutants of RANTES have been produced by selection or recombinant methods and exhibit antagonist or partial agonist functions. For example, N-terminal peptide fragments RANTES(1-14) (166), RANTES (3-68)(167), RANTES (4-68)(168), RANTES (8-68) (169), RANTES (9-68) (81,169) and RANTES (10-68) (169) truncated mutants were reported to be antagonists in CCR5 binding and block HIV fusion. Met-RANTES and Leu-RANTES are mutants that are extended at the N-terminus by nature amino acids. They are found to be partial agonists (90,97,170-173). Subsequently, a range of N-terminal artificial chemical modification derivatives of RANTES were widely reported, for example, AOP-RANTES (174), NNY-RANTES(175), PSC-RANTES (93,168,176,177).

Recently, towards improving the function of blocking the HIV entry property of RANTES, a phage display techniques was applied to select RANTES mutants against living cell expressing CCR5 (100). From this work, came potent anti-HIV mutant, named P2, which has a modified N-terminal sequence: FSPLSSQSS-RANTES (9-68) (100) (Figure 1-7). The chemically synthesized polypeptide of P2-RANTES has been shown by Hartley et al. to only selectively activate CCR5, not CCR1 or CCR3 in calcium release signal transduction experiments. It shows improved binding affinity to CCR5 in competition radioactive assays. In env-mediated cell-cell fusion assays and PBMC HIV-1 infection assays, P2-RANTES resembles AOP-RANTES function because of its tight binding affinity and strong CCR5 down modulation function (100). In order to investigate the structural basis of this unique mutant, we produced this mutant

using the *E. coli* overexpression and refolding techniques and solved the structure by X-ray crystallography. Our AUC studies show P2-RANTES is a monomer in solution, but the crystal structure of P2-RANTES shows it is a unique tetramer. The N-terminal extended residue, Phe0, plays an important role in the oligomerzation and packing. The first 9 residues on the N-terminus of P2-RANTES in the subunit A and B are clearly defined due to the oligomerization restraints. In particular the first 3 residues are well defined while these residues on the x-ray structure of wild type RANTES are not defined (15,16,178). These structural studies reveal the structural basis of activity of the unique variant. These findings may lead to further design of potent anti-HIV entry inhibitors. This structural work may also be therapeutically useful to further design antagonists for CCR1 and CCR3 in the future.

Experimental Procedures

Chemicals and reagents

All cell culture media, supplements, and sera were purchased from Invitrogen (Carlsbad, CA). Fusion inhibitor (N-acetylated derivative), T-20 (catalog No: 9845) was obtained from the NIH AIDS Research and Reference Reagent Program through Roche. Mouse monoclonal antibody to human CCR5 was obtained through the NIH AIDS Research and Reference Reagent Program, Division of AIDS, NIAD, NIH: mouse anti human CCR5 monoclonal antibody from R&D system (catalog number: FABSP1, clone: 45502). FITC (fluorescein isothiocyanate) labeled F(ab')2 fragment of polyclonal goat anti-mouse IgG second antibody was purchased from Sigma (catalog number: F 2653).

Cell culture and cell lines

HeLa cell line stably expressing HIV-1 ADA (R5) env (referred to as HeLa-ADA) was a kind gift from Dr. M. Alizon (Cochin Institute, Paris, France) (179). Cells were cultured in DMEM supplemented with 10 % FBS, and 100 units of penicillin and 0.1 mg/ml of streptomycin and the ADA (R5) env was selectively expressed by adding 2 μM methotrexate (Sigma) as previously published (180). A HeLa cell line stably expressing human receptor CD4 and CCR5 (referred to as HeLa-P5L) was a kind gift from Dr. M. Alizon (Cochin Institute, Paris, France) (179). Cells were cultured in RPMI-1640 (Invitrogen) supplemented with 10 % FBS, and 100 units of penicillin and 0.1 mg/ml streptomycin. The expression of CCR5 was selected by adding zeocin (Invitrogen) 0.5 mg/ml. A HeLa-TZM cell line was obtained through the NIH AIDS Research and Reference Reagent Program, Division of AIDS, NIAID, NIH: TZM-bl from Dr. John C. Kappes, Dr. Xiaoyun Wu and Tranzyme Inc.(181). The cells were cultured at DMEM supplemented with 10% FBS, 100 units of penicillin and 0.1 mg/ml of streptomycin as mentioned in the instruction. 3T3 cell are cultured in DMEM supplanted with 10% FCS with 100 units of penicillin and 0.1 mg/ml streptomycin.

Protein expression and purification

The wild type RANTES was purified as shown previously (115). For the RANTES mutant, P2-RANTES, its corresponding gene (100) with an upstream Factor Xa cut site was amplified using PCR with the wild type RANTES as a template. The PCR product of P2-RANTES was ligated into pET32-Xa (Novagen) at the Nde I-BamH I sites, and the DNA sequence of this mutant was confirmed through DNA sequencing. Protein

production was induced by addition of IPTG to 1 mM in 37ºC culture of BL21(DE3) (Novagen) bearing the constructed plasmids for 7 hours, and the cells were harvested by centrifugation at 6,000 x g in an F10S-6X500y rotor (Piramoon Technologies Inc.) for 30 minutes. The cells were resuspended in 30 mL of 500 mM NaCl, 20 mM Tris (pH 8), and 10 mM benzamidine and French pressed twice at 16,000 psi. After centrifugation for 30 minutes at 17,000 x g in an SS34 rotor (Sorvall Instruments), the pellet was resuspended in 20 mL of 5 M guanidinium chloride, 50 mM Tris (pH 8), 500 mM NaCl. The solution was stirred overnight and then centrifuged for 30 minutes at 17,000 x g to remove the remaining insoluble pellet. The soluble denatured proteins were loaded onto a 5ml Ni-chelating column (Amersham Pharmacia Biotech) equilibrated with same buffer (5 M guanidinium chloride, 50 mM Tris (pH 8), 500 mM NaCl). The denatured proteins were purified through the Ni-chelating column using a gradient from 10% to 100% of 500 mM imidazole in 5 M guanidinium chloride, 50 mM Tris (pH 8), 500 mM NaCl. The fractions containing purified denatured protein were pooled together and slowly shaked (~50 rpm) for 2 hours in room temperature after adding 10mM β-mercaptoethanol. The purified denatured proteins were dialyzed against 20mM Tris-HCl, pH8.0 buffer overnight at 4ºC. After dialysis, precipitated matter was removed by centrifugation for 30 minutes at 15,000 x g in an F14S-6X250y rotor (Piramoon Technologies Inc.) and the protein was purified on a C4 reversed phase chromatography column (Vydac, Hesperia, CA), and lyophilized by the Labconco freeze dry system (Labconco Corporation). To remove the fusion tag, the protein powder was solubilized

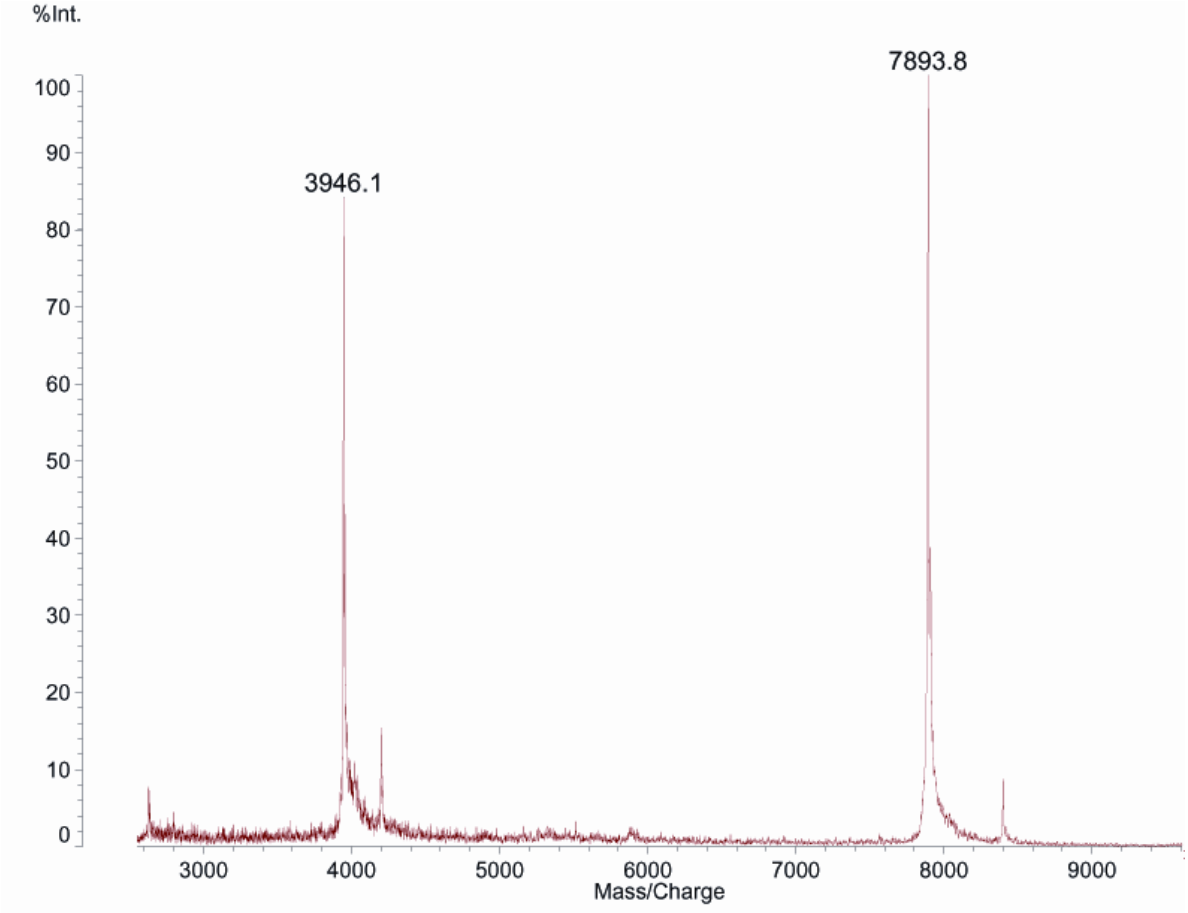

Figure 4-1: Characterization of purified P2-RANTES on MALDI-TOF Mass spectrum. There are two main peaks shown in the spectrum. The left peak is the double charged peak (molecular weight /charge= 3946.1) and right peak is the single charged peak (molecular weight /charge = 7893.8). The observed molecular weight of P2-RANTES from this experiment is 7894 ± 8 Da. The calculated molecular weight from the amino acid composition (using average isotope composition) is 7906 Da.

into ~1mL of 20 mM sodium phosphate (pH 2.5) and the volume was increased to ~ 40 mL in 20 mM Tris (pH 8), 50mM NaCl, and 2 mM $CaCl_2$. Factor Xa (Novagen) was used for the proteolytic cleavage, which typically took 2 weeks at room temperature. SDS-PAGE was used to monitor the cutting reaction. Finally, the cut proteins were purified over a C4 reversed phase chromatography column and lyophilized into powder.

MALDI-TOF mass spectroscopy

The lyophilized powder of P2-RANTES sample was dissolved in 100 μl of 0.1% TFA and mixed 1:1 with a-Cyano-4-hydroxycinnamic (6 mg/ml solution in 50% acetonitrile, 0.05% TFA). The MALDI-TOF mass spectra of the samples were acquired using a Shimadzu Kratos Axima-CFR mass spectrometer equipped with a pulsed nitrogen laser emitting at 337 nm (Shimadzu Biotech). All spectra were acquired in the positive ion mode using 20 kV acceleration voltage. The spectrum is the average of 400 laser pulses and was analyzed with Kompact Software Version 2.4.1 by Shimadzu Biotech. Calibration was performed using the doubly and singly charged ions of cytochrome C (Figure 4-1).

Structural determination and refinement

The structure of P2-RANTES was determined by molecular replacement using the structural model of AOP-RANTES (PDB id: 1B3A) as search model. The first ten residues were deleted from the search model. Four molecules of the search model were located in the unit cell using the program MOLREP in the CCP4 suit (182). The solution was improved by rigid body refinement using CNS (183). The electron density map

Table 4-1: Data collection and refinement statistics.

	P2-RANTES
Data collection	
Space group	***C2***
Cell dimensions	
***a*, *b*, *c* (Å)**	**116.68, 51.98, 61.69**
α, β, γ (°)	**90, 117.87, 90.0**
Resolution (Å)	**50–1.70 (1.76-1.70)**
R_{merge}	**4.6 (19.9)**
$I / \sigma I$	**49.9 (6.5)**
Completeness (%)	**97.4 (79.6)**
Redundancy	**3.4 (2.5)**
Refinement	
Resolution (Å)	**50–1.70**
No. reflections	**34,463**
R_{work} / R_{free}	**21.7 / 24.8**
No. atoms	
Protein	**2,123**
Water	**313**
***B*-factors**	
Protein	**36.0**
Water	**50.4**
R.m.s. deviations	
Bond lengths (Å)	**0.010**
Bond angles (°)	**1.56**

Data were collected from a single crystal for each structure. Values in parentheses are for highest-resolution shell. This work was done in collaboration with Dr. Pingwei Li.

calculated from the model after rigid body refinement showed clear and complete electron density for the first 10 residues for one of the mutant molecule and fragmented density for another molecule. No electron density was observed for the first 9 residues of the other two molecules in the asymmetric unit, which are supposed to be disordered. The molecular model was completely rebuilt for the first ten residues of molecule A and B according to 2|Fo|-|Fc| simulated annealing omit map. The model was refined by several cycles of positional refinement and remodeling. In the final stage of the refinement, individual B factors were refined and solvent molecules were added to peaks higher than 3σ in the difference map. The crystallographic R factor for the final model is 21.7% and R_{free} is 24.8%, with good geometry. Statistics of the crystallographic data and refinement is listed in Table 4-1.

Analytical ultracentrifugation

Sedimentation equilibrium and sedimentation velocity measurements were carried out with a temperature-controlled Beckman XL-I analytical ultracentrifuge equipped with an An-60 Ti rotor and a photoelectric scanner (Beckman Instruments, Palo Alto, CA). For equilibrium experiments, varying concentration (20 μM, 25 μM and 35 μM) of P2-RANTES were carried out in the buffer containing 50 mM Tris-Bis, pH 5.0, with 200 mM NaCl. Samples were loaded onto the 12 mm aluminum 6 channel centerpiece and set the speed for 35,000 rpm, 45,000 rpm and 55,000 rpm at 20°C for 16 hours for each speed in a step scan model. For velocity experiments, 40 μM of P2-RANTES was carried out in the buffer containing 50 mM Tris-Bis, pH 5.0, with 1000 mM NaCl. Protein sample was loaded in a double sector 12 mm aluminum centerpiece and at a

rotor speed of 60,000 rpm at 20°C for 24 hours in a continues scan model. For both equilibrium and velocity experiments, the reference compartments were loaded with the matching buffer without proteins and samples were monitored the absorbance at 280 nm with setup rotor speed. Analysis of the raw data was carried out using UltraScan version 8.0 (http: //ultrascan.uthsca.edu). The partial specific volume of P2-RANTES was estimated using the amino acid composition methods implemented in UltraScan. The hydrodynamic corrections for buffer conditions were calculated by UltraScan. For the equilibrium experiments, data were analyzed using the Global Nonlinear Least-Squares fitting methods implemented in UltraScan. The equilibrium data are also applied to the Origin program (Beckman), and the fitting results are very consistent with UltraScan. For velocity experiments, data were analyzed using the enhanced van Hode-Weschet method, which reports sedimentation coefficient distributions transformed into molecular weight distributions by applying the Svedberg equation and assuming a particle shape that corresponds to an expected frictional ratio, f1/f0 (184,185).

Nuclear magnetic resonance

^{15}N labeled wild type RANTES and P2-RANTES were produced in $^{15-}NH_4Cl$ isotopically labeled minimal medium following the standard procedure. The purified lyophilized powders were dissolved in 10% D_2O with 20 mM sodium phosphate, pH 3.0. The samples were placed in Shigemi tubes (Allison Park, PA) and the spectra referenced relative to DSS (123). NMR spectra were acquired at 25 °C on a Varian Unity Plus 500 MHz spectrometer equipped with an *xyz* gradient penta probe. ^{15}N-^{1}H HSQC (heteronuclear single quantum coherence) spectra were collected with 512* points in the

proton dimension and 128* points in the nitrogen dimension. A spectral width of 6000 was used in the ^{1}H dimension and 1500.68 Hz for ^{15}N. The data were processed using the program nmrPipe (124) and analyzed using the program PIPP (125).

Cell-cell fusion assay

Envelope-mediated cell-cell fusion assays were carried out as described in reference (179,180) with HeLa-P5L and HeLa-ADA cell lines with minor modifications. Briefly, HeLa-P5L 10^4 cells were seeded in 96-well culture plate in 50μl RPMI-1640 medium per well for 2-3 hours. For 3T3 competition assay, HeLa-P5L cells10^4 in 25μl were mixed with 1×10^5 3T3 cells in 25μl for each well. The sample of P2-RANTES or T-20 were added into the cell medium with serial dilutions from 4 μM to 0.4 pM (protein concentration was quantified by measuring the absorbance at 280nm using the extinction coefficient method published by Pace (186).) After preincubation in 37ºC for 30 min, 50 μl HeLa-ADA 10^4 cells per well in RPMI-1640 medium were added into 96-well culture plate. After further 24 hours of incubation at 37ºC for complete fusion, cells in the 96-well culture plate were washed once by 1× PBS, lysed by adding 0.5% NP-40 (USBiological) in PBS for 15 min at room temperature and assayed for β-galactosidase activity by the addition of 8 mM substrate CRPG in PBS with 20 mM KCl and 10mM β-mercaptoethanol (Sigma) for 2 hours in the dark at room temperature. The A570 was read on Benchmark microplate reader (BioRad). The percentage of the cell-cell fusion was expressed as 100 × (mean absorbance of treated well - mean absorbance of HeLa-P5L only well) / (mean absorbance of untreated well - absorbance of HeLa-P5L only well). Experiments were performed in triplicate, and dose dependent inhibition curves

were fitted with four-parameter logistic equation (187) using KaleidaGraph (version 3.6, Synergy Software).

FACS analysis

HeLa-TZM cells (10^5) were incubated for 30min at 37°C in culture medium containing various concentrations of (0-100 nM) of drugs in 10× 75mm culture tubes (Fisher Scientific). After washing 4 times with 10 mL cold PBS, cells were incubated in 300 µl of 500 µg/ml mouse anti-human CCR5 monoclonal antibody in PBS-0.5% BSA (Sigma), and kept on ice for 45 min. The cells were then washed 3 times with cold PBS-0.5% BSA and incubated in 300 µl of 50 µg/ml FITC labeled polyclonal goat anti-mouse antibody in PBS-0.5% BSA, and kept on ice for 30 min. 1 aliquot of untreated cells were incubated with PBS-BSA for 30 minutes followed by 3 washes and incubation with the FITC-labeled goat anti-mouse IgG as control. Then the cells were washed 3 times with cold PBS-0.5% BSA and kept in PBS-0.5% BSA, and analyzed with a FACSCalibur (BD Biosciences, San Jose, CA) flow cytometer using CellQuest (BD Biosciences) acquisition software. Cell viability was determined by staining with propidium iodide (PI) at 1µg/ml final concentration 1 minute prior to analysis. FITC fluorescence was collected through a 515/30 band pass filter, and PI fluorescence through a 650LP filter. List mode data were acquired on a minimum of 10,000 viable cells defined by a light scatter and lack of PI staining. Data were analyzed using FlowJo (Tree Star, Inc., Ashland, OR). First, a region to define cells was set using a forward and side light scatter plot, then viable (PI-negative) cells were determined by

a plot of forward light scatter and PI fluorescence. Results are presented as histograms of FITC fluorescence.

Heparin sepharose chromatography of GAG binding studies.

GAG binding capacity of chemokine mutants were studied using heparin Sepharose chromatography as mentioned in previous publications (188). Briefly, equal amounts of wild type RANTEE and P2-RANTES (approximately 10 μg of lyophilized protein) was taken up in 0.5 mL of 50 mM Tris (pH7.4) and injected onto a 1 mL Hi-Trap heparin column (Pharmacia) using the AKTA HPLC system (GE Healthcare). The column was equilibrated with 5 mL of the same buffer followed by a gradient of 0 to 1200 mM NaCl in 50 mM Tris (pH7.4) at a rate of 0.5 mL/min for 60 min. The elution profile was monitored by UV absorbance at 280nm. The salt concentration corresponding to the center of each eluted peak is a relative determinant of the GAG binding ability of that mutant. Experiments were performed in duplicate and the results were reported as average plus the standard deviation.

Results

Protein production and characterization

The RANTES mutant (P2-RANTES) was overexpressed largely as inclusion bodies in the E. coli strain Bl21 (DE3). By utilizing a refolding protocol followed by proteolysis of the fusion tag, the tag free P2-RANTES was found to be folded as judged by NMR (Figure 4-2). The 15N-1H HSQC (Heteronuclear Single Quantum Coherence)

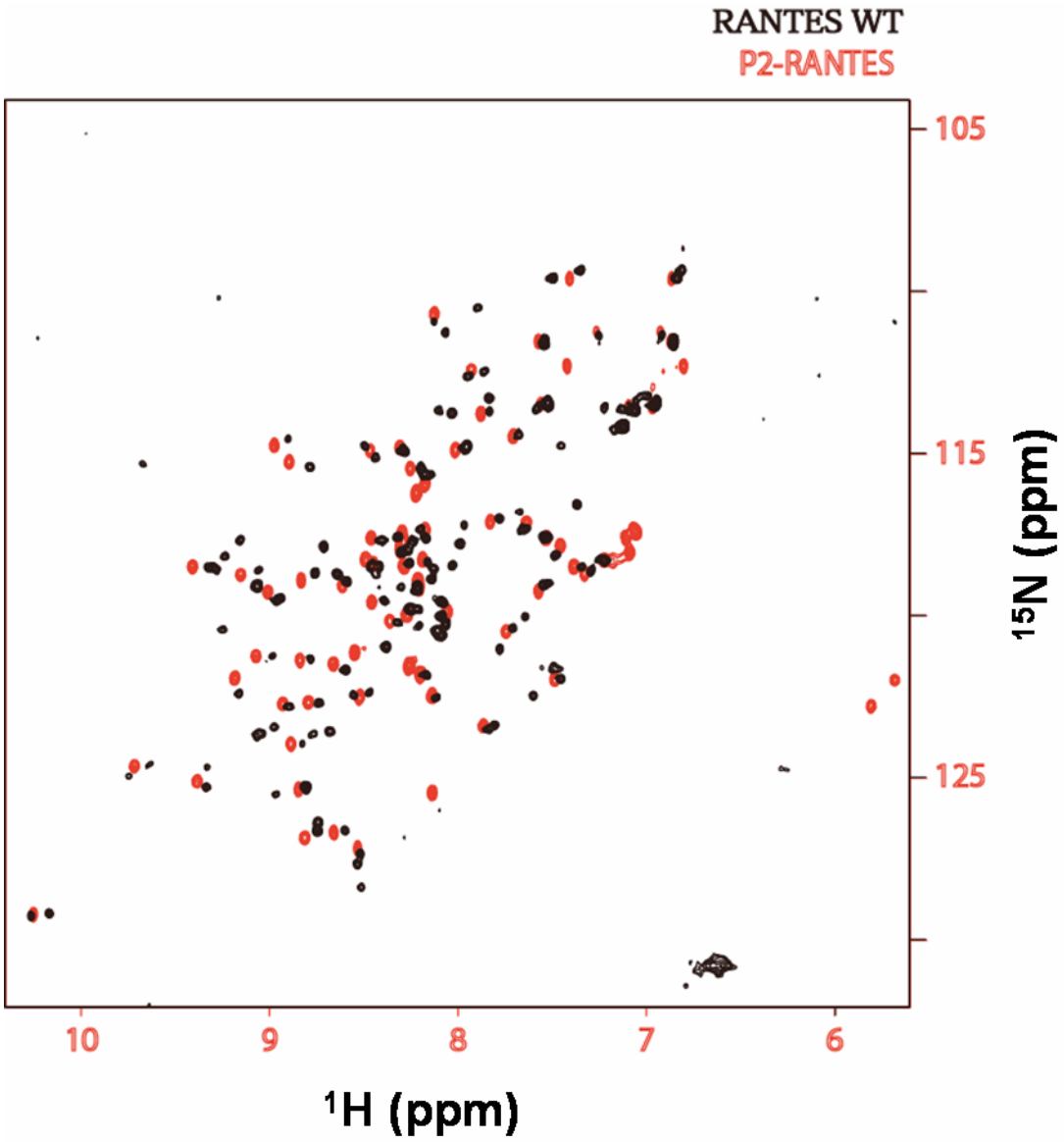

Figure 4-2: In the NMR-HSQC experiments each peak corresponds to each covalently bonded ^{15}N-^{1}H pair in the protein. The chemical shift position of a peak is dependent on the local molecular environment. If the protein is folded, all peaks will be nicely spread in the 1H dimension, because each individual peak has a unique conformation. If the protein is not folded, all peaks will be in the middle of the spectrum and not spread because all ^{15}N-^{1}H bonds are similar to each other. The peaks from P2-RANTES are nicely spread indicating that the protein P2-RANTES is nicely folded. The overlay of P2-RANTES(red) with wild type RANTES (black) reveals that these two proteins have very similar "fingerprint" and highly are similar in structure.

experiment provides a spectrum showing a single peak corresponding to each covalently bonded 15N-1H pair in the protein. The chemical shift position of a peak is dependent on the local molecular environment and as a result the HSQC spectrum for each protein is unique, providing a "fingerprint" of the protein. The overlay of spectrum of P2-RANTES (red) with wild type RANTES (black) indicates that P2-RANTES has similar "fingerprint" as RANTES protein. Moreover, P2-RANTES has about 60 peaks while the wild type RANTES has about 80 peaks. This may indicate this mutant has a different oligomerization state. Further experiments using ultracentrifugation were applied to this matter in a later section of this chapter. The Mass spectrum indicated that the protein is nearly 97% pure and the molecular weight is 7894 ±8 Dalton (Figure 4-1). This matches closely the calculated molecular weigh 0f 7906 Dalton. This indicates that P2- RANTES produced from the *E. coli* overexpression has the expected amino acids composition.

Anti-HIV fusion function

In order to test the biological function of P2-RANTES produced from the *E. coli* overexpression, we carried out an HIV R5 tropic env mediated cell-cell fusion assay. The 50% inhibition of the cell-cell fusion for P2-RANTES is 0.71± 0.09 nM (Fig 4-3). This is the same as the published results of P2-RANTES produced using complete chemical synthesis (100). Moreover, we also found that this potent anti-HIV chemokine mutant has advantages over the widely used fusion inhibitor: T-20.

There are several studies revealing that T-20 in addition to bind to gp41 can bind to an undefined target such as cell membranes or lipids (77,104,108,109). This could

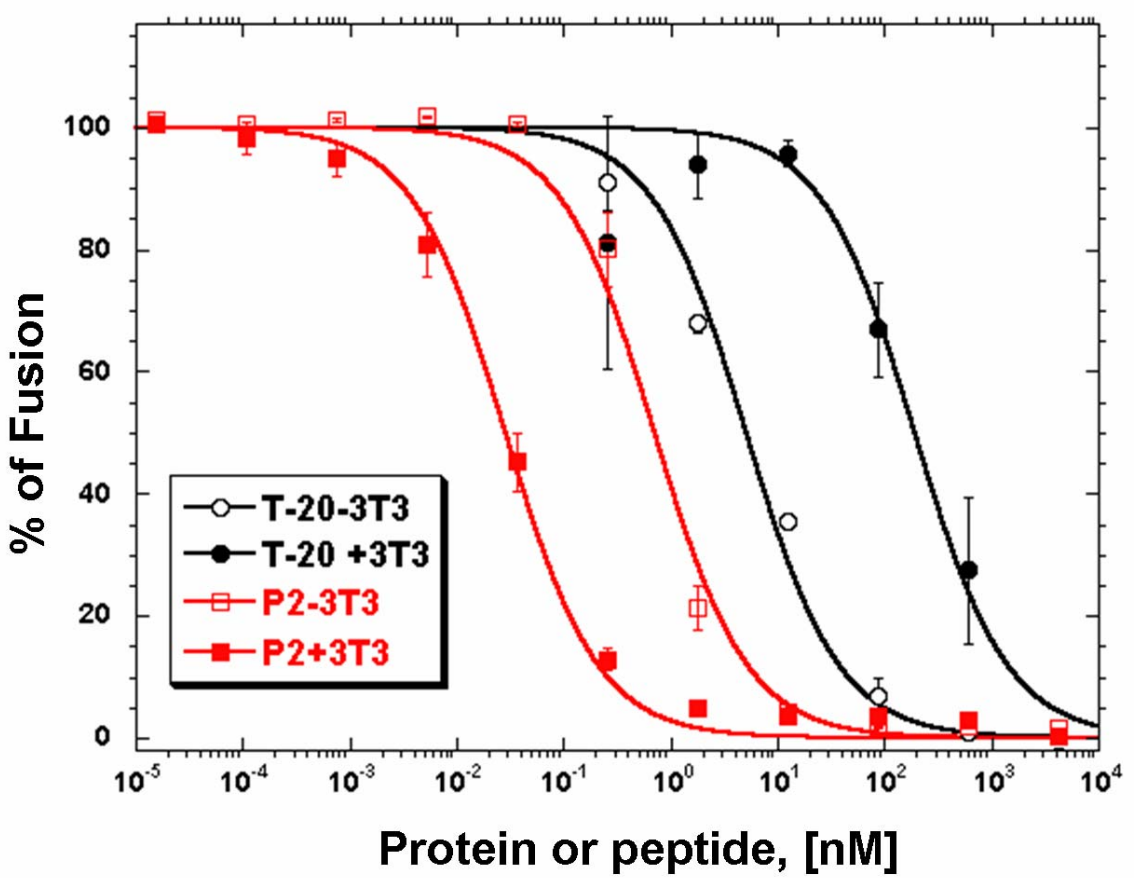

Figure 4-3: Dose dependent inhibition curve in the R5-tropic cell-cell fusion assay with or without the competitive 3T3 cells. The inhibition of HIV-1 fusion is presented using the plot of the percentage of fusion versus the concentration (nM) of T-20 (with 3T3, black filled circles; without 3T3 cells, black open circles), P2-RANTES (with 3T3 cells, red filled circles; without 3T3 cells, red open circles) in the HeLa-ADA and HeLa-P5L R5 tropic cell-cell fusion assay. Error bars indicate the triplicate standard deviation (± SD). Curves were fitted with four-parameter logistic equation using KaleidaGraph. The IC50 for T-20 with and without 3T3 cells are 193 ± 62 nM and 5.1 ± 0.8nM respectively. The IC50 for P2-RANTES with and without 3T3 cells are 0.027 ± 0.003 nM and 0.71 ± 0.09 nM respectively.

explain the high dose requirement when T-20 is administered in the clinic. In our cell-cell fusion experiments, we tried to change the standard assay to use *in vitro* conditions to mimic the actual cell environment *in vivo*: Mice 3T3 cell which do not contain human CD4, CCR5 or HIV env on the surface were used as a competitor. Without the 3T3 competitive cells, (i.e. in a standard HIV cell-cell fusion assay) T-20 was shown to have 50% inhibition at 5.1 ± 0.8 nM. With the 3T3 competitive cell present (10^5 3T3 cell / well, $1e^4$ HeLa-ADA / well,10^4 HeLa- P5L / well), T-20 was shown to have 50% inhibition 193 ± 62 nM (Figure 4-3). This significant decrease (~40 fold) of potency in the inhibition of cell-cell fusion of T-20 is only due to the presence of 3T3 cells because the control wells (HeLa-P5L cell only as negative, HeLa-P5L adding HeLa-ADA without treatment as positive) with 3T3 cells and without 3T3 cells did not show any significant difference (data not shown). In the same experiment, P2-RANTES was shown to have 50% inhibition 0.027± 0.003 nM when 3T3 cells are present and 0.71±0.09 nM when 3T3 cells are absent (Figure 4-3). The dramatic increased (~25 fold) in potency of inhibition of cell-cell fusion is only due to the presence of the competitive 3T3 cells. This effect can be explained by the strong selectivity of P2-RANTES to CCR5. When competitive 3T3 cells are present, the HeLa-ADA cells (representing the HIV surface) may have less chance to recognize the target cells. In this situation, the overall fusion is less efficient, making apparent inhibition by P2-RANTES more efficient. The fusion is more difficult to inhibit by T-20 when competitive 3T3 cells are present because T-20 has nonspecific interactions to unrelated cell membrane or lipids (77,104,108,109).

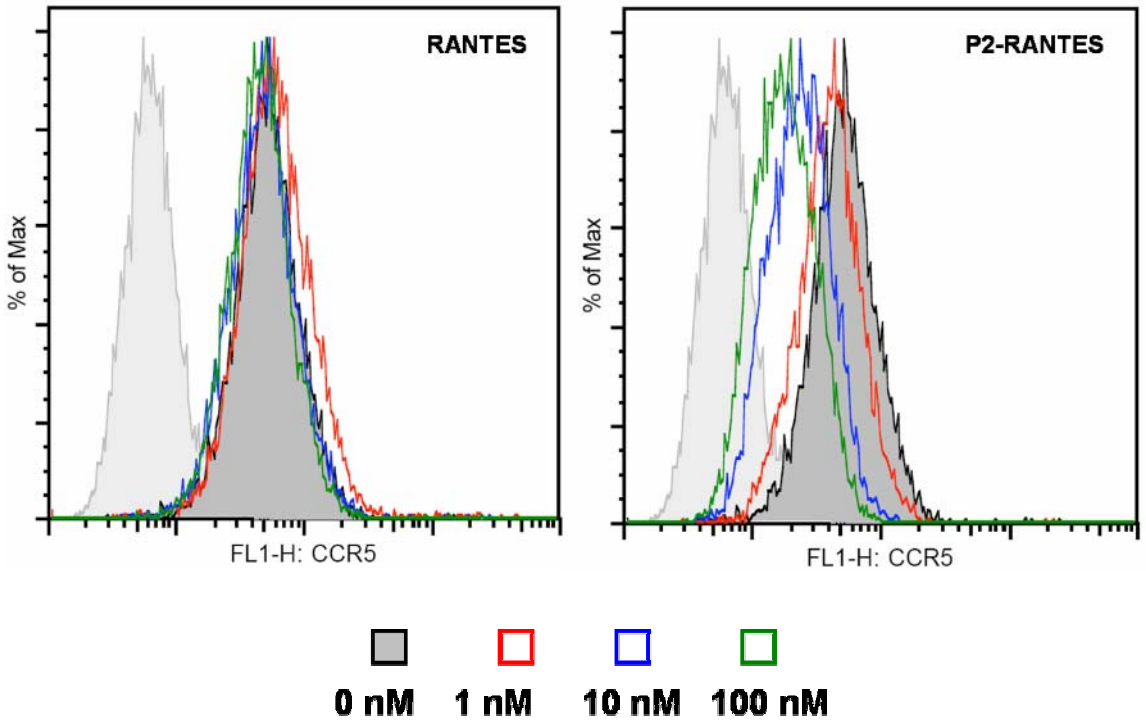

Figure 4- 4: CCR5 internalization induced by wild type RANTES and P2-RANTES in the steady–state CCR5 down modulation FACS experiment. Data are plotted as histograms of fluorescence intensity (cell surface CCR5), with the cell number normalized for each sample. FITC fluorescence intensity from different concentration drug treated HeLa-TZM and stained with same CCR5 antibody and second antibody are presented with different color: black (0 nM); red (1 nM); blue (10 nM) and green (100nM). The cells stained without CCR5 antibodies are showed as gray curve.

This result may also be explained that P2-RANTES can strongly reduce the expression of CCR5 on the target cell, which lead to a longer period windows for the prehairpin state of gp41. This result may need further investigation in future. But the overall function of P2-RANTES in the same experiments is much greater than T-20. Without competitive cells, P2-RANTES has ~10 fold improvement compared to T-20. With competitive cells, P2-RANTES has ~6000 fold improvement compared to T-20.

CCR5 down modulation

As mentioned by Hartley (100) there are two mechanisms underlying improved anti-HIV activity of P2-RANTES: increased binding affinity for CCR5 and enhanced capacity of internalization of CCR5. We repeated similar CCR5 internalization experiments. Compared to wild type RANTES, P2-RANTES produced in our hands also showed stronger capacity to reduce the CCR5 expression level in steady-state CCR5 down modulation experiments than the wild type RANTES. As show in Figure 4-4, in the FACS experiments, P2-RANTES was shown to strongly internalize CCR5 expression on the HeLa-TZM cell in a concentration dependent manner while the wild type RANTES control did not show any significant changes using the same set up. This is in agreement with previously published work with different CCR5 expressing cell lines using a synthesized P2-RANTES polypeptide (100).

GAG binding studies

Most chemokines are highly positively charged. This property facilitates the binding to GAGs on the surface of cells, which immobilizes and presents the chemokine

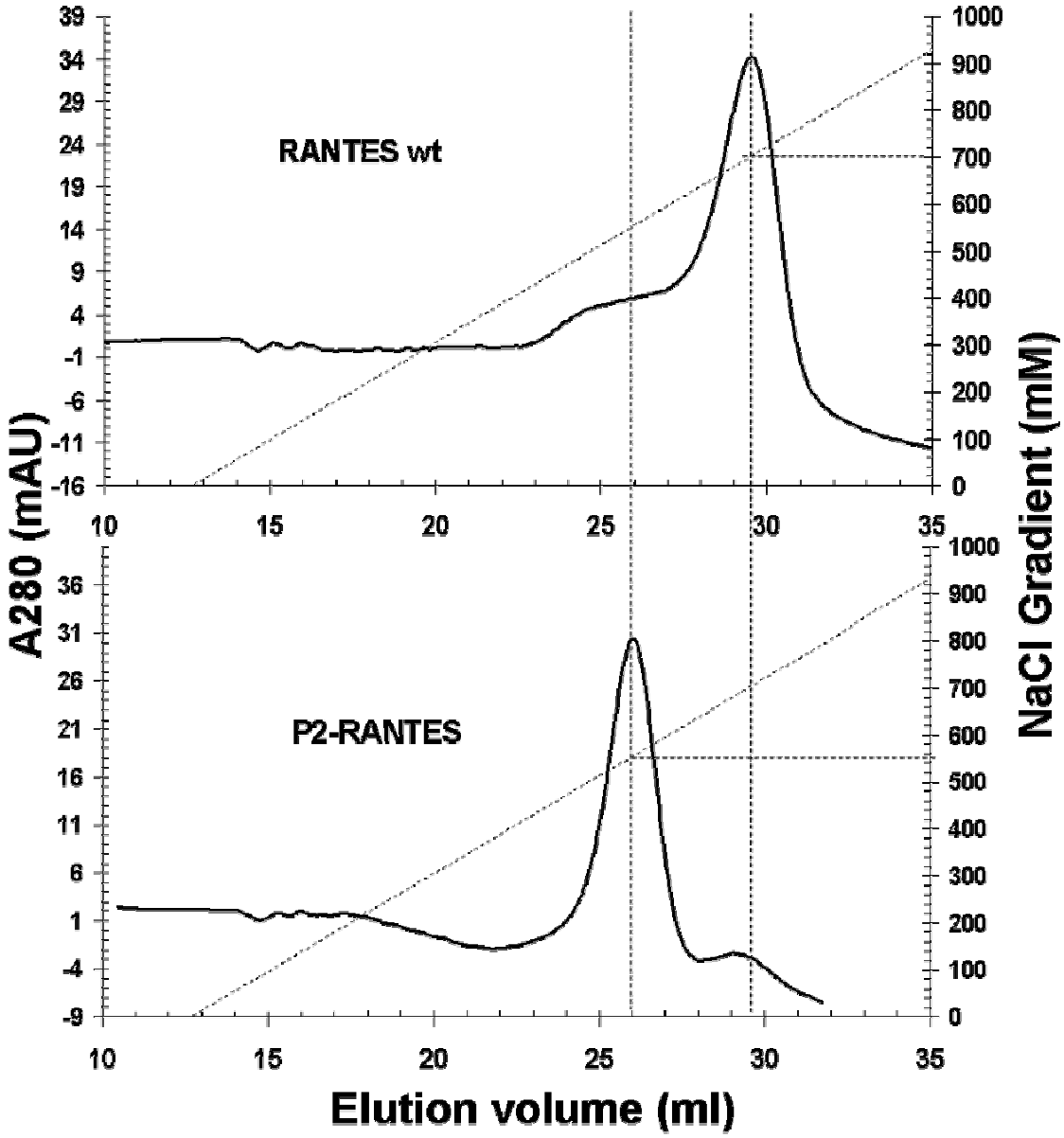

Figure 4-5: Heparin sepharose chromatography of wild type RANTES and P2-RANTES. Equal amounts of wild type RANTES and P2-RANTES were loaded onto a heparin sepharose column and eluted using a NaCl gradient. The dashed lines indicating the elution gradient. The experiments from duplicate indicate that the gradient for wild type RANTES is 698 ± 5mM and P2-RANTES is 550 ± 3 mM.

gradients for chemotaxis. Previous studies of AOP-RANTES indicated that the AOP group may alter the GAG binding capacity (178). We wanted to verify whether the N-terminal amino acid mutagenesis modification of RANTES, P2-RANTES has any effect on the GAG binding capacity. The result of our heparin column binding studies suggested that P2-RANTES indeed has less capacity to bind GAG compared to the wild type protein. As shown in Figure 4-5, when the same amount of protein was loaded onto the heparin column with low salt, the wild type RANTES was found to require 698 ± 5 mM NaCl to completely elute, while P2-RANTES eluted around 550 ± 3mM NaCl. This result indicates that the N-terminal modification of P2-RANTES reduced the GAG binding capacity compared to wild type RANTES.

Analytical ultracentrifugation sedimentation

RANTES can dimerize in solution as many other chemokines (15,16). The dimerization of RANTES or other chemokines plays an important role in the regulation of GAG binding (9,29,189). Since P2-RANTES shows a different profile of GAG binding compared to the wild type RANTES, it may indicate that P2-RANTES has a different oligomerization state (Figure 4-5). We carried out analytical ultracentrifugation sedimentation equilibrium and velocity experiments to determine the quaternary structure of P2-RANTES. Our results with multiple concentrations and multiple speeds suggest that P2-RANTES is predominantly in a monomeric conformation in solution. As show in Figure 4-6, the sedimentation equilibrium experiments revealed that P2-RANTES fits the single component model. The data can not fit to either the monomer-dimer equilibrium or the monomer-tetramer equilibrium model. The fitted molecular

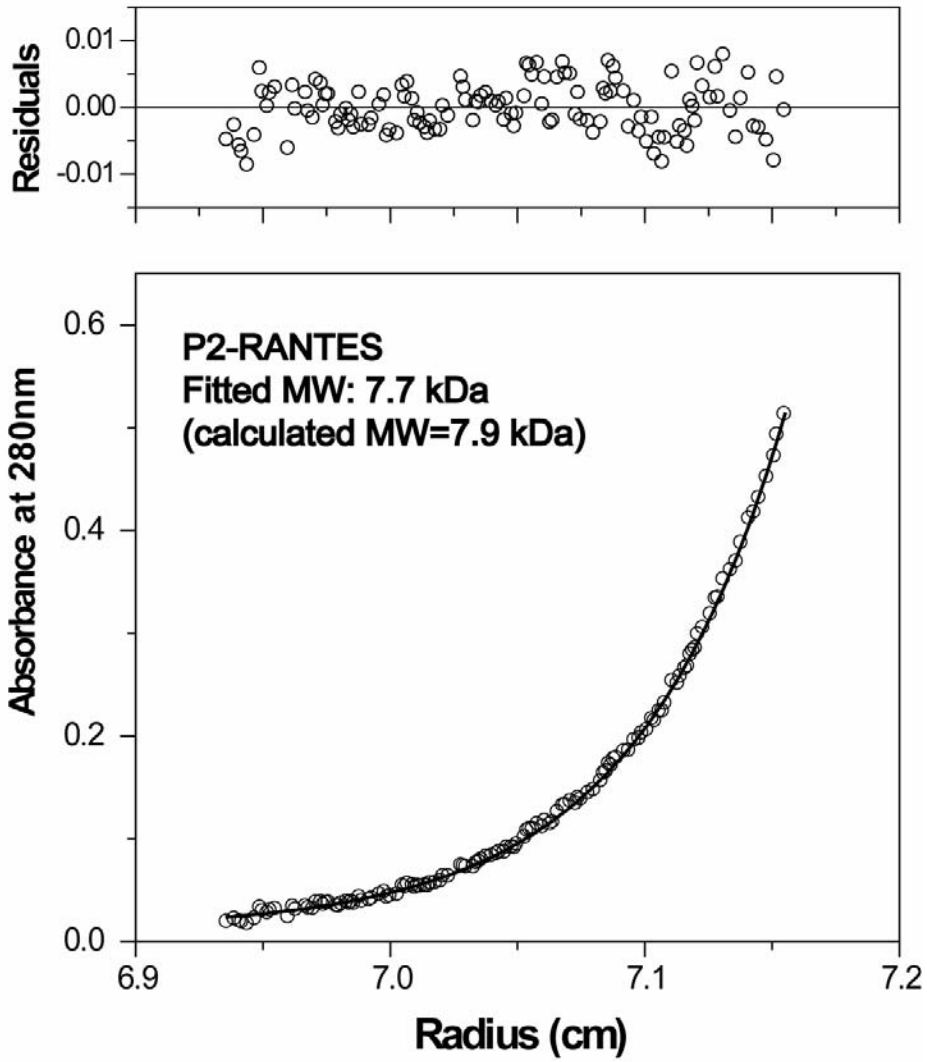

Figure 4-6: Oligomerization state of P2-RANTES in solution. The selected AUC sedimentation equilibrium experiment (24 μM of P2-RANTES in 50mM Tris-Bis, 200 mM NaCl, pH 5.0, speed rate at 55,000rpm) is showing with the raw data by the plot of absorbance at 280nm versus the radius, and curve fitting with the single component model. The fitted molecular weight (MW) is around 7.7 kDa in this set up using the Origin 3.78 (Beckman) program while the calculated MW from amino acid composition is 7.9 kDa.

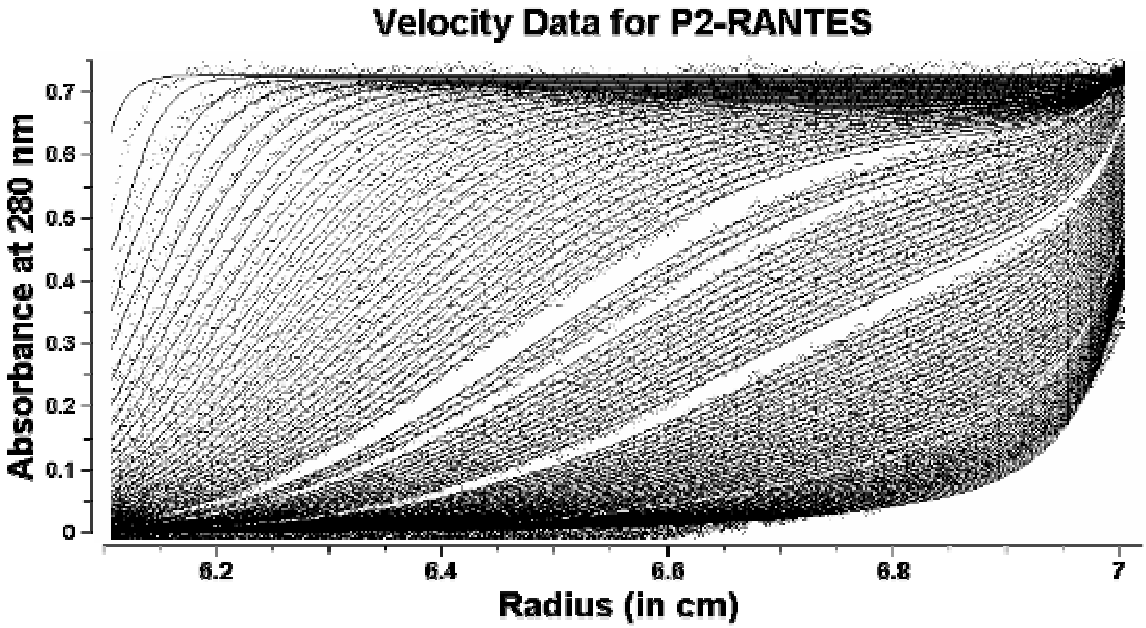

Figure 4-7: AUC sedimentation velocity experiment showing boundary movements in the plot of absorbance at 280nm versus the radius in cm.

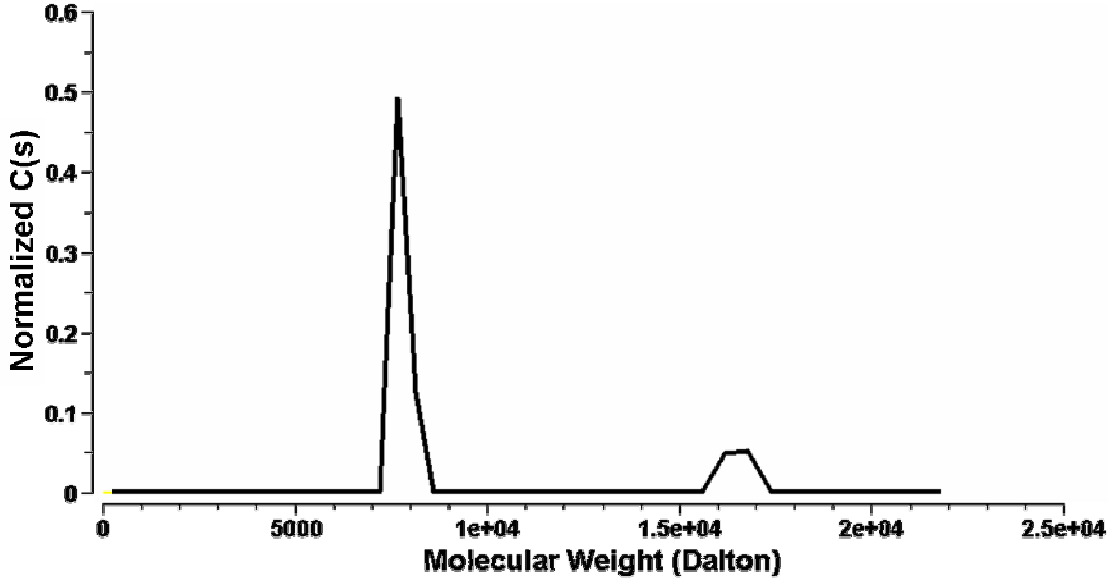

Figure 4-8: Species of population versus molecular weight by converting the raw sedimentation velocity data. Molecular weight distribution of P2-RANTES at 50mM Tris-Bis, pH5.0, 1000 mM NaCl indicates that 90% of the population is a monomer (around 8 kDa) and 10% of the population is a dimer (around 16 kDa).

weight is around 7.7 kDalton in solution conditions: 50mM Tris-Bis, pH5.0, 200mM NaCl. Other studies suggested that the chemokine oligomerization is salt dependent with more salt generally favoring the dimer (29,115). We therefore carried out further sedimentation velocity experiments with higher salt concentrations: 50mM Tris-Bis, pH 5.0, 1000mM NaCl. We transformed the raw sedimentation experiments (Figure 4-7) into the species population plot using the enhance Hode-Weschet method implemented in the UltraScan (184,185) . As shown in Figure 4-8, 90% of the population of P2-RANTES is a monomer and 10% of the population is a dimer. This indicates that again P2-RANTES is predominantly a monomer but it has the tendency to dimerize under certain conditions (for instance high concentration of salt).

Structure determination and description

The crystal structure of P2-RANTES was determined in collaboration with Dr. Pingwei Li. The crystal structure of P2-RANTES is well defined in 1.7Å resolution with the R free factor 24.8% (Table 4-1). The overall structure of P2-RANTES is a homotetramer containing four subunits, labeled as chain A, B, C and D (Figure 4-9). Chain A and chain B have a completely defined structure from residues Phe0 to Ser 68. The N-terminal mutated region in chain A and B is clearly defined due to the restraints of the oligomerization (Figure 4-10). The N-terminal mutated region in chain C (Phe0-Ser4) and chain D (Phe0-Ser5) is disordered, but the rest of the core structure, from residue (chain C: Ser5 to Ser68; chain D: Ser6-Ser68), are well defined. All monomers of P2-RANTES from chain A to D share the same topology as other CC and CXC chemokines monomers, with three anti-parallel β sheets and an α-helix connected to the

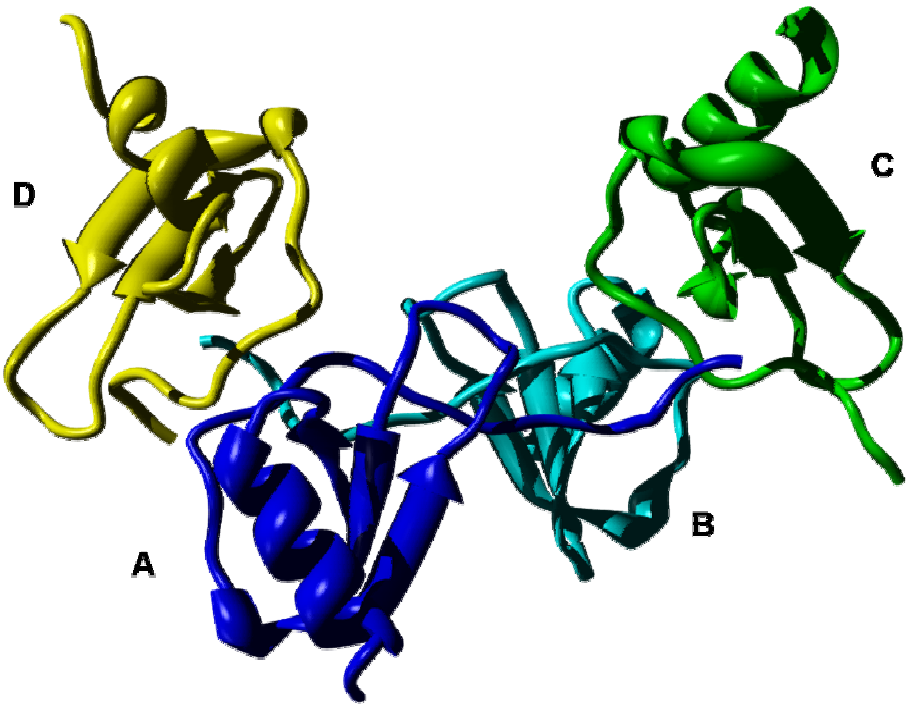

Figure 4-9: Structure of P2-RANTES. Overview of the tetramer structure of P2-RANTES. The four subunits in this ribbon drawing are labeled with A (blue), B (cyan), C (green) and D (yellow).

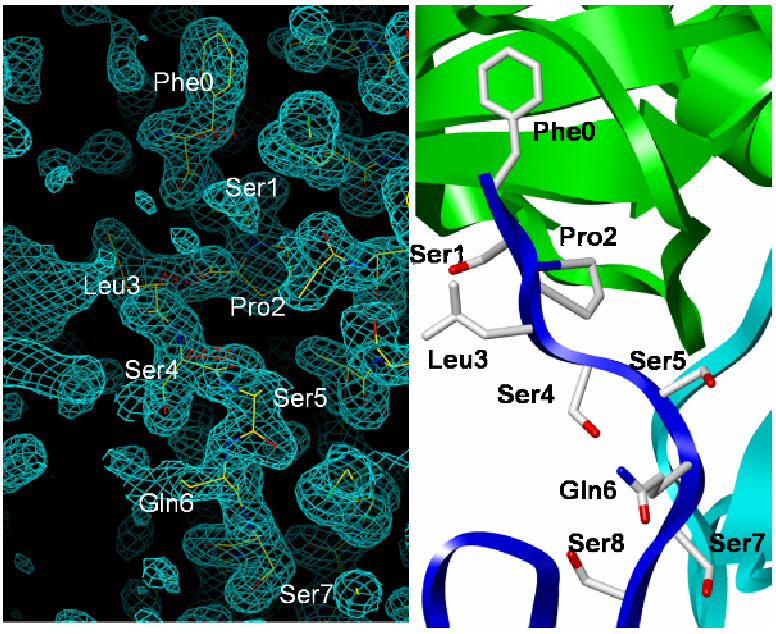

Figure 4-10: Close-up view of N-terminal residues of a P2-RANTES monomer A. Based on the electron density map, the N-terminal residues, from Phe0 to Ser8 (stick model) are clearly defined due to the restraints of oligomerization.

third β-sheet with a flexible loop. Two left-handed disulfide bridges (Cys10-Cys34, Cys11-Cys50) restrain the overall core of the chemokine fold. A short β-sheet (β0) is formed in monomers chain A and chain B from residues Ser8 to Cys10. This region is reported to cause the dimerization for wild type RANTES (15,16,178,190), but the wild type RANTES has the Pro9 in the middle of β sheet, while P2-RANTES has Ala9 in the middle instead. This makes the β0-β0 dimer in P2-RANTES slightly weaker than wild type RANTES. All monomers contain a long loop (N-loop, sometimes referred to as the 20's loop) between Cys11 and Pro20. This loop region is previously reported for the determinant of binding to CCR5 (136). After a short 3^{10} helix (Arg21–His23, α0), there are three main anti-parallel β-strands formed by Ile24–Tyr29 (β1), Val39–Thr43 (β2) and Gln48–Ala51 (β3). The structure of all monomers end with a C-terminal α-helix (α1) formed by residues from Lys56 to Glu66 with extended residues Met67 and Ser68 as a tail. The loop between β1 and β2 contains a type III reverse turn (Ser31–Cys34, sometimes referred to as the 30's loop); the loop between β2 and β3 contains a type I reverse turn (Thr43–Asn46, sometimes referred to as the 40's loop); and the loop between β3 and α1 is a type I reverse turn (Asn52–Lys55, sometimes referred to as the 50's loop). Secondary structure elements were defined using the program CNS (183).

There are several contacts between monomer A and B that are involved in forming the wild type dimer. For example, the antiparallel β0-β0 interactions are formed by residues Ser8-Ala9-Cys10, hydrogen bonds are formed between Ser7 (N) and Gln48' (O), Ser7 (OG) and Gln48' (OE1), Ser8 (N) and Cys10' (O), Cys10 (N) and Ser8' (O),

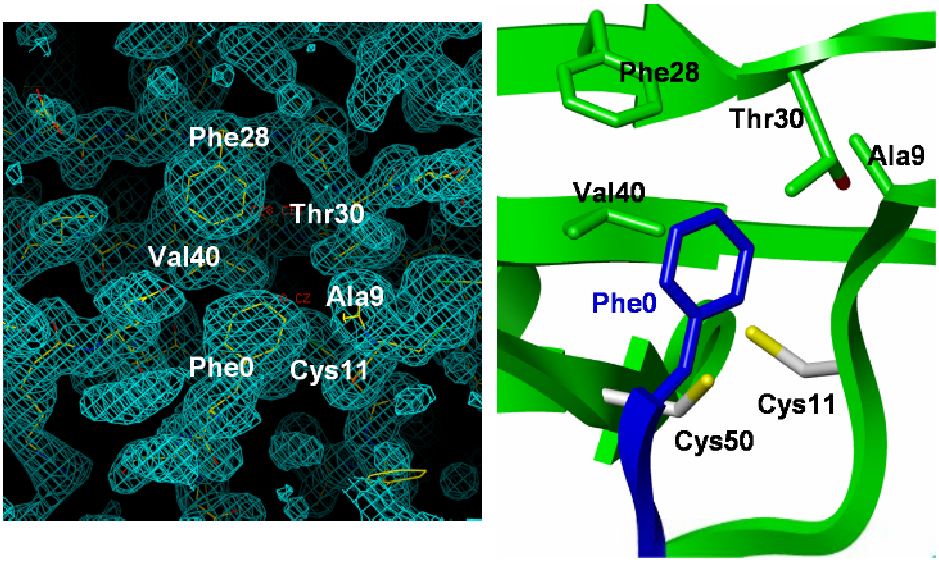

Figure 4-11: Close-up view of the contact interface between Phe0 of monomer A and the hydrophobic cleft of monomer C. Based on electron density map, Phe0 (blue, stick model) from monomer A interacts to Phe28, Thr30, Ala9, Val40, Cys11, Cys50 (green stick model) of monomer C (green ribbon) by hydrophobic interactions.

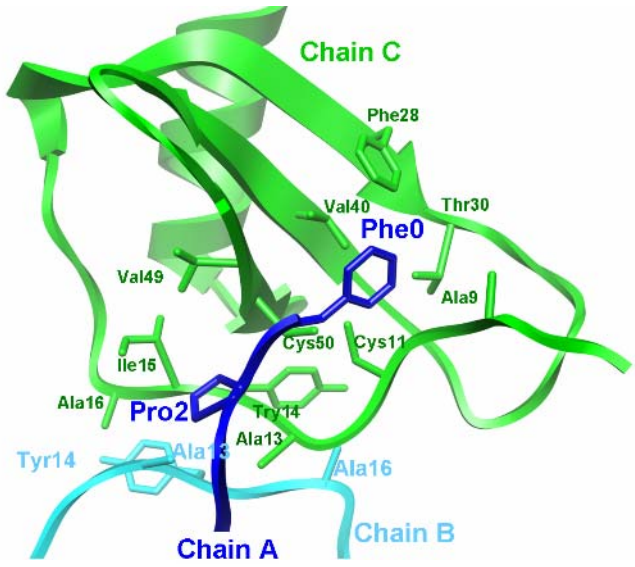

Figure 4-12: Close-up view of the contact interface between monomer B (cyan) and monomer C(green). The hydrophobic interactions are also found between monomer B and C: Try14 from monomer B to Ala16 from monomer C, Ala16 from monomer B to Tyr14 from monomer C and Ala 13 from monomer B to Ala 16 from monomer C. Same as Figure 4-11, Phe0 from monomer A (blue) interacts to Phe28, Thr30, Ala9, Val40, Cys11, and Cys50 of monomer C (green) by hydrophobic interactions. The residue Pro2 of monomer A also contacts to Ile15, Val49 and Ala13 of monomer C by hydrophobic interactions.

Cys50 (N) and Ser 5' (O). This is slightly different from the AOP-RANTES(190) and Met-RANTES in which the hydrogen bonds are formed between Ser5 (O) and Cys50'(N), Asp6(N) and Gln48'(O) and Thr7(OG1) and Gln48'(OE1) (178). Phe12 has een shown to be important for binding to CCR5 and dimerization (191,192). In the P2-RANTES dimer, between chain A and chain B, Phe12 is still intact and involved in corresponding interactions to create the dimer interface. Comparison of the N-termini from both monomers shows the N-termini of monomer A to be better resolved and more highly ordered than monomer B, with clearer density and lower temperature factors.

Residue Phe0 from chain A (or chain B) contacts hydrophobic clefts on chain C (or chain D). As shown in Figure 4-11, based on theelectronic density map, Phe0 from monomer A interacts with Phe28, Thr30, Ala9, Val40, Cys11, Cys50 of monomer C by hydrophobic interactions. Residue Pro2 of chain A (or B) is also found to contact Ile15, Val49 and Ala13 of chain C (or D) by hydrophobic interactions. The hydrophobic contacts between monomer B and C (or between A and D) are also found through Try14 (chain B) to Ala16 (chain C), Ala16 (chain B) to Tyr14 (chain C) and Ala 13 (chain B) to Ala 16 (chain C) (Figure 4-12). However, the buried surface area of this dimer interface is much smaller compared to the dimer interface between monomer A and B (Table 4-2).

Comparison of P2-RANTES structure with other crystal structures of RANTES

There is very little difference in the secondary structure between the crystal structure of P2-RANTES described here and the crystal structures of RANTES: Met-RANTES (193) and AOP-RANTES (190). The root mean square deviation (rmsd) values for

Table 4-2: The buried surface area of the dimer interface.

RANTES variants		Monomer 1 ($Å^2$)	Monomer 2 ($Å^2$)	Dimer ($Å^2$)	Buried surface area ($Å^2$)
P2-RANTES	A-B	5242	5286	9064	1464
	A-C	5242	4692	9318	616
	A-D	5242	4609	9082	769
	B-C	5286	4692	9131	847
	B-D	5286	4609	9257	638
RANTES wt (1rto)		5314	5316	9186	1444
AOP-RANTES (1b3a)		5125	4917	8081	1961

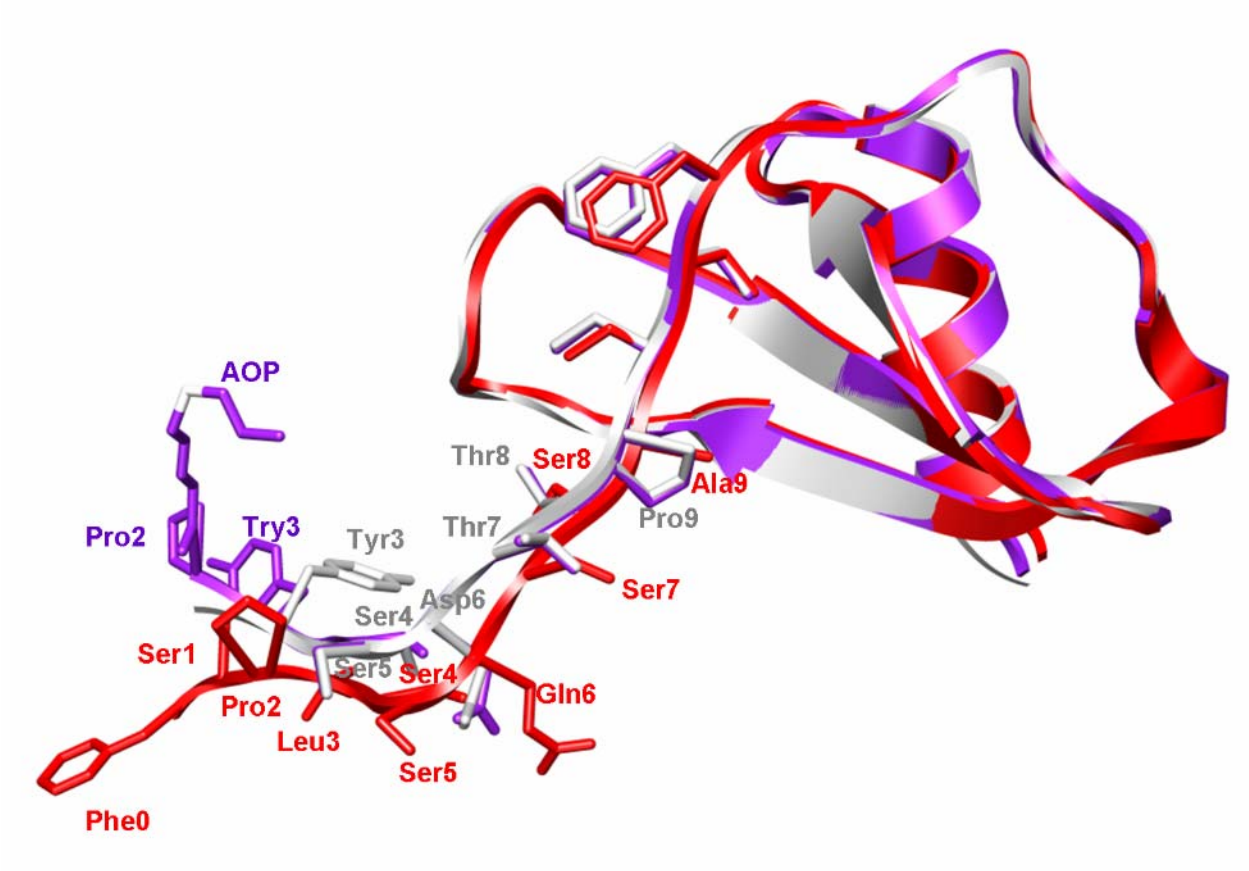

Figure 4-13: Overlay of monomer structure of P2-RANTES (red) to Met-RANTES (gray) and AOP-RANTES (purple). The conserved four Cys residues set as a control to superimpose the monomer structure of these three using the "super match" function implemented in UCSF Chimera (194). Most of the core structures are well overlapped. The most different part are the N-terminal regions. In P2-RANTES, Pro9 is mutated into Ala, Thr7 is mutated into Ser, Thr8 is mutated into Ser, Asp6 is mutated into Gln and Tyr3 is mutated into Leu3. All these mutations make the N-terminal dimer contacts weaker than wild type RANTES. The extended residue Phe0 is pointing in a completely different direction compared to the AOP group.

superpositioning the backbone atoms of P2-RANTES residues 6–68 onto the equivalent atoms of the 1eqt (Met-RANTES) and 1b3a (AOP-RANTES) structures are 0.461 Å and 0.461 Å, respectively. But, there is a lot of difference in the N-terminal regions as seen in the overlay of these three crystal structure (Figure 4-12). In contrast to Met-RANTES structure, in which the conformation of the first 3 residues was not determined, the extended Phe0, Ser1, Pro2 and Leu3 are seen quite clearly in the P2-RANTES crystal structure between monomer A and monomer B (Figure 4-12). Moreover, in AOP-RANTES and Met-RANTES, there are contacts between the peptide Pro2–Tyr3 of one monomer and the symmetry-related ring of Tyr29, which cause the N-termini to push closer to the protein. In P2-RANTES, the Tyr3 is mutated to Leu, this seems to push monomer B away from monomer A. This seems to make a less packed dimer interface that can explain why the protein is mainly a monomer in solution.

The largest differences are found at the dimer interface. The sparse contacts between the monomers of P2-RANTES seem to allow the dimer to flex, as seen in a comparison of the P2 RANTES dimer with Met-RANTES and AOP-RANTES. Although the two monomers are linked through a short β0-β0 interaction by residues Ser8–Cys10, the relative orientations of the monomers to each other are quite different. The dimeric structure of P2-RANTES is less compact than the AOP-RANTES structure, as reflected in the total buried surfaces (Table 4-2) (Figure 4-13). AOP-RANTES (1b3a) buries 24% of the total monomeric solvent accessible surface on dimerization (monomer A = 5125 Å2, monomer B = 4917 Å2, dimer = 8081 Å2), whereas P2-RANTES bury only 16% (monomer A = 5451 Å2, monomer B = 5429 Å2, dimer = 9142 Å2). The

difference in the buried surface area between P2-RANTES and AOP-RANTES is due mainly to the tight fit between the Pro2 and AOP groups wrapped around the surface of the neighboring monomer while Pro2 and Phe0 in P2-RANTES are pointing in different directions (Figure 4-13, 4-14).

Monomers A and B of P2-RANTES shows the N- termini to be clearly defined and the extended Phe0 bound to the hydrophobic clefts of monomer C and D. This is very different to the disordered amino terminus of native RANTES, and different to AOP-RANTES which the AOP group binds to the surface of the other monomer (190). As seen in AOP-RANTES, movement of the N- terminus from solution to the surface might therefore disallow specific interactions with CCR5. Or, these interactions seen in the crystal structure may reflect the interaction on how the N-termini of RANTES inserts into the transmember region to trigger transduction signaling. Very interestingly, in P2-RANTES the Phe0 is not moved back to the surface of the other monomer as seen in the AOP group, but it is pointing toward the hydrophobic cleft of monomer C (or D) instead. Alternatively, the presence of the extended Phe0, mutation Tyr 3 to Leu, mutation of Pro9 to Ala might disturb the monomer/dimer equilibrium, which might or might not play a role in receptor binding and activation. Without a complete understanding of chemokine receptor activation, it is difficult to state the reasons for the antagonist properties of P2-RANTES. Further studies of other RANTES derivatives would be helpful in evaluating different hypotheses.

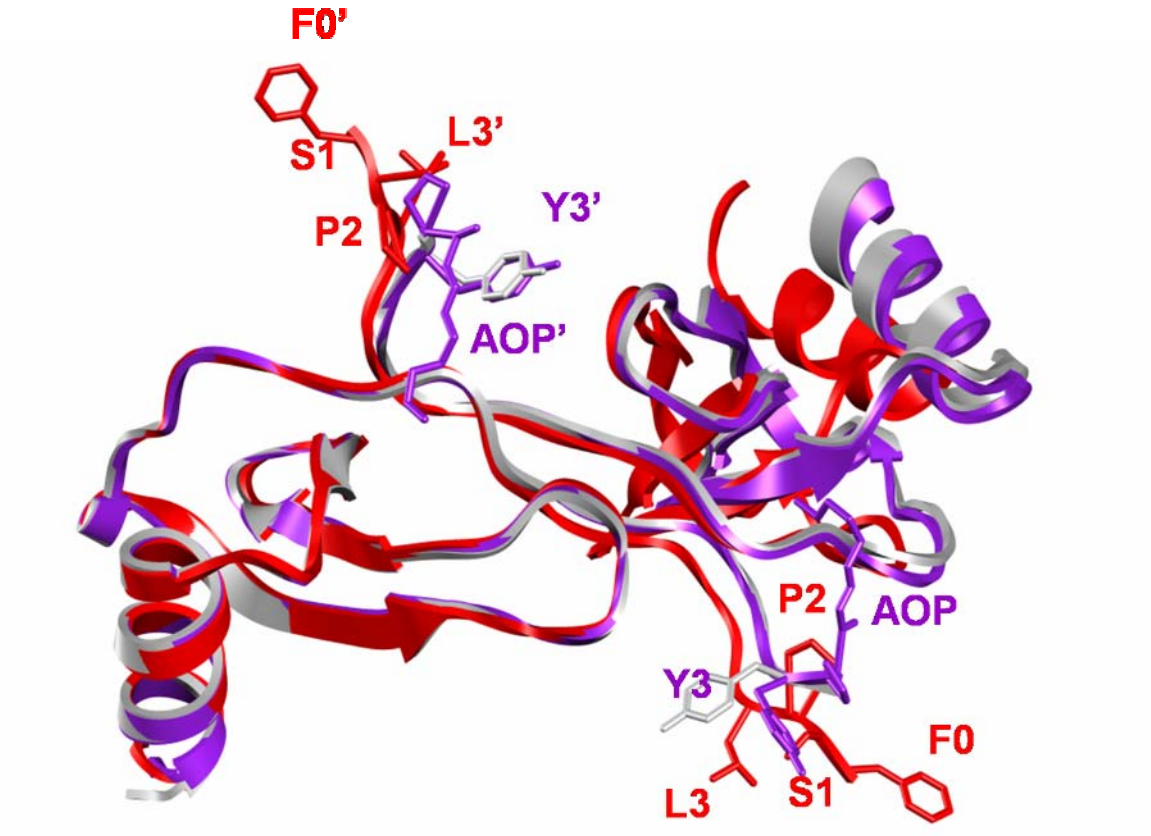

Figure 4-14: Overlay of the dimer structure of P2-RANTES to Met-RANTES and AOP-RANTES. Monomer A from P2-RANTES was set as reference, all dimer structures were overlaid by "super match" function implemented in UCSF Chimera (194). It shows that monomer to monomer orientation in the dimer of P2-RANTES (red) is very different to AOP-RANTES (purple) or Met-RANTES (gray). Especially, due to the N-terminal regions mutations, the lacking of dimer contact in P2-RANTES makes the C-terminal α-Helix orientate away from the referenced monomer. Beside, Phe0 (red stick model) is pointing very different direction comparing to AOP group (purple stick model). Other residues including Ser1, Pro2 and Tyr3 (in P2-RANTES is Leu3) are all showing different orientation. All figures were made using UCSF Chimera (194).

Discussion

RANTES possesses the unique capacity to bind and activate a range of receptors including CCR1, CCR3, CCR4 and CCR5. In order to make it a more potent anti-HIV entry inhibitor, Hartley et al. improved CCR5 binding affinity and CCR5 selectivity using a phage display, resulting in the mutant, P2-RANTES (100). The structure studies of this mutant protein from our work revealed that in contrast to wild type RANTES which is a tight dimer both in solution and in crystallization conditions, P2-RANTES is a monomer in solution while it is unique tetramer in crystallization conditions.

The different quaternary structures between the solution (from AUC) and crystal forms of P2-RANTES correspond with obvious differences between monomer C (or D) and monomer A (or B). Residues 1-4 in monomers C and D structure are highly disordered as also seen in the crystal structure of Met-RANTES (178) or the NMR structure of wild type RANTES (15,16). However, these residues protrude into the surrounding solvent as seen in monomers C and D, are closely packed at the dimer interface on monomer A and monomer B (as well as the dimer between monomer A and C) and contribute to the dimerization. The factors that promote stabilization of the N-terminus and formation of complementary monomer-monomer interactions are not known.

P2-RANTES is a pure monomer in solution judged using analytical ultracentrifugation (Figure 4-6), but the crystal structure shown in this study is a very unique tetramer. Because of the tendency to dimerize in certain conditions (Figure 4-8), P2-RANTES might energetically favor a monomer in solution. But, with high

concentration and less solvent environment, for instance, in the x-ray crystallization conditions, P2-RANTES might favor the oligomerization state as we described here. To our knowledge, this is not an isolated case. Several chemokines are found to be a monomers in solution, but the crystal structures are oligomers (1,25,195). In binding assays and activation assays reported by Hartley, the residue Phe0 seems to be very critical for its function (100). Here, the reported structure of P2-RANTES also indicates that Phe0 is very important in forming the unique tetramer structure. But it is not clear whether this structural importance reflects a functional importance. Further studies of a complex between P2-RANTES with CCR5 would be helpful in evaluating on how P2-RANTES directly interact with CCR5.

Moreover, it is well-known that at physiological conditions RANTES can form higher-order oligomers at high concentration (15) or in the presence of GAGs (160). It has been shown in several studies that GAG binding can alter the oligomermization of chemokines (9,29). Yet the exact role of the extension of Phe0 in this effect is not known. It possibly is due to a change in transfer to the cell surface as mediated by GAG, although the binding to GAG has been shown to be mediated primarily by positively charged residues on a surface far from the N-terminus. The attachment of aromatic Phe0 to the amino terminus alters the chemical nature and surface features of the RANTES molecule. Several other mutations, such as Tyr3Leu, Asp6Gln, Thr7Ser, Thr8Ser and Pro9Ala also strongly reduce the dimerization as seen in the structure. Also, as we showed in the Heparin column results, P2-RANTES lost one third of its capacity to bind to GAG (Figure 4-5). This could give rise to the possibility that P2-RANTES strong

anti-HIV-1 fusion activity is due to its binding less to GAG on the cell surface. This may also need further investigation to clarify.

Although it is not clear exactly how the extended residue Phe0 in P2-RANTES interacts with CCR5, comparison of the N-termini of the structure that we reported here to other available RANTES crystal structure, shows that Phe0 is largely different with Met0 in Met-RANTES or AOP group in AOP-RANTES: Met0 is undefined in the crystal structure; the AOP group folds back onto the surface of the other monomer. Phe0, however, is pointing away from the dimer of monomer A and monomer B and binds to the hydrophobic cleft of monomer C. Since Phe0 is critical for the function for P2-RANTES, this might indicate that Phe0 interacts with CCR5 in a different manner compared to the AOP group interacting with CCR5. In the crystal structure we showed here, Ser1 is pointing in the same direction as the AOP group, it may be very interesting to mutate Ser1 to Phe to see whether the property of blocking HIV entry can be affected. Interestingly, a novel natural mutant Ser1Phe of wild type RANTES was reported in a recent paper from 95 Cameroon samples (196). This mutant was found to only activate CCR5 not CCR1 or CCR3 (196). This might suggest that, as we showed in the structure here, Ser1 is pointing in a similar direction as the AOP group.

CHAPTER V

STRONG SYNERGY BETWEEN CC CHEMOKINES AND FUSION INHIBITORS LEADS TO POTENT EFFECTIVE ANTI-HIV-1 AGENTS IN BLOCKING CELL-CELL FUSION AND VIRUS INFECTION

Introduction

In addition to the more established anti-HIV-1 strategies such as inhibition of protease or reverse transcriptase, viral entry inhibition has great potential in the fight against AIDS. Entry inhibition entails stopping HIV-1 before it breaches the cell, either as a strategy to prevent infection altogether or to curtail infection of new cells in an HIV-positive individual. Several strategies have proven effective at HIV-1 entry inhibition either *in vitro* or *in vivo*: binding to viral surface proteins gp120 and gp41, binding to human cell surface receptor CD4, and binding to human cell surface co-receptors CCR5 and CXCR4 (1,77,161,197). In particular, the synthesized peptide T-20 is believed to act by binding to gp41 (198,199) and is currently in clinical use. But several recent studies revealed that T-20 does not block the six-helix bundle pre-hairpin formation (104,197). Another peptide, C37, derived from C-terminus of gp41 (covering the widely reported C-peptide C34 (101,104,200)) is also reported to have strong anti-HIV entry activity due to tightly binding to the gp41 N-terminal helices; this peptide can be easily produced through *E.coli*. overexpression (200,201).

The potential for synergy between two entry inhibitors is an important for two reasons. First, the therapeutic dose of the drugs will be lowered, and second, the ability

of the virus to develop resistance to two agents at the same time is harder than to a single agent. Several studies have established that synergy can occasionally be observed when two fusion inhibitors are combined in a viral assay or in vitro fusion assay (202-208). For example, some synergy is observed in the combination of CCR5 antibodies with T-20 (202,204), the combination of small molecular antagonists of coreceptors with T-20 (207,208), combination of small molecular antagonists of CCR5 with CCR5 antibodies (202,204,206) and the combination small molecular antagonists of CCR5 with chemokines (204,207). A potent synergy was observed between PRO 542 (a multivalent CD4-immunoglobulin fusion) and T-20, in which the IC_{50} of each component was 0.84 nM and 1.3 nM, respectively, but in combination the IC_{50} was reduced to 0.039 nM and 0.35 nM, respectively in cell-cell fusion assays (205).

In this study I report that potent synergy can also be observed when CCR5 ligands MIP-1β and RANTES are combined with gp41 binding peptides C37 and/or T-20. In particular, a combination of the RANTES mutant P2-RANTES (100) and C37 in a fixed 10:1 ratio yields an IC_{50} of 1 pM and IC_{90} of 39 pM in an R5 tropic cell-cell fusion assay, which we believe to be the most potent combination of entry inhibitors yet reported.

Experimental Procedures

Reagents

All cell culture media and supplements and fetal bovine sera were purchased from Invitrogen (Carlsbad, CA). Fusion inhibitor (N-acetylated derivative), T-20 (catalog No:

9845) was obtained from the NIH AIDS Research and Reference Reagent Program through Roche. The gene of HIV (HXB2) (catalog number: 1069) env was obtained through the NIH AIDS Research and Reference Reagent Program, Division of AIDS, NIAD, NIH: HXB2-env from Dr. Kathleen Page and Dr. Dan Littman (209). Mouse monoclonal antibody to human CCR5 was obtained through the NIH AIDS Research and Reference Reagent Program, Division of AIDS, NIAD, NIH: mouse anti human CCR5 monoclonal antibody from R&D system (catalog number: FABSP1, clone: 45502). FITC (fluorescein isothiocyanate) labeled $F(ab')_2$ fragment of polyclonal goat anti-mouse IgG second antibody was purchased from Sigma (catalog number: F 2653). PHA-P (catalog number: L8754) and AZT (catalog number: A2169) were purchased from Aldrich-Sigma (St.Louis, MO). IL-2 (catalog number: 0801017) and the Retro-Tek p24 antigen ELISA kits (catalog number: 0801200) were purchased from Zeptometrix Corp. (Buffalo, NY).

Protein production and purification

For wild type chemokine MIP-1β and RANTES, protein expression and purification followed a standard chemokine refolding and purification method published previously (29,47,138,188).

For the C37 peptide, its corresponding gene (200) was amplified through standard thermocycling using the gene of HIV (HXB2) env as template, adding the sequence of a Factor Xa cutting site upstream. The PCR product was placed into pET15b (Novagen, Madison, WI) at the Nde I-BamH I sites, and the DNA sequence of this mutant was

confirmed through DNA sequencing. When it is expressed, the protein has a 6 histidine tag on the N-terminus that is subsequently cleaved.

The gene for the RANTES mutant, P2-RANTES, was amplified through standard thermocycling using the wild type RANTES as template (100), also adding the sequence for a Factor Xa cutting site upstream. This was inserted into pET32-Xa (Novagen) at the Nde I-BamH I sites, and the DNA sequence of this mutant was confirmed through DNA sequencing. Upon expression, the protein has a 6 histidine tag and a thioredoxin fusion protein thioredoxin on the N-terminus to facilitate the purification. When the fusion tag is removed (see below) the N-terminus of the P2-RANTES is exactly as published (100).

For production of peptide C37 and protein P2-RANTES, a slight variation on the standard chemokine refolding procedure was used. Protein production was induced by addition of IPTG to 1 mM in 37ºC culture of BL21(DE3) (Novagen) bearing the constructed plasmids for 7 hours, and the cells were harvested by centrifugation at 6,000 x g in an F10S-6X500y rotor (Piramoon Technologies Inc.) for 30 minutes. The cells were resuspended in 30 mL of 500 mM NaCl, 20 mM Tris (pH 8), and 10 mM benzamidine and French pressed twice at 16,000 psi. After centrifugation for 30 minutes at 17,000 x g in an SS34 rotor (Sorvall Instruments), the pellet was resuspended in 20 mL of 5 M guanidinium chloride, 50 mM Tris (pH 8), 500 mM NaCl. The solution was stirred overnight and then centrifuged for 30 minutes at 17,000 x g to remove remaining insoluble pellet. The soluble denatured proteins were loaded onto a 5 mL chelating column (Amersham Pharmacia Biotech) equilibrated with same buffer (5 M

guanidinium chloride, 50 mM Tris (pH 8), 500 mM NaCl). The denatured proteins were purified through the chelating column using a gradient from 10% to 100% of 500 mM imidazole in 5 M guanidinium chloride, 50 mM Tris (pH 8), 500 mM NaCl. The fractions containing purified denatured protein were pooled together and slowly shaken (50 rpm) for 2 hours at room temperature after adding β-mercaptoethanol to 10mM. The purified denatured proteins were dialyzed against 20 mM Tris-HCl, pH 8.0 buffer overnight at 4ºC. After dialysis, precipitated matter was removed by centrifugation for 30 minutes at 15,000 x g in an F14S-6X250y rotor (Piramoon Technologies Inc.) and the protein was purified on a C4 reversed phase chromatography column (Vydac, Hesperia, CA), and lyophilized by the Labconco freeze dry system (Labconco Corporation). To remove the fusion tag, the protein powder was solubilized into ~1mL of 20 mM sodium phosphate (pH 2.5) and the volume was increased to ~ 40 mL in 20 mM Tris (pH 8), 50mM NaCl, and 2 mM $CaCl_2$. Factor Xa (Novagen) was used for the proteolytic cleavage, which typically took 2 weeks at room temperature. SDS-PAGE was used to monitor the cutting reaction. Finally, the cut proteins were purified over a C4 reversed phase chromatography column and lyophilized into powder.

Cell culture

The HeLa cell line stably expressing HIV-1 ADA (R5) env (referred to as HeLa-ADA) was a kind gift from Dr. M. Alizon (Cochin Institute, Paris, France) (179). Cells were cultured in DMEM supplemented with 10 % FBS, and 100 units of penicillin and 0.1 mg/ml of streptomycin and the ADA (R5) env was selectively expressed by adding 2 μM methotrexate (Sigma) as previously published (100,179,180). A HeLa cell line

stably expressing human receptor CD4 and CCR5 (referred to as HeLa-P5L) was a kind gift from Dr. M. Alizon (Cochin Institute, Paris, France) (179). Cells were cultured in RPMI-1640 (Invitrogen) supplemented with 10 % FBS, and 100 units of penicillin and 0.1 mg/ml streptomycin. The expression of CCR5 was selectively expressed by adding zeocin (Invitrogen) 0.5 mg/ml. A HeLa-TZM cell line was obtained through the NIH AIDS Research and Reference Reagent Program, Division of AIDS, NIAID, NIH: TZM-bl from Dr. John C. Kappes, Dr. Xiaoyun Wu and Tranzyme Inc. (181,210,211). The cells were cultured at DMEM supplemented with 10% FBS, 100 units of penicillin and 0.1 mg/ml of streptomycin as mentioned in the instructions provided by the NIH-ARRR.

Cell-cell fusion assay

Envelope-mediated cell fusion assays were carried out as described (100,175,179,180) with HeLa-P5L and HeLa-ADA cell lines (100,175,179,180), with minor modification. Briefly, 10^4 HeLa-P5L cells were seeded in a 96-well culture plate in 50 μl RPMI-1640 medium per well for 2-3 hours. The individual chemokine or the combination of chemokines with C37 or T-20 were added into the cell medium with serial dilution from 4 μM to 0.4 pM. Protein concentration was quantified by measuring the absorbance of the concentrated stock solution at 280nm using the extinction coefficient method published by Pace (186), followed by serial dilution. After preincubation in 37ºC for 30min, 50 μl HeLa-ADA (10^4 cells per well) in RPMI-1640 medium were overlaid into 96-well culture plate. After a further 24 hours of incubation at 37ºC for complete fusion, cells in the 96-well culture plate were washed once by 1× PBS, lysed by adding 0.5% NP-40 (USBiological) in PBS for 15 min at room temperature and assayed for β-

galactosidase activity by the addition of 8 mM substrate CRPG (chlorphenol red-β-D-galactopyranoside, Calbiochem) in PBS with 20mM KCl and 10mM β-mercaptoethanol (Sigma) for 2 hours in the dark at room temperature. The absorbance at 570 nm was read on a Benchmark microplate reader (BioRad). The percentage of the cell-cell fusion was expressed as 100 × (mean absorbance of treated well - mean absorbance of HeLa-P5L-only well) / (mean absorbance of untreated well - absorbance of HeLa-P5L-only well). Experiments were performed in triplicate, and dose dependent inhibition curves were fitted with a four-parameter logistic equation (187) using KaleidaGraph (version 3.6, Synergy Software).

HIV infection assay

Peripheral blood mononuclear cells (PBMC) were isolated from leucopaks (Gulf Coast Regional Blood Center, Houston, TX) drawn from eligible blood donors. Blood was layered over a Ficoll-Paque Plus (GE Healthcare Bio-Scoience Corp, Pittsburgh, PA) gradient, and centrifuged. Buffy coats were harvested and washed 3 times with PBS, and the cells were subsequently placed in RPMI-1640 medium supplemented with 20% FBS - 3% IL-2 - 5 μg/mL PHA-P, and allowed to stimulate for 2-3 days (37°C - 5% CO2) at a density of 1×10^6 PBMC/mL. Following stimulation, culture medium consisted of RPMI-1640 supplemented with 20% FBS - and 5% IL-2 (complete medium). Chemokines or combination with C37 initially diluted 1,000 nM in 5 mM sodium phosphate buffer, pH 3.0. Further serial working dilutions (from 500 nM to 5 pM) were made in complete medium, and were pre-incubated with the cells for a minimum of 1-2 hours. Cells were plated in 24-well cell culture plates at a density of 2×10^6 PBMC/mL.

Each well, except for the negative virus control, received 50 μL containing sufficient virus to achieve a concentration of 1,000 $TCID_{50}$ units of HIV-1 stock (R5 tropic strain, Ba-L) per 1×10^6 PBMC/mL and incubated overnight. During the initial 1-2 hours of incubation, the cell-culture plate(s) were agitated every 15 min to redistribute the virus dilution. Following overnight incubation the wells were washed 3 times with PBS to remove the virus, and each well received the analogous medium to that that was originally used to pre-treat the cells before virus infection. Following washing, the wells contents were split into three aliquots and placed into a 48-well cell culture plate (0.5×10^6 PBMC/0.5 mL per well). Samples were composed of three replicates each. All cell culture plates were incubated as indicated above. ELISA testing of culture supernatants was typically done after 6-7 days to determine HIV-1 p24 levels. ELISA determinations were performed using the Retro-Tek HIV-1 p24 antigen ELISA kit (Zeptometrix Corp.). In each experiment, the positive inhibition control was treatment with 5 μM AZT and the negative inhibition control was no treatment of any kind. The percentage of inhibition was expressed as 100 × [1- (mean A450 of negative wells - mean A450 with drug treatment wells) / (mean A450 of negative wells- mean A450 of positive wells)]. Experiments were performed in triplicate, and dose dependent inhibition curves were fitted with four-parameter logistic equation (187) using KaleidaGraph (version 3.6, Synergy Software).

Evaluation of synergy

Analysis of synergy, additivity or antagonism between chemokines and C37/T-20 was performed using fixed ratios of drug combinations in antiviral assays according to

the median effect principle of Chou and Talalay (212). Chemokines and C37/T-20 were tested individually and in a fixed molar ratio combination over a range of serial dilutions (4 μM-0.1 pM range). The values of the doses required for percentage inhibition (IC_5-IC_{95}) by each of the two drugs (alone and in combination), the Combination Index (CI), and the Dose Reduction Index (DRI) are calculated based on the published protocol from Chou (212) using Microsoft Excel. Based on this analysis, CI value reflects the nature of the interaction between the drugs. CI < 1 indicates synergy; CI = 1 indicates additivity; and CI > 1 indicates antagonism. The DRI is a measure of how much the dose of each drug in a synergistic combination is reduced at a given effect level compared with the dose for each drug alone.

FACS analysis

HeLa-TZM cells (10^5) were incubated for 30min at 37°C in culture medium containing various concentration of (0-100 nM) of drugs in 10× 75mm culture tubes (Fisher Scientific). After washing 4 times with 10 mL cold PBS, cells were incubated in 300 μl of 500 μg/ml mouse anti-human CCR5 monoclonal antibody in PBS-0.5% BSA (Sigma), and kept on ice for 45 min. The cells were then washed 3 times with cold PBS-0.5% BSA and incubated in 300 μl of 50 μg/ml FITC labeled polyclonal goat anti-mouse antibody in PBS-0.5% BSA, and kept on ice for 30 min. 1 aliquot of untreated cells were incubated with PBS-BSA for 30 minutes followed by 3 washes and incubation with the FITC-labeled goat anti-mouse IgG as control. Then the cells were washed 3 times with cold PBS-0.5% BSA and kept in PBS-0.5% BSA, and analyzed with a FACSCalibur (BD Biosciences, San Jose, CA) flow cytometer using CellQuest (BD Biosciences)

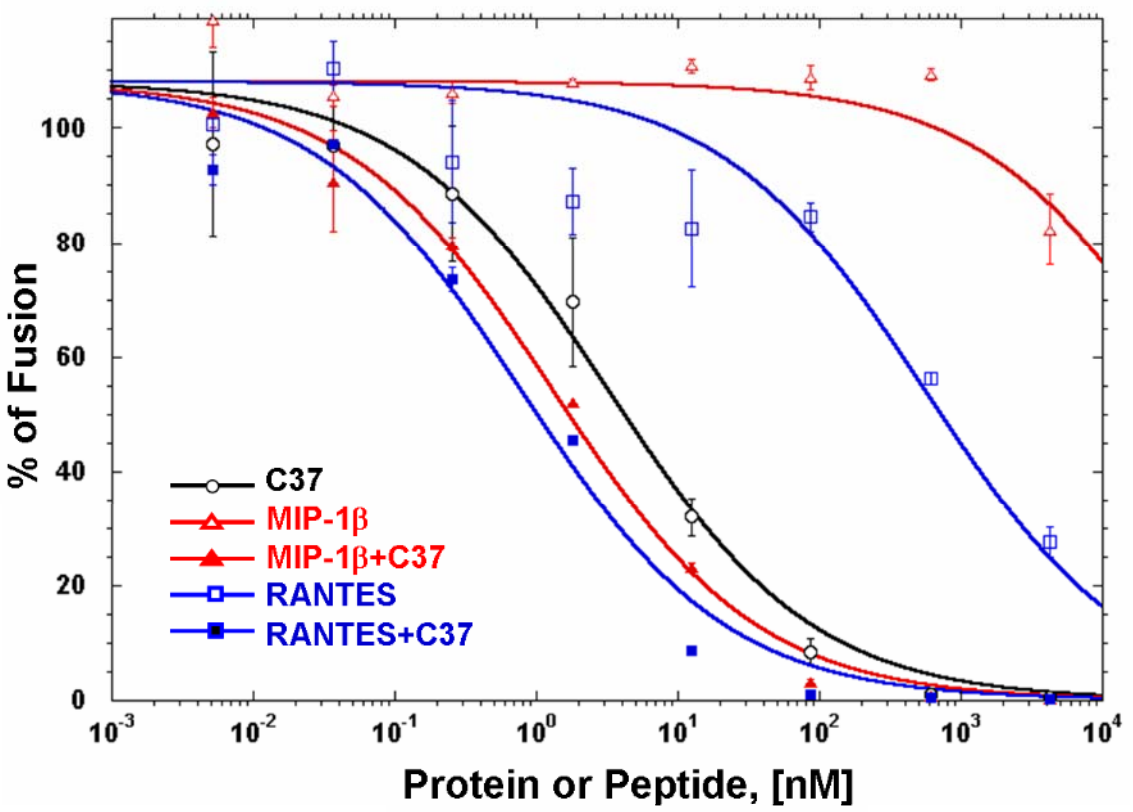

Figure 5-1: The dose dependent inhibition curve in the R5-tropic cell-cell fusion assay for combination of chemokines with C37. The free C37 (black open circle), free MIP-1β (red open triangle), free RANTES(blue open square), C37 combination (1 to 1 ratio) with MIP-1β(red filled triangle), and C37 combination with RANTES (blue filled square) are presented using the plot of the percentage of fusion in the HeLa-ADA and HeLa-P5L R5 tropic cell-cell fusion assay versus the concentration (nM).

acquisition software. Cell viability was determined by staining with propidium iodide (PI) at 1ug/ml final concentration 1 minute prior to analysis. FITC fluorescence was collected through a 530/30 bandpass filter, and PI fluorescence through a 650LP filter. List mode data were acquired on a minimum of 10,000 viable cells defined by a light scatter and lack of PI staining. Data were analyzed using FlowJo (Tree Star, Inc., Ashland, OR). First, a region to define cells was set using a forward and side light scatter plot, and then viable (PI-negative) cells were determined by a plot of forward light scatter and PI fluorescence. Results are presented as histograms of FITC fluorescence.

Results

Cell-cell fusion assays

The CC chemokine MIP-1β has been shown to inhibit infection by HIV-1, and this ability to block entry helped lead to the discovery of CCR5 as the HIV-1 coreceptor (80,213). In later years, however, it became clear that MIP-1β was not as effective as other CCR5 ligands in HIV-1 inhibition (94,100,214). As shown in Figure5-1 and Figure5-2, MIP-1β alone does not significantly inhibit fusion in a standard *in vitro* fusion assay, nor is it notably effective in viral assays (12, 26 and unpublished). Upon combination of MIP-1β with gp41-binding peptide C37 (1:1 ratio), significant inhibition of fusion is observed, but a comparison with C37 alone indicates that fusion inhibition is largely, if not completely, mediated by C37 itself (Figure 5-1). Similarly, the combination of MIP-1β and fusion inhibitor peptide T-20 (1:1 ratio) shows only weak improvement over the effect of T-20 alone (Figure 5-2). In each case, although some

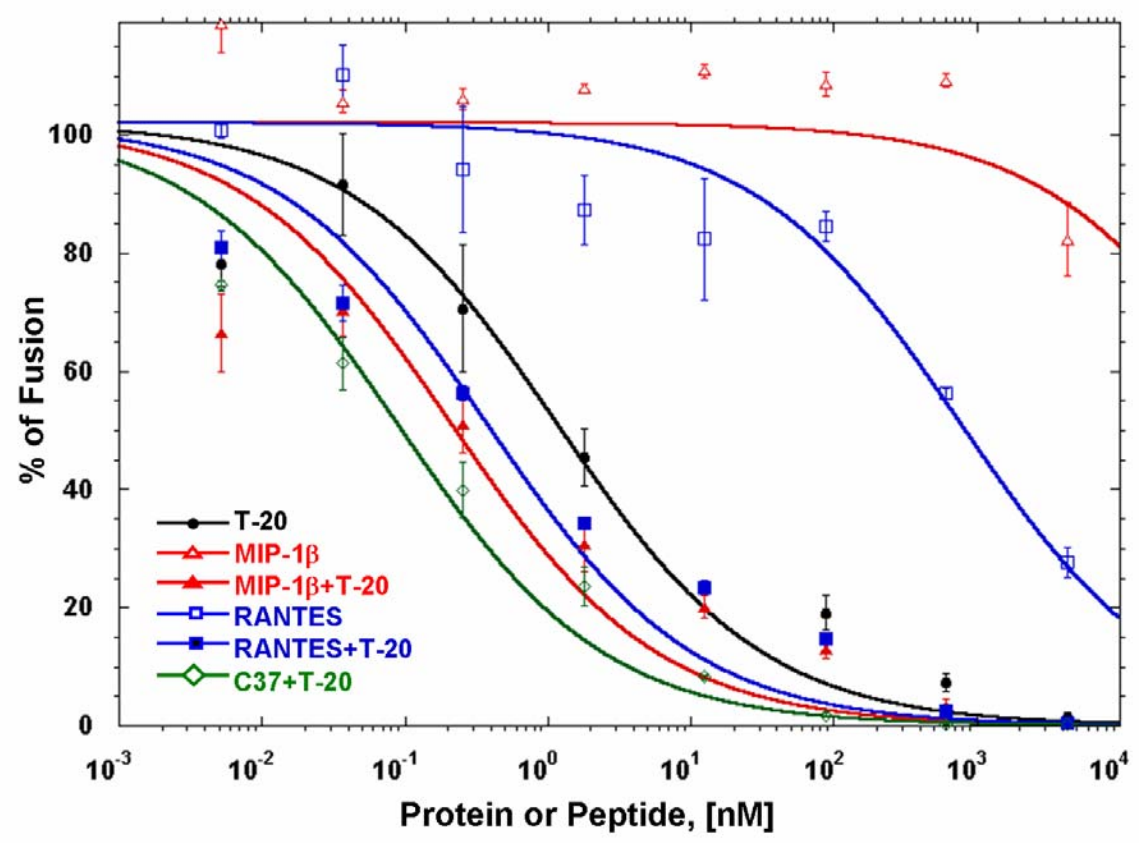

Figure 5-2: The dose dependent inhibition curve in the R5-tropic cell-cell fusion assay for combination of chemokines with T-20. The free T-20 (black filled circle), free MIP-1β (red open triangle), free RANTES (blue open square), T-20 combination (1 to 1 ratio) with MIP-1β (red filled triangle), T-20 combination with RANTES (blue filled square), and T-20 combination with C37 (green open diamond) are presented using the plot of the percentage of fusion in the HeLa-ADA and HeLa-P5L R5 tropic cell-cell fusion assay versus the concentration (nM).

Table 5-1: Combination index values for the T-20 (and /or C37) in combination (1 to 1 ratio) with MIP-1β, RANTES and P2-RANTES in the HIV-1 (ADA) env mediated cell–cell fusion.

Drugs	Inhibitor one IC_{50}, nM	Inhibitor two IC_{50}, nM	Combination of First Inhibitor and Second Inhibitor, IC_{50}, nM	Combination Index
MIP-1β/T-20	1000±100	1.65±0.79	0.49±0.25	0.29
MIP-1β/C37	1000±100	8.31±1.21	7.27±1.39	0.887
RANTES/T-20	109±126	1.65±0.79	0.56±0.26	0.344
RANTES/C37	109±126	8.31±1.21	2.32±0.24	0.306
P2-RANTES /T-20	0.88±0.25	1.65±0.79	0.0077±0.00099	0.0135
P2-RANTES /C37	0.88±0.25	8.31±1.21	0.0080±0.0014	0.0101
T-20/C37	1.65±0.79	8.31±1.21	0.63±0.21	0.487

synergy may be observable, it is not quantifiable because the lack of effectiveness of MIP-1β in the fusion assay made such calculations incomplete.

The CC chemokine RANTES has been shown to be more effective in fusion assays (and viral assays) than MIP-1β (94,100,214). Therefore, the combinations of wild type RANTES with C37 (1 to 1 ratio) and RANTES with T-20 (1 to 1 ratio) were assessed for fusion inhibition. As shown in Table 5-1, RANTES alone produced an IC_{50} for inhibition of 109 ±126 nM, C37 alone had an IC_{50} of inhibition of 8.33 ±1.21 nM, and a combination inhibited at 2.32 ±0.34 nM. This modest but repeatable effect was assessed using the combination index formula described by Chou and Talalay (212). The combination index (CI) of a two drug combination can be used to study the interactions of two drugs where 1 indicates no synergy between the two drugs (that is, their effects are merely additive), and values lower than 1 indicate synergy, with values closer to zero indicating more synergy. The combination of RANTES and C37 showed moderate synergy, with a CI value of 0.3056 (Table 5-1). Similarly, RANTES in combination with T-20 showed modest synergy, giving a CI value of 0.3442.

The RANTES variant "P2-RANTES" was discovered by Hartley et al who used phage selection of randomly N-terminally mutated RANTES to discover this analog that tightly binds CCR5 and internalizes the receptor with high efficiency (100). P2-RANTES performs quite well in fusion assays, having an IC_{50} of 0.88nM in our hands (Figure 5-3) and 0.6-0.9 nM as reported by Hartley (100). However, in a 1:1 combination of P2-RANTES with C37, the IC_{50} of inhibition drops to 0.008 nM, giving a CI value of 0.01 (Figure 5-3 and Table 5-1). This value indicates a highly synergistic

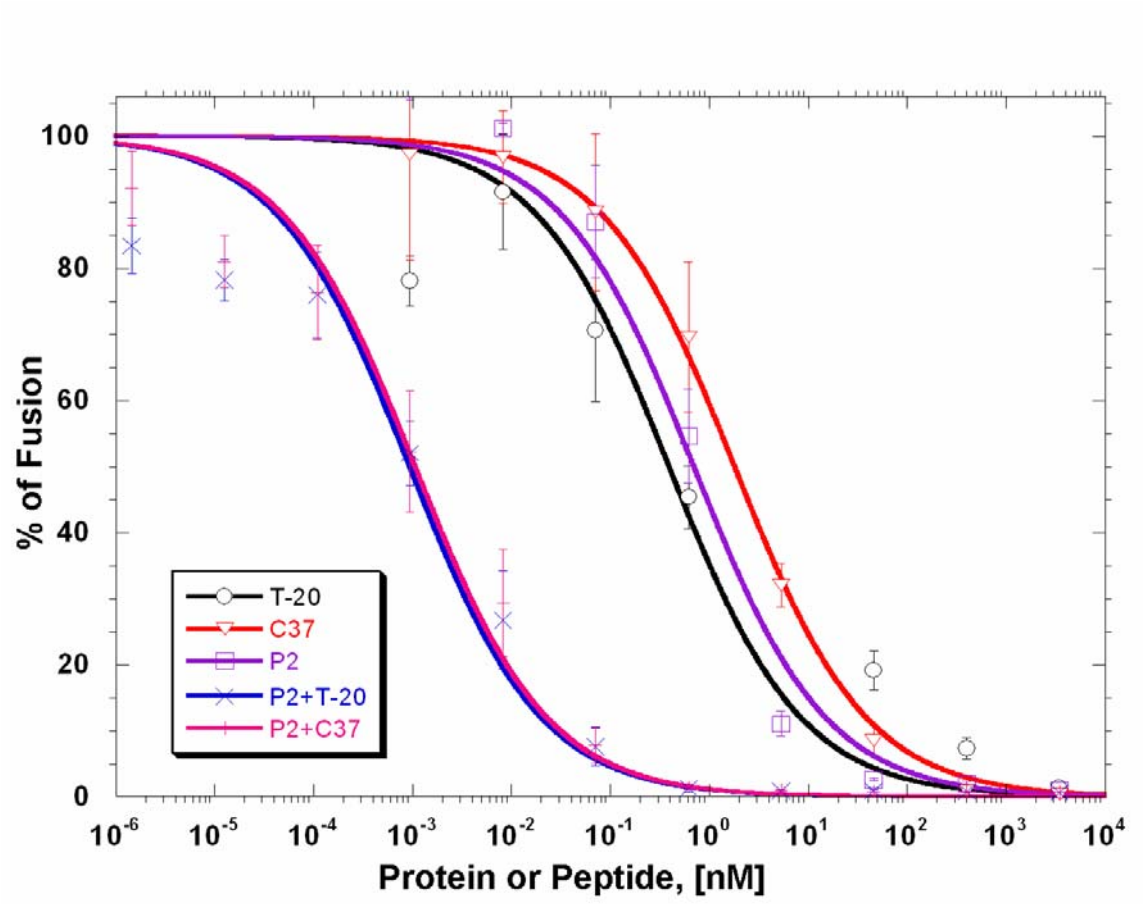

Figure 5-3: The dose dependent inhibition curve in the R5-tropic cell-cell fusion assay for combination of P2-RANTES with C37 or T-20. The free C37 (red open triangle), free T-20 (black open circle), free P2-RANTES (purple open square), C37 combination (1 to 1 ratio) with P2-RANTES (pink plus) and T-20 combination (1 to 1 ratio) with P2-RANTES (blue cross) are presented using the plot of the percentage of fusion in the HeLa-ADA and HeLa-P5L R5 tropic cell-cell fusion assay versus the concentration (nM).

and potent combination. Similarly, the combination of P2-RANTES and T-20 also resulted in high synergy and effectiveness (Figure 5-3 and Table 5-1).

To determine which ratio of P2-RANTES and C37 best inhibits HIV-1 fusion, ratios of 20:1, 10:1, 1:1 and 1:10 were also tested. As shown in Table 5-2, the ratio of P2-RANTES:C37 10:1 has an IC_{50} of 0.001 nM, with a CI of 0.0025. To our knowledge, this is the most potent combination of fusion inhibitors yet reported, both in terms of concentration for effectiveness and in terms of the CI value.

Interestingly, the combination between C37 and T-20 also showed a moderate synergistic effect, with a CI of 0.49. As shown in Table 5-1, the 1:1 ratio of C37/T20 combination has an IC_{50} of 0.63 ± 0.21 nM, where C37 alone and T-20 alone only gave IC_{50} of 8.33 ± 1.21 nM and 1.65 ± 0.79 nM, respectively. This may indicate that the two peptides have different functions in HIV inhibition. While it is generally postulated that both C37 and T-20 bind to the N-terminal coiled coil of gp41, a recent report suggests that T-20 may have alternate binding modes (104).

Table 5-2: Combination index values and dose reductions for inhibition of HIV-1 (ADA) env mediated cell –cell fusion with combination of P2-RANTES and C37 with different molar ratio.

Ratio of P2-RANTES /C37	% of Inhibition	CI	P2-RANTES Concentration (nM)		DRI	C37 Concentration (nM)		DRI
			Alone	Mix		Alone	Mix	
20:1	95	0.011	53.1	0.56	94	284	0.028	10100
	90	0.0089	18.7	0.16	113	77.3	0.0083	9370
	70	0.0065	2.82	0.018	158	7.37	0.00089	8250
	50	0.0053	0.861	0.0044	195	1.68	0.00022	7620
10:1	95	0.010	12.64	0.12	105	16.1	0.012	1330
	90	0.0071	5.36	0.036	149	8.94	0.0036	2480
	70	0.0037	1.14	0.0041	279	3.10	0.00041	7620
	50	0.0025	0.429	0.0010	415	1.59	0.000103	15400
1:1	95	0.068	12.6	0.47	27	16.1	0.47	34
	90	0.047	5.35	0.16	34	8.94	0.16	57
	70	0.025	1.13	0.021	54	3.10	0.021	148
	50	0.018	0.43	0.0059	72	1.59	0.0059	267
1:10	95	0.061	12.6	0.087	145	16.1	0.87	18
	90	0.051	5.35	0.039	137	8.94	0.39	23
	70	0.038	1.14	0.0093	123	3.10	0.092	34
	50	0.032	0.43	0.0037	115	1.59	0.037	43

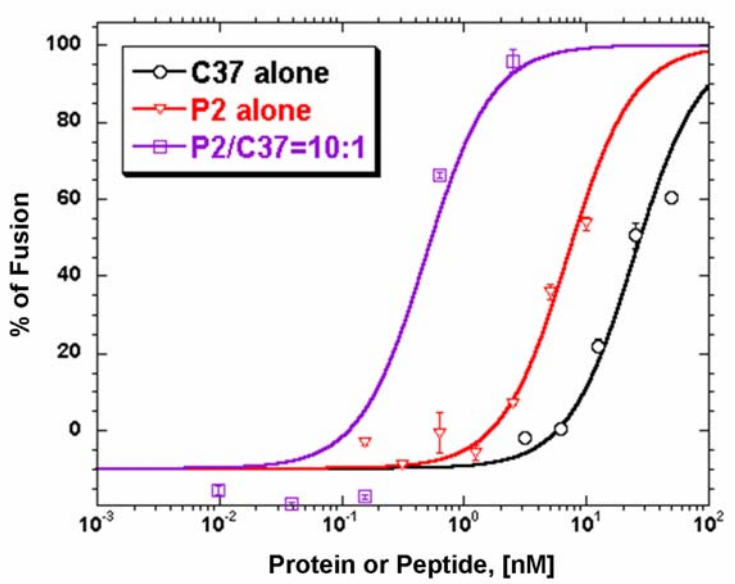

Figure 5-4: HIV (Ba-L) infection assay of combination of P2-RANTES with C37 (10 to 1 ratio). The free C37 (black), free P2-RANTES (orange) or C37 combination with P2-RANTES (with P2-RANTES /C37=10:1 ratio, purple) are presented using the plot of the percentage of inhibition versus the concentration (nM) in the HIV-1 strain Ba-L infection assay. Error bars indicate the triplicate standard deviation (±SD). Curves were fitted with four-parameter logistic equation (187) using KaleidaGraph.

Table 5-3: Combination index values and dose reductions for inhibition of HIV-1 (Ba-L) infection assay with combination of P2-RANTES with C37 (10 to 1 ratio).

% of Inhibition of HIV (Ba-L) infection	CI	P2-RANTES Concentration (nM)		DRI	C37 Concentration (nM)		DRI
		Alone	Mix		Alone	Mix	
95	0.014	39.52	0.55	72	344.79	0.054	6270
90	0.017	26.49	0.44	60	187.48	0.044	4265
70	0.023	12.86	0.29	44	62.36	0.029	2125
50	0.029	8.17	0.23	36	31.25	0.023	1373

HIV-1 infection assays

The best combination studied from the cell-cell fusion assay, P2-RANTES and C37 with fixed ratio as 10:1, was tested for inhibitory capacity against HIV-1 (Ba-L) in PBMC. As shown in Figure 5-4, P2-RANTES and C37 were each effective inhibitors, as reported previously (95,100,104). The combination of P2-RANTES and C37 (10 to 1 ratio) shows 90% inhibition at 0.48 nM and the CI of 0.016 (Table 5-3). This indicates that combination of P2-RANTES and C37 indeed gives strong synergy in the real HIV infection assay as well as the *in vitro* cell-cell fusion assay.

FACS analysis

In order to study the mechanism of this strong synergy between P2-RATNES and gp41 binding peptides, we hypothesized that the internalization of CCR5 to remove it from the cell surface by P2-RANTES may play an important role. As published by Hartley et al.(100), P2-RANTES not only tightly binds to CCR5 as other chemokines do, but also strongly internalizes the CCR5 on the cell surface. We used steady-state CCR5 down-modulation FACS experiments to study the internalization of CCR5 by treatment with individual or combination drugs in 30 min of incubation at 37ºC. As shown in Figure 5-5, free C37 or free wild type RANTES did not induce significant CCR5 internalization with the highest concentration (100 nM), but free P2-RANTES or P2-RANTES combined with C37 (1:1 ratio) showed significant internalization of CCR5 in a concentration dependent manner. This significant difference between wild type RANTES and P2-RANTES may play a role in the stronger synergy observed by P2-RANTES:C37 compared to wild type RANTES:C37.

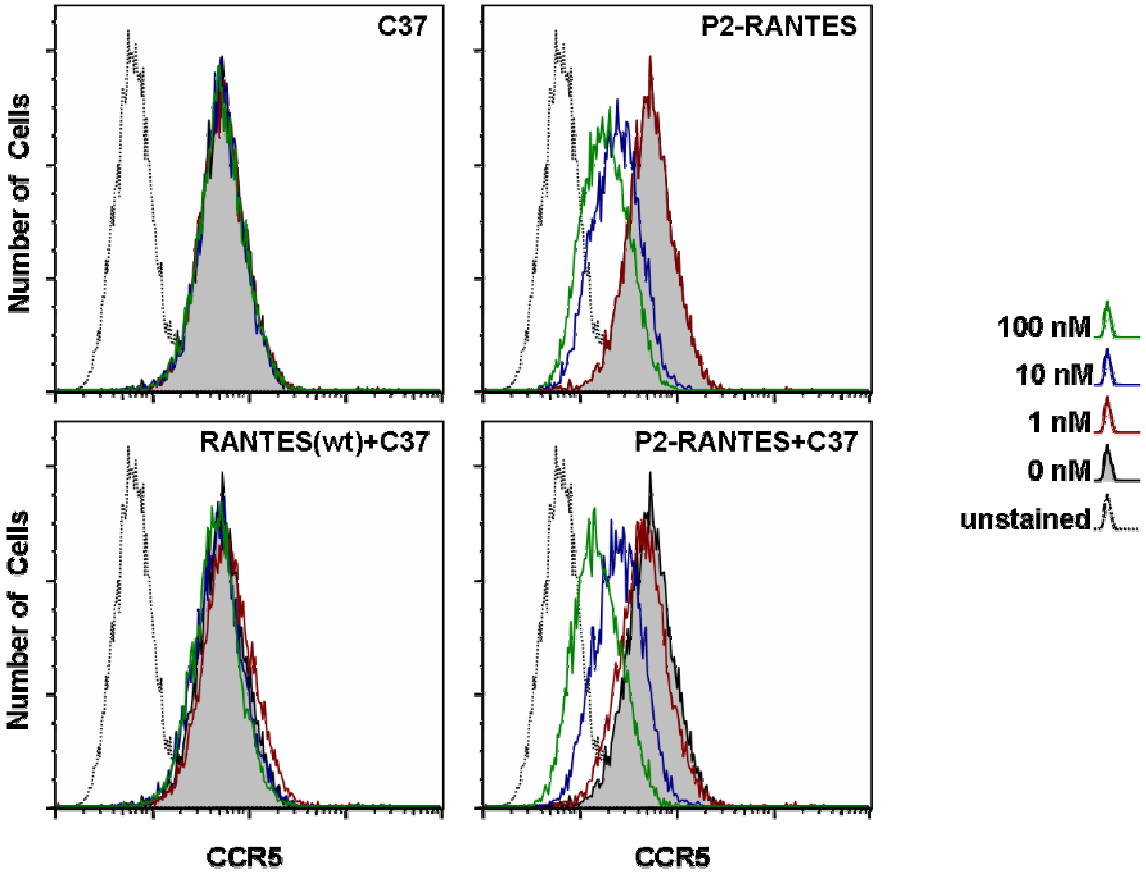

Figure 5-5: CCR5 internalization, as measured by FACS. The effect of free C37, P2-RANTES and the combination of wild type RANTES/ C37 (1:1 ratio) and P2-RANTES/C37 (1:1 ratio) on the cell surface CCR5 population was measured. Data are plotted as histograms of fluorescence intensity (cell surface CCR5), with the cell number normalized for each sample. The level of CCR5 expression is represented for cells treated with: 0 nM drug (black, shaded), 1 nM (brown), 10 nM (blue) and 100nM (green). The cells stained with the second antibody but in the absence of CCR5 antibodies are shaded in light gray. Each histogram represents between 9000 and 9400 viable cells. Viability of the cells varied from 95% to 97%.

Discussion

HIV-1 entry in cells requires cell surface proteins CD4 and coreceptor CCR5 or CXCR4 (215-218). CCR5 serves as the main coreceptor for transmitting infection of HIV-1 (219-221), and CCR5 density level (molecules/cell) on CD4 T cells have been shown to be the driving force of cell-cell fusion (211,222,223). Reeves et al (224,225) have shown that "low" CCR5 density levels on cell lines lead to slower kinetics of fusion and increased susceptibility to T-20. In addition, CCR5 levels were shown to affect sensitivity of primary cells to T-20 (226). Rapamycin, which reduces CCR5 density oncells, was recently shown to moderately synergize with T-20, giving a dose reduction in T-20 of about 33-fold (227)

Synergy between drug therapies is an important strategy to allow effective disease control at low doses of drug (202,203,205-208,228,229). Several combinations of anti-HIV compounds have been reported that involve fusion inhibitors, including CCR5 antibodies, CCR5 antagonists and fusion inhibitors (13, 23, 37, 38). Among the best of these, PRO 542 (a multivalent CD4-immunoglobulin fusion) and T-20 were shown to have strong synergy with a combination index value of 0.34 at 50% inhibition in a cell-cell fusion assay (205). Even better synergy was reported by Safarian et al. who observed a CI_{50} of 0.06 for the combination of anti-CCR5 antibody PA14 and small molecule SCH-C (206). However, these authors do not report a dose reduction and the combination appears to work no better than nanomolar levels.

We report here an even more effective combination of anti-HIV agents, namely the combination of P2-RANTES and the gp41-binding peptide C37 in a ratio of 10:1. This

combination shows highly potent anti-HIV activity both in fusion assays and against viral infection in PBMC, which gave a CI value of 0.0025 in the cell-cell fusion assay and 0.029 in the HIV infection assay (50% inhibition). This combination was found giving a dose reduction in T-20 of about 1373-fold (50% inhibition) (Table 3). To our knowledge, the synergy observed using these combinations is far greater than for any other combination of fusion inhibitors yet reported. Since FACS analysis shows that P2-RANTES greatly decreases cell surface CCR5 on HeLa-TZM cells, overall this suggests that chemokine-mediated internalization of CCR5 strongly increases the sensitivity of HIV-1 to inhibition by C37/T20.

CHAPTER VI

SUMMARY AND CONCLUSIONS

The chemokine monomeric fold can support very different dimer forms: CC chemokine and CXC chemokine subfamily. Both rational and random mutagenesis were used to study chemokine monomers and dimerization. A novel use of a bacterial homodimer selection system geared toward understanding quaternary structure formation in chemokines is reported. The results indicate that, while the goal of attaining folded monomeric variants from the wild type chemokine dimer is achievable, neither structure based design of mutations nor a λ repressor based homodimer selection system was successful in revealing a pathway to obtain a CC chemokine-type dimer from a monomeric CXC chemokine, or a CXC chemokine-type dimer from a CC chemokine monomer. When expressed and purified, all folded variants were judged to be monomers, not dimers. It can be concluded that the chemokine fold is a robust arrangement that can be attained by a wide variety of amino acid sequences, while the chemokine dimer can only be formed by very specific placement of amino acids. However, further design and investigation of chemokine quaternary forms may be possible using computational methods and phylogenetic calculations.

The dimer of MIP-1β does not bind to CCR5. Since the dimer of chemokine is very important in several *in vivo* studies. We used a "trapped dimer", MIP-1β-A10C, to study whether the dimer CC chemokine has ability to bind or activate its receptor. Our data indicate that dimer of the CC chemokine does not bind or activate the CCR5 receptor

even though it fully retain the ability to bind GAGs. This result supports a model of chemokine action in which the chemokine is immobilized on the endothelial surface in the dimeric (or higher order oligomeric) form by binding to cell surface GAGs. The ability to dimerize is likely critical for GAG affinity, for chemokine gradient formation, or for the ability of the chemokine to be presented appropriately to the receptor on the surface of a chemotaxing leukocyte that is passing nearby. Dissociation of the chemokine oligomer into monomeric subunits likely occurs as part of the process of transferring the chemokine from the GAG to the receptor. This dissociation from the dimer (or oligomer) form to the monomer form is evidently necessary in order to bind and activate the cognate receptor, at least in the case of CC chemokines, as shown by the present work on the CC chemokine MIP-1β.

Unique structure of N-terminal six-site mutant of RANTES: P2-RANTES. We produced the previously reported potent anti-HIV-1 protein P2-RANTES from *E. coli* and found this unique mutant protein to have ~6000 fold improvement in the 3T3 completive cell-cell fusion comparing to the widely used HIV fusion inhibitor, T-20. The crystal structure of this mutant protein was determined at 1.7Å resolution. Several contact area were identified by this tetramer crystal structure. This structure study illustrated detailed information of this potent anti-HIV-1 chemokine mutant protein.

Synergistic effect of P2-RANTES and C37. CCR5 serves as the main coreceptor for transmitting strains of HIV-1 in primary infection. In this Ph.D. study, we demonstrate that treatment of CD4+ CCR5+ cells with P2-RANTES combined with C37 or T-20 resulted in significant suppression of HIV-1 entry, both in cell-cell fusion assay and HIV

infection assay of PBMC. Further FACS analysis suggested that the reason for the synergy is that P2-RANTES has a strong internalization on CCR5 expression on the HeLa-TZM cell while wild type RANTES has a modest effect in the same experiment. The significant difference between wild type RANTES/C37 and P2-RANTES/C37 suggests that the strong internalization of CCR5 by P2-RANTES makes the combination of P2-RANTES/C37 more synergistic than wild type RANTES/C37.

NOMENCLATURE

AIDS	Acquired Immune Deficiency Syndrome
AOP	aminooxypentane
AUC	analytical ultracentrifugation
BSA	bovine serum albumin
BME	β-mercaptoethanol
B.M.	Bachelor of Medicine
CCR	CC chemokine receptor
CXCR	CXC chemokine receptor
CHO	Chinese hamster ovary
CNS	Crystallography and NMR system
CRPG	chlorphenol red-β-D-galactopyranoside
DTT	dithiothreitol
EDTA	EthyleneDiamineTetraacetic Acid
NNY	N-nonanoyl
NOE	Nuclear Overhauser Effect
PSC	[L-ThiaPro2, L-α-cyclohexyl-Gly3]-NNY
Da	Dalton
DSS	4, 4-dimethyl-4-silapentane-1-sulfonate
DMEM	Dulbecco's Modified Eagle's Medium
EC_{50}	concentration of 50% effect (i.e. activation)

env	HIV-1 envelope protein
FACS	fluorescence activated cell sorting
FCS	fetal calf serum
FDA	Food and Food Administration
FITC	fluorescein isothiocyanate
FBC	fetal bovine serum
GAG	glycosaminoglycan
HPLC	High Performance Chromatography
HIV	human immunodeficiency virus
HSQC	heteronuclear single-quantum coherence
IC_{50}	concentration of 50% inhibition
IL-8	interleukin-8 (CXC chemokine Ligand 8 or CXCL8)
IPTG	isopropyl-β-D-thiogalactopyranoside
Kd	dissociation constant
MALDI-TOF	Matrix Assisted Laser Desorption /Ionization- Time Of Flight
MCP	monocyte chemotactic protein, MCP-1(CCL2), MCP-2 (CCL8), MCP-3 (CCL7) are mentioned in this thesis
MIP	macrophage inflammatory protein (MIP-1α, CCL4; MIP-1β, CCL3)
MW	Molecular Weight
NMR	nuclear magnetic resonance

PBS	phosphate buffered saline
PBMC	peripheral blood mononuclear cells
PCR	polymerase chain reaction
PEEA	Polyethyleneamine
PEG	polyethylene glycol
PF-4	platelet factor 4 (CXCL4)
PI	propidium iodide
RANTES	regulated on activation of normal T cell expressed and secreted (CCL5)
RMSD	root mean square deviation
RPMI	Roswell Park Memorial Institute
SD	Standard deviation
SDS-PAGE	sodium dodecyl sulfate polyacrylamide gel electrophoresis
SDF-1α	stromal cell-derived factor-1α (CXCL12)
TFA	Trifluroacetic acid
WT	Wild Type

REFERENCES

1. Allen, S. J., Crown, S. E., and Handel, T. M. (2007) *Annu. Rev. Immunol.* **25**, 787-820

2. Cartier, L., Hartley, O., Dubois-Dauphin, M., and Krause, K. H. (2005) *Brain Res. Brain Res. Rev.* **48**(1), 16-42

3. Sheikine, Y., and Hansson, G. K. (2004) *Anna. Med.* **36**, 98-118

4. Le, Y., Zhou, Y., Iribarren, P., and Wang, J. (2004) *Cell Mol. Immunol.* **1**(2), 95-104

5. Weber, C. (2003) *J. Mol. Med.* **81**(1), 4-19

6. Butcher, E. C., and Picker, L. J. (1996) *Science* **272**(5258), 60-66

7. Springer, T. A. (1994) *Cell* **76**(2), 301-314

8. Dwir, O., Grabovsky, V., and Alon, R. (2004) *Ernst. Schering Res. Found. Workshop* **44**, 109-135

9. Proudfoot, A. E., Handel, T. M., Johnson, Z., Lau, E. K., LiWang, P., Clark-Lewis, I., Borlat, F., Wells, T. N., and Kosco-Vilbois, M. H. (2003) *Proc. Natl. Acad .Sci. USA* **100**(4**)**, 1885-1890

10. Bazan, J. F., Bacon, K. B., Hardiman, G., Wang, W., Soo, K., Rossi, D., Greaves, D. R., Zlotnik, A., and Schall, T. J. (1997) *Nature* **385**, 640-644

11. Kelner, G. S., Kennedy, J., Bacon, K. B., Kleyensteuber, S., Largaespada, D. A., Jenkins, N. A., Copeland, N. G., Bazan, J. F., Moore, K. W., Schall, T. J., et al., (1994) *Science* **266**, 1395-1399

12. Clore, G. M., Appella, E., Yamada, M., Matsushima, K., Gronenborn, A.M. (1990) *Biochemistry* **29**, 1689-1696

13. Rajarathnam, K., Clark-Lewis, I., and Sykes, B. D. (1995) *Biochemistry* **34**(40), 12983-12990

14. Lodi, P. J., Garrett, D. S., Kuszewski, J., Tsang, M. L.-S., Weatherbee, J. A., Leonard, W. J., Gronenborn, A. M., and Clore, G. M. (1994) *Science* **263**, 1762-1767

15. Skelton, N. J., Aspiras, F., Ogez, J., Schall, T.J. (1995) *Biochemistry* **34**, 5329-5342

16. Chung, C., Cooke, R.M., Proudfoot, A.E.I. and Wells, T.N.C. (1995) *Biochemistry* **34**(29), 3907-9314

17. Handel, T. M., and Domaille, P. J. (1996) *Biochemistry* **35**(21), 6569-6584

18. Lubkowski, J., Bujacz, G., Boque, L., Domaille, P. J., Handel, T. M., and Wlodawer, A. (1997) *Nature. Stru. Biol.* **4**(1), 64-69

19. Crump, M. P., Rajarathnam, K., Kim, K.-S., Clark-Lewis, I., and Sykes, B. D. (1998) *J. Biol. Chem.* **273**, 22471-22479

20. Mizoue, L. S., Bazan, J. F., Johnson, E. C., and Handel, T. M. (1999) *Biochemistry* **38**, 1402-1414

21. Zhang, X., Chen, L., Bancroft, D. P., Lai, C. K., and Maione, T. E. (1994) *Biochemistry* **33**(27), 8361-8366

22. Swaminathan, G. J., Holloway, D. E., Colvin, R. A., Campanella, G. K., Papageorgiou, A. C., Luster, A. D., and Acharya, K. R. (2003) *Structure* **11**(5), 521-532

23. Blaszczyk, J., Coillie, E. V., Proost, P., Damme, J. V., Opdenakker, G., Bujacz, G. D., Wang, J. M., and Ji, X. (2000) *Biochemistry* **39**(46), 14075-14081

24. LiWang, A. C., Wang, Z.-x., Sun, Y., Peiper, S. C., and LiWang, P. J. (1999) *Protein Sci.* **8**, 2270-2279

25. Fernandez, E. J., and Lolis, E. (2002) *Annu. Rev. Pharmacol. Toxicol.* **42**, 469-499

26. Johnson, Z., Proudfoot, A. E., and Handel, T. M. (2005) *Cytokine Growth Factor Rev.* **16**(6), 625-636

27. Handel, T. M., Johnson, Z., Crown, S. E., Lau, E. K., and Proudfoot, A. E. (2005) *Annu. Rev. Biochem.* **74**, 385-410

28. Lau, E. K., Paavola, C. D., Johnson, Z., Gaudry, J. P., Geretti, E., Borlat, F., Kungl, A. J., Proudfoot, A. E., and Handel, T. M. (2004) *J. Biol. Chem.* **279**(21), 22294-22305

29. McCornack, M. A., Boren, D. M., and LiWang, P. J. (2004) *Biochemistry* **43**(31), 10090-10101

30. Hoover, D. M., Boulegue, C., Yang, D., Oppenheim, J. J., Tucker, K., Lu, W., and Lubkowski, J. (2002) *J. Biol. Chem.* **277**(40), 37647-37654

31. Lortat-Jacob, H., Grosdidier, A., and Imberty, A. (2002) *Proc. Natl. Acad. Sci. USA* **99**(3), 1229-1234

32. Crump, M. P., Gong, J.-H., Loetscher, P., Rajarathnam, K., Amara, A., Arenzana-Seisdedos, F., Virelizier, J.-L., Baggiolini, M., Sykes, B., and Clark-Lewis, I. (1997) *EMBO J.* **16**(23), 6996-7007

33. Shao, W., Jerva, L. F., West, J., Lolis, E., and Schweitzer, B. I. (1998) *Biochemistry* **37**, 8303-8313

34. Kim, K.-S., Clark-Lewis, I., and Sykes, B.D. (1994) *J. Biol. Chem.* **269**, 32909-32915

35. Czaplewski, L. G., McKeating, J., Craven, C. J., Higgins, L. D., Appay, V., Brown, A., Dudgeon, T., Howard, L. A., Meyers, T., Owen, J., Palan, S. R., Tan, P., Wilson, G., Woods, N. R., Heyworth, C. M., Lord, B. I., Brotherton, D., Christison, R., Craig, S., Cribbes, S., Edwards, R. M., Evans, S. J., Gilbert, R., Morgan, P., Randle, E., Schofield, N., Varley, P. G., Fisher, J., Waltho, J. P., and Hunter, M. G. (1999) *J. Biol. Chem.* **274**, 16077-16084

36. Clark-Lewis, I., Schumacher, C., Baggiolini, M., and Moser, B. (1991) *J. Biol. Chem.* **266**, 23128-23134

37. Rajarathnam, K., Sykes, B.D., Kay, C.M., Dewald, B., Geiser, T., Baggiolini, M., and Clark-Lewis, I. (1994) *Science* **264**, 90-92

38. Paavola, C. D., Hemmerich, S., Grunberger, D., Polsky, I., Bloom, A., Freedman, R., Mulkins, M., Bhakta, S., McCarley, D., Wiesent, L., Wong, B., Jarnagin, K., and Handel, T. M. (1998) *J. Biol. Chem.* **273**, 33157-33165

39. Laurence, J. S., Blanpain, C., Parmentier, M., Burgner, J. W., and LiWang, P. J. (2000) *Biochemistry* **39**, 3401-3409

40. Clark-Lewis, I., Kim, K.-S., Rajarathnam, K., Gong, J.-H., Dewald, B., Moser, B., Baggiolini, M., and Sykes, B. D. (1995) *J. Leukoc. Biol.* **57**, 703-711

41. Rajarathnam, K., Prado, G. N., Fernando, H., Clark-Lewis, I., and Navarro, J. (2006) *Biochemistry* **45**(25), 7882-7888

42. Williams, G., Borkakoti, N., Bottomley, G. A., Cowan, I., Fallowfield, A. G., Jones, P. S., Kirtland, S. J., Price, G. J., and Price, L. (1996) *J. Biol. Chem.* **271**(16), 9579-9586

43. Zhang, Y., and Rollins, B. J. (1995) *Mol. Cell. Biol.* **15**(9), 4851-4855

44. Moser, B., Dewald, B., Barella, L., Schumacher, C., Baggiolini, M., and Clark-Lewis, I. (1993) *J. Biol. Chem.* **268**, 7125-7128

45. Clark-Lewis, I., Dewald, B., Loetscher, M., Moser, B., and Baggiolini, M. (1994) *J. Biol. Chem.* **269**(23), 16075-16081

46. Pakianathan, D. R., Kuta, E. G., Artis, D. R., Skelton, N. J., and Hebert, C. A. (1997) *Biochemistry* **36**(32), 9642-9648

47. Laurence, J. S., Blanpain, C., De Leener, A., Parmentier, M., and LiWang, P. J. (2001) *Biochemistry* **40**, 4990-4999

48. Hemmerich, S., Paavola, C., Bloom, A., Bhakta, S., Freedman, R., Grunberger, D., Krstenansky, J., Lee, S., McCarley, D., Mulkins, M., Wong, B., Pease, J., Mizoue, L., Mirzadegan, T., Polsky, I., Thompson, K., Handel, T. M., and Jarnagin, K. (1999) *Biochemistry* **38**, 13013-13025

49. Jarnagin, K., Grunberger, D., Mulkins, M., Wong, B., Hemmerich, S., Paavola, C., Bloom, A., Bhakta, S., Diehl, F., Freedman, R., McCarley, D., Polsky, I., Ping-Tsou, A., Kosaka, A., and Handel, T. M. (1999) *Biochemistry* **38**, 16167-16177

50. Laurence, J. S., LiWang, A. C., and LiWang, P. J. (1998) *Biochemistry* **37**, 9346-9354

51. Blanpain, C., Doranz, B. J., Bondue, A., Govaerts, C., De Leener, A., Vassart, G., Doms, R. W., Proudfoot, A., and Parmentier, M. (2003) *J.Biol. Chem.* **278**(7), 5179-5187

52. Ho, H. H., Du, D., and Gershengorn, M. C. (1999) *J. Biol. Chem.* **274**(44), 31327-31332

53. Katancik, J. A., Sharma, A., Radel, S. J., and De Nardin, E. (1997) *Biochem. Biophys. Res. Commun.* **232**(3), 663-668

54. Monteclaro, F. S., and Charo, I. F. (1997) *J. Biol. Chem.* **272**(37), 23186-23190

55. Xanthou, G., Williams, T. J., and Pease, J. E. (2003) *Eur. J. Immunol.* **33**(10), 2927-2936

56. Booth, V., Keizer, D. W., Kamphuis, M. B., Clark-Lewis, I., and Sykes, B. D. (2002) *Biochemistry* **41**(33), 10418-10425

57. Handel, T. M., and Lau, E. K. (2004) *Ernst. Schering. Res. Found. Workshop* **45**, 101-124

58. Mayer, K. L., and Stone, M. J. (2000) *Biochemistry* **39**(29), 8382-8395

59. Mizoue, L. S., Bazan, J. F., Johnson, E. C., and Handel, T. M. (1999) *Biochemistry* **38**(5), 1402-1414

60. Skelton, N. J., Quan, C., Reilly, D., and Lowman, H. (1999) *Structure* **7**(2), 157-168

61. Farzan, M., Mirzabekov, T., Kolchinsky, P., Wyatt, R., Cayabyab, M., Gerard, N. P., Gerard, C., Sodroski, J., and Choe, H. (1999) *Cell* **96**(5), 667-676

62. Farzan, M., Babcock, G. J., Vasilieva, N., Wright, P. L., Kiprilov, E., Mirzabekov, T., and Choe, H. (2002) *J. Biol. Chem.* **277**(33), 29484-29489

63. Farzan, M., Chung, S., Li, W., Vasilieva, N., Wright, P. L., Schnitzler, C. E., Marchione, R. J., Gerard, C., Gerard, N. P., Sodroski, J., and Choe, H. (2002) *J. Biol. Chem.* **277**(43), 40397-40402

64. Fong, A. M., Alam, S. M., Imai, T., Haribabu, B., and Patel, D. D. (2002) *J. Biol. Chem.* **277**(22), 19418-19423

65. Saita, Y., Kodama, E., Orita, M., Kondo, M., Miyazaki, T., Sudo, K., Kajiwara, K., Matsuoka, M., and Shimizu, Y. (2006) *J. Immunol.* **177**(5), 3116-3122

66. Liu, S., Fan, S., and Sun, Z. (2003) *J. Mol. Model.* **9**(5), 329-336

67. Fano, A., Ritchie, D. W., and Carrieri, A. (2006) *J. Chem. Inform. Model.* **46**(3), 1223-1235

68. Paterlini, M. G. (2002) *Biophys. J.* **83**(6), 3012-3031

69. Dragic, T., Trkola, A., Thompson, D. A., Cormier, E. G., Kajumo, F. A., Maxwell, E., Lin, S. W., Ying, W., Smith, S. O., Sakmar, T. P., and Moore, J. P. (2000) *Proc. Natl. Acad. Sci. USA* **97**(10), 5639-5644

70. Mirzadegan, T., Diehl, F., Ebi, B., Bhakta, S., Polsky, I., McCarley, D., Mulkins, M., Weatherhead, G. S., Lapierre, J. M., Dankwardt, J., Morgans, D., Jr., Wilhelm, R., and Jarnagin, K. (2000) *J. Biol. Chem.* **275**(33), 25562-25571

71. Onuffer, J. J., and Horuk, R. (2002) *Trends. Pharmacol. Sci.* **23**(10), 459-467

72. Onuffer, J., McCarrick, M. A., Dunning, L., Liang, M., Rosser, M., Wei, G. P., Ng, H., and Horuk, R. (2003) *J. Immunol.* **170**(4), 1910-1916

73. Zoffmann, S., Chollet, A., and Galzi, J. L. (2002) *Mol Pharmacol* **62**(3), 729-736

74. Dragic, T., Litwin, V., Allaway, G. P., Martin, S. R., Huang, Y., Nagashima, K. A., Cayanan, C., Maddon, P. J., Koup, R. A., Moore, J. P., and Paxton, W. A. (1996) *Nature* **381**, 667-673

75. Deng, H., Liu, R., Ellmeier, W., Choe, S., Unutmaz, D., Burkhart, M., Di Marzio, P., Marmon, S., Sutton, R. E., Hill, C. M., Davis, C.B., Peiper, S. C., Schall, T. J., Littman, D. R., and Landau, N. R. (1996) *Nature* **381**, 661-666

76. Alkhatib, G., Combadiere, C., Broder, C. C., Feng, Y., Kennedy, P. E., Murphy, P. M., and Berger, E. A. (1996) *Science* **272**, 1955-1958

77. Root, M. J., and Steger, H. K. (2004) *Curr. Pharm. Des.* **10**(15), 1805-1825

78. Lee, B., Doranz, B. J., Ratajczak, M. Z., and Doms, R. W. (1998) *Stem. Cells* **16**, 79-88

79. Brandt, S. M., Mariani, R., Holland, A. U., Hope, T. J., and Landau, N. R. (2002) *J. Biol. Chem.* **277**(19), 17291-17299

80. Alkhatib, G., Locati, M., Kennedy, P. E., Murphy, P. M., and Berger, E. A. (1997) *Virology* **234**(2), 340-348

81. Amara, A., Gall, S. L., Schwartz, O., Salamero, J., Montes, M., Loetscher, P., Baggiolini, M., Virelizier, J. L., and Arenzana-Seisdedos, F. (1997) *J.Exp. Med.* **186**(1), 139-146

82. Cocchi, F., Devico, A.L., Garzinodemo, A., Lusso, P., Gallo, R.C. (1995) *Science* **270**, 1811

83. Bleul, C. C., Farzan, M., Choe, H., Parolin, C., Clark-Lewis, I., Sodroski, J., and Springer, T. A. (1996) *Nature* **382**, 829-833

84. Oberlin, E., Amara, A., Bachelerie, F., Bessia, C., Virelizier, J.-L., Arenzana-Seisdedos, Schwartz, O., Heard, J.-M., Clark-Lewis, I., Legler, D.F., Loetscher, M., Baggiolini, M., Moser, B. (1996) *Nature* **382**, 833-835

85. Pakianathan, D. R., Kuta, E. G., Artis, D. R., Skelton, N. J., and Hebert, C. A. (1997) *Biochemistry* **36**(32), 9642-9648

86. Graham, G. J., Wilkinson, P. C., Nibbs, R. J. B., Lowe, S., Kolset, S. O., Parker, A., Freshney, M. G., Tsang, M. L.-S., and Pragnell, I. B. (1996) *EMBO J.* **15**, 6506-6515

87. Lederman, M. M., Veazey, R. S., Offord, R., Mosier, D. E., Dufour, J., Mefford, M., Piatak, M., Jr., Lifson, J. D., Salkowitz, J. R., Rodriguez, B., Blauvelt, A., and Hartley, O. (2004) *Science* **306**(5695), 485-487

88. Johnson, Z., Kosco-Vilbois, M. H., Herren, S., Cirillo, R., Muzio, V., Zaratin, P., Carbonatto, M., Mack, M., Smailbegovic, A., Rose, M., Lever, R., Page, C., Wells, T. N., and Proudfoot, A. E. (2004) *J. Immunol.* **173**(9), 5776-5785

89. Mack, M., Luckow, B., Cihak, J., Simmons, G., Clapham, P. R., Signoret, N., Marsh, M., Strassinger, M., Borlat, F., Wells, T., Scholondorff, D., and Proudfoot, A. E. I. (1998) *J. Exp. Med.* **187**, 1215-1224

90. Polo, S., Nardese, V., De Santis, C., Arcelloni, C., Paroni, R., Sironi, F., Verani, A., Rizzi, M., Bolognesi, M., and Lusso, P. (2000) *Eur. J. Immunol.* **30**(11), 3190-3198

91. Signoret, N., Pelchen-Matthews, A., Mack, M., Proudfoot, A. E., and Marsh, M. (2000) *J. Cell Biol.* **151**(6), 1281-1294

92. Simmons, G., Clapham, P. R., Picard, L., Offord, R. E., Rosenkilde, M. M., Schwartz, T. W., Buser, R., Wells, T. N. C., and Proudfoot, A. E. I. (1997) *Science* **276**, 276-279

93. Pastore, C., Picchio, G. R., Galimi, F., Fish, R., Hartley, O., Offord, R. E., and Mosier, D. E. (2003) *Antimicrob. Agents. Chemother.* **47**(2), 509-517

94. Mosier, D. E., Picchio, G. R., Gulizia, R. J., Sabbe, R., Poignard, P., Picard, L., Offord, R. E., Thompson, D. A., and Wilken, J. (1999) *J. Virol.* **73**(5), 3544-3550

95. Hartley, O., and Offord, R. E. (2005) *Curr. Protein Pept. Sci*. **6**(3), 207-219

96. Kawamura, T., Bruse, S. E., Abraha, A., Sugaya, M., Hartley, O., Offord, R. E., Arts, E. J., Zimmerman, P. A., and Blauvelt, A. (2004) *J. Virol.* **78**(14), 7602-7609

97. Proudfoot, A. E., Power, C. A., Hoogewerf, A. J., Montjovent, M. O., Borlat, F., Offord, R. E., and Wells, T. N. (1996) *J. Biol. Chem.* **271**(5), 2599-2603

98. Yang, O. O., Swanberg, S. L., Lu, Z., Dziejman, M., McCoy, J., Luster, A. D., Walker, B. D., and Herrmann, S. H. (1999) *J. Virol.* **73**(6), 4582-4589

99. Hartley, O., Gaertner, H., Wilken, J., Thompson, D., Fish, R., Ramos, A., Pastore, C., Dufour, B., Cerini, F., Melotti, A., Heveker, N., Picard, L., Alizon, M., Mosier, D., Kent, S., and Offord, R. (2004) *Proc. Natl. Acad. Sci. U S A* **101**(47), 16460-16465

100. Hartley, O., Dorgham, K., Perez-Bercoff, D., Cerini, F., Heimann, A., Gaertner, H., Offord, R. E., Pancino, G., Debre, P., and Gorochov, G. (2003) *J. Virol.* **77**(12), 6637-6644

101. Chan, D. C., Fass, D., Berger, J. M., and Kim, P. S. (1997) *Cell* **89**(2), 263-273

102. Weissenhorn, W., Dessen, A., Harrison, S. C., Skehel, J. J., and Wiley, D. C. (1997) *Nature* **387**(6631), 426-430

103. Weng, Y., and Weiss, C. D. (1998) *J. Virol.* **72**(12), 9676-9682

104. Liu, S., Lu, H., Niu, J., Xu, Y., Wu, S., and Jiang, S. (2005) *J. Biol. Chem.* **280**(12), 11259-11273

105. Sodroski, J. G. (1999) *Cell* **99**(3), 243-246

106. Lalezari, J. P., DeJesus, E., Northfelt, D. W., Richmond, G., Wolfe, P., Haubrich, R., Henry, D., Powderly, W., Becker, S., Thompson, M., Valentine, F., Wright, D., Carlson, M., Riddler, S., Haas, F. F., DeMasi, R., Sista, P. R., Salgo, M., and Delehanty, J. (2003) *Antivir. Ther.* **8**(4), 279-287

107. Lalezari, J. P. (2003) *AIDS Read.* **13**(3 Suppl), S9-13

108. Veiga, A. S., Santos, N. C., Loura, L. M., Fedorov, A., and Castanho, M. A. (2004) *J. Am. Chem. Soc.* **126**(45), 14758-14763

109. Barretina, J., Blanco, J., Armand-Ugon, M., Gutierrez, A., Clotet, B., and Este, J. A. (2003) *Antivir. Ther.* **8**(2), 155-161

110. Samson, M., Libert, F., Doranz, B. J., Rucker, J., Liesnard, C., Farber, C. M., Saragosti, S., Lapoumeroulie, C., Cognaux, J., Forceille, C., Muyldermans, G., Verhofstede, C., Burtonboy, G., Georges, M., Imai, T., Rana, S., Yi, Y., Smyth, R. J., Collman, R. G., Doms, R. W., Vassart, G., and Parmentier, M. (1996) *Nature* **382**(6593), 722-725

111. Liu, R., Paxton, W. A., Choe, S., Ceradini, D., Martin, S. R., Horuk, R., MacDonald, M. E., Stuhlmann, H., Koup, R. A., and Landau, N. R. (1996) *Cell* **86**(3), 367-377

112. Zlotnik, A., and Yoshie, O. (2000) *Immunity* **12**, 121-127

113. Baggiolini, M. (2001) *J. Intern. Med.* **249**, 1-14

114. Baggiolini, M., Dewald, B., and Moser, B. (1997) *Annu. Rev. Immunol.* **15**, 675-705

115. McCornack, M. A., Cassidy, C. K., and LiWang, P. J. (2003) *J. Biol. Chem.* **278**, 1946-1956

116. Williams MA, Cave CM, Quaid G, Robinson C, Daly TJ, Witt D, Lentsch AB, and JS., S. (2005) *Shock* **23**(4), 371-376

117. Marino-Ramirez, L., Campbell, L., and Hu, J. C. (2003) *Methods. Mol. Biol.* **205**, 235-250

118. Hu, J. C., Kornacker, M. G., and Hochschild, A. (2000) *Methods (Duluth)* **20**(1), 80-94

119. Marino-Ramirez, L., Minor, Jonathan L., Reading, Nicola, Hu,James C. (2004) *J.Bacteriol.* **186**(5), 1311-1319

120. Voelker, P., and McRorie, D. (1994) *Beckman Instruments, Inc.* **Publication: T-1782A**(Technical information), Analytical Ultracentrifugation: 1-7

121. Johnson, M. L., and Correia, J. J. (1981) *Biophys. J.* **36**, 575-588

122. Correia, J. J., Chacko, B. M., Lam, S. S., and Lin, K. (2001) *Biochemistry* **40**, 1473-1482

123. Wishart, D. S., Bigam, C. G., Yao, J., Abildgaard, F., Dyson, H. J., Oldfield, E., Markley, J. L., and Sykes, B. D. (1995) *J. Biomol. NMR* **6**, 135-140

124. Delaglio, F., Grzesiek, S., Vuister, G.W., Zhu, G., Pfeifer, J., Bax, A. (1995) *J. Biomol. NMR* **6**, 277-293

125. Garrett, D. S., Powers, R., Gronenborn, A.M., Clore, G.M. (1991) *J. Magn. Reson.* **95**, 214-220

126. Kim, S., Jao, S.-c., Laurence, J. S., and LiWang, P. J. (2001) *Biochemistry* **40**, 10782-10791

127. Rajarathnam, K., Kay, C. M., Clark-Lewis, I., and Sykes, B. D. (1997) *Methods. Enzymol.* **287**, 89-105

128. Lowman, H. B., Fairbrother, W. J., Slagle, P. H., Kabakoff, R., Liu, J., Shire, S., and Hebert, C. A. (1997) *Protein Sci.* **6**, 598-608

129. Hu, J. C., Newell, N. E., Tidor, B., and Sauer, R. T. (1993) *Protein Sci.* **2**(7), 1072-1084

130. Hu, J. C., O'Shea, E. K., Kim, P. S., and Sauer, R. T. (1990) *Science* **250**, 1400-1403

131. Zhang, Z., Murphy, A., Hu, J. C., and Kodadek, T. (1999) *Curr. Biol.* **9**(8), 417-420

132. Koonin, E. V., Wolf , Y. I., and Karev, G. P. (2002) *Nature* **420**, 218-223

133. Meunier, A., Bernassau, J.-M., Guillemot, J.-C., Ferrara, P. & Darbon, H. (1997) *Biochemistry* **36**(15), 4412-4422

134. Kim, K.-S., Rajarathnam, K., Clark-Lewis, I., and Sykes, B. D. (1996) *FEBS Lett.* **395**, 277-282

135. Mayer, K. L., and Stone, M. S. (2000) *Biochemistry* **39**, 8382-8395

136. Mellado, M., Rodriguez-Frade, J. M., Manes, S., and Martinez, A. C. (2001) *Annu. Rev. Immunol.* **19**, 397-421

137. Rodriguez-Frade, J. M., Vila-Coro, A. J., Martin de Ana, A., Albar, J. P., Martinez-A, C., and Mellado, M. (1999) *Proc. Natl. Acad. Sci. USA* **96**, 3628-3633

138. Jin, H., Hayes, G. L., Darbha, N. S., Meyer, E., and Liwang, P. J. (2005) *Biochem. Biophys. Res. Commun.* **338**(2), 987-999

139. Grzesiek, S., and Bax, A. (1992) *J. Magn. Reson.* **99**, 201-207

140. Wittekind, M., and Mueller, L. (1993) *J. Magn. Reson. Ser.B* **101**(2), 201-205

141. Grzesiek, S., and Bax, A. (1992) *J. Am. Chem. Soc.* **114**, 6291-6293

142. Grzesiek, S., and Bax, A. (1993) *J. Biomol. NMR* **3**, 185-204

143. Grzesiek, S., Anglister, J., and Bax, A. (1993) *J. Magn. Reson. Ser.B* **101**(1), 114-119

144. Muhandiram, D. R., Kay, L. E. (1994) *J. Magn. Reson. Ser. B.* **103**, 203-216

145. Logan, T. M., Olejniczak, E. T., Xu, R. X., and Fesik, S. W. (1993) *J. Biomol. NMR* **3**(2), 225-231

146. Ikura, M., Kay, L.E. and Bax, A. (1991) *J. Biomol. NMR* **1**, 299-304

147. Vuister, G. W., Clore, G. M., Gronenborn, A. M., Powers, R., Garrett, D. S., Tschudin, R., and Bax, A. (1993) *J. Magn. Reson. Ser. B* **101**(2), 210-213

148. Blanpain, C., Lee, B., Vakili, J., Doranz, B.J., Govaerts, C., Migeotte, I., Sharron, M., Dupriez, V., Vassart, G., Doms, R.W., and Parmentier, M. (1999) *J. Biol. Chem.* **274**, 18902-18908

149. Derdeyn, C. A., Decker, J. M., Sfakianos, J. N., Wu, X., O'Brien, W. A., Ratner, L., Kappes, J. C., Shaw, G. M., and Hunter, E. (2000) *J. Virol.* **74**(18), 8358-8367

150. Wei, X., Decker, J. M., Liu, H., Zhang, Z., Arani, R. B., Kilby, J. M., Saag, M. S., Wu, X., Shaw, G. M., and Kappes, J. C. (2002) *Antimicrob. Agents. Chemother.* **46**(6), 1896-1905

151. Chackerian, B., Lowy, D. R., and Schiller, J. T. (1999) *Proc. Natl. Acad. Sci. USA* **96**(5), 2373-2378

152. Blanpain, C., Doranz, B. J., Vakili, J., Rucker, J., Govaerts, C., Baik, S. S. W., Lorthioir, O., Migeotte, I., Libert, F., Baleux, F., Vassart, G., Doms, R. W., and Parmentier, M. (1999) *J. Biol. Chem.* **274**, 34719-34727

153. Koopmann, W., Ediriwickrema, C., and Krangel, M. S. (1999) *J. Immunol.* **163**, 2120-2127

154. Kuschert, G. S., Coulin, F., Power, C. A., Proudfoot, A. E., Hubbard, R. E., Hoogewerf, A. J., and Wells, T. N. (1999) *Biochemistry* **38**(39), 12959-12968

155. Sharma, D., and Rajarathnam, K. (2000) *J. Biomol. NMR* **18**(2), 165-171

156. Veldkamp, C. T., Peterson, F. C., Pelzek, A. J., and Volkman, B. F. (2005) *Protein Sci.* **14**(4), 1071-1081

157. Leong, S. R., Lowman, H. B., Liu, J., Shire, S., Deforge, L. E., Gillece-Castro, B. L., McDowell, R., and Hébert, C. A. (1997) *Protein Sci.* **6**, 609-617

158. Fernando, H., Chin, C., Rosgen, J., and Rajarathnam, K. (2004) *J. Biol. Chem.* **279**(35), 36175-36178

159. Bondue, A., Jao, S. C., Blanpain, C., Parmentier, M., and LiWang, P. J. (2002) *Biochemistry* **41**(46), 13548-13555

160. Hoogewerf, A. J., Kuschert, G. S. V., Proudfoot, A. E. I., Borlat, F., Clark-Lewis, I., Power, C. A., and Wells, T. N. C. (1997) *Biochemistry* **36**(44), 13570-13578

161. Leonard, J. T., and Roy, K. (2006) *Curr. Med. Chem.* **13**(8), 911-934

162. Gerard, C., and Rollins, B. J. (2001) *Nature Immunol.* **2**, 108-115

163. Wells, T. N., Proudfoot, A. E., and Power, C. A. (1999) *Immunol. Lett.* **65**(1-2), 35-40

164. Homey, B., Muller, A., and Zlotnik, A. (2002) *Nature Rev. Immunol.* **2**(3), 175-184

165. Amzazi, S., Ylisastigui, L., Bakri, Y., Rabehi, L., Gattegno, L., Parmentier, M., Gluckman, J. C., and Benjouad, A. (1998) *Virology* **252**(1), 96-105

166. Ramnarine, E. J., Devico, A. L., and Vigil-Cruz, S. C. (2006) *Bioorg. Med. Chem. Lett.* **16**(1), 93-95

167. Struyf, S., De Meester, I., Scharpe, S., Lenaerts, J. P., Menten, P., Wang, J. M., Proost, P., and Van Damme, J. (1998) *Eur. J. Immunol.* **28**(4), 1262-1271

168. Lim, J. K., Lu, W., Hartley, O., and DeVico, A. L. (2006) *J. Leuk. Biol.* **80**(6), 1395-1404

169. Ylisastigui, L., Vizzavona, J., Drakopoulou, E., Paindavoine, P., Calvo, C. F., Parmentier, M., Gluckman, J. C., Vita, C., and Benjouad, A. (1998) *AIDS* **12**(9), 977-984

170. Elsner, J., Petering, H., Hochstetter, R., Kimmig, D., Wells, T. N., Kapp, A., and Proudfoot, A. E. (1997) *Eur. J. Immunol.* **27**(11), 2892-2898

171. Elsner, J., Petering, H., Kimmig, D., Wells, T. N., Proudfoot, A. E., and Kapp, A. (1999) *Internat. Arch. Aller. Immunol.* **118**(2-4), 462-465

172. Grone, H. J., Weber, C., Weber, K. S., Grone, E. F., Rabelink, T., Klier, C. M., Wells, T. N., Proudfood, A. E., Schlondorff, D., and Nelson, P. J. (1999) *FASEB J.* **13**(11), 1371-1383

173. Proudfoot, A. E., Buser, R., Borlat, F., Alouani, S., Soler, D., Offord, R. E., Schroder, J. M., Power, C. A., and Wells, T. N. (1999) *J. Biol. Chem.* **274**(45), 32478-32485

174. Mack, M., Luckow, B., Nelson, P. J., Cihak, J., Simmons, G., Clapham, P. R., Signoret, N., Marsh, M., Stangassinger, M., Borlat, F., Wells, T. N., Schlondorff, D., and Proudfoot, A. E. (1998) *J. Exp. Med.* **187**(8), 1215-1224

175. Sabbe, R., Picchio, G. R., Pastore, C., Chaloin, O., Hartley, O., Offord, R., and Mosier, D. E. (2001) *J. Virol.* **75**(2), 661-671

176. Kawamura, T., Bruse, S. E., Abraha, A., Sugaya, M., Hartley, O., Offord, R. E., Arts, E. J., Zimmerman, P. A., and Blauvelt, A. (2004) *J. Virol.* **78**(14), 7602-7609

177. Hartley, O., Gaertner, H., Wilken, J., Thompson, D., Fish, R., Ramos, A., Pastore, C., Dufour, B., Cerini, F., Melotti, A., Heveker, N., Picard, L., Alizon, M., Mosier, D., Kent, S., and Offord, R. (2004) *Proc. Natl. Acad. Sci. USA* **101**(47), 16460-16465

178. Hoover, D. M., Shaw, J., Gryczynski, Z., Proudfoot, A. E. I., Wells, T., and Lubkowski, J. (2000) *Protein Pep. Lett.* **7**(2), 73-82

179. Pleskoff, O., Treboute, C., Brelot, A., Heveker, N., Seman, M., and Alizon, M. (1997) *Science* **276**(5320), 1874-1878

180. Mkrtchyan, S. R., Markosyan, R. M., Eadon, M. T., Moore, J. P., Melikyan, G. B., and Cohen, F. S. (2005) *J. Virol.* **79**(17), 11161-11169

181. Wei, X., Decker, J. M., Liu, H., Zhang, Z., Arani, R. B., Kilby, J. M., Saag, M. S., Wu, X., Shaw, G. M., and Kappes, J. C. (2002) *Antimicrob. Agents. Chemother.* **46**(6), 1896-1905

182. Potterton, L., McNicholas, S., Krissinel, E., Gruber, J., Cowtan, K., Emsley, P., Murshudov, G. N., Cohen, S., Perrakis, A., and Noble, M. (2004) *Acta Crystal. Sec. D-Biol. Crystal.* **60**, 2288-2294

183. Brunger, A. T., Adams, P. D., Clore, G. M., DeLano, W. L., Gros, P., Grosse-Kunstleve, R. W., Jiang, J. S., Kuszewski, J., Nilges, M., Pannu, N. S., Read, R. J., Rice, L. M., Simonson, T., and Warren, G. L. (1998) *Acta Crystal. Sec. D-Biol. Crystal.* **54**(Pt 5), 905-921

184. Demeler, B., Saber, H., and Hansen, J. C. (1997) *Biophys. J.* **72**(1), 397-407

185. K. E. Van Holde, W. O. W. (1978) *Biopolymers* **17**(6), 1387-1403

186. Pace, C. N., Vajdos, F., Fee, L., Grimsley, G., and Gray, T. (1995) *Protein Sci.* **4**(11), 2411-2423

187. DeLean, A., Munson, P. J., and Rodbard, D. (1978) *Am. J. Physiol.* **235**(2), E97-102

188. Jin, H., Shen, X., Baggett, B. R., Kong, X., and LiWang, P. J. (2007) *J. Biol. Chem.*, **282** (38), 27976-27983

189. Martin, L., Blanpain, C., Garnier, P., Wittamer, V., Parmentier, M., and Vita, C. (2001) *Biochemistry* **40**(21), 6303-6318

190. Wilken, J., Hoover, D., Thompson, D. A., Barlow, P. N., McSparron, H., Picard, L., Wlodawer, A., Lubkowski, J., and Kent, S. B. (1999) *Chem. Biol.* **6**(1), 43-51

191. Nardese, V., Longhi, R., Polo, S., Sironi, F., Arcelloni, C., Paroni, R., DeSantis, C., Sarmientos, P., Rizzi, M., Bolognesi, M., Pavone, V., and Lusso, P. (2001) *Nature Stru. Biol.* **8**, 611-615

192. Ali, S., Palmer, A. C. V., Banerjee, B., Fritchley, S. J., and Kirby, J. A. (2000) *J. Biol. Chem.* **275**, 11721-11727

193. Hoover, D. M., Mizoue, L. S., Handel, T. M., and Lubkowski, J. (2000) *J. Biol. Chem.* **275**(30), 23187-23193

194. Pettersen, E. F., Goddard, T. D., Huang, C. C., Couch, G. S., Greenblatt, D. M., Meng, E. C., and Ferrin, T. E. (2004) *J. Comput. Chem.* **25**(13), 1605-1612

195. Oppermann, M. (2004) *Cell Signal* **16**(11), 1201-1210

196. Capoulade-Metay, C., Ayouba, A., Kfutwah, A., Lole, K., Petres, S., Dudoit, Y., Deterre, P., Menu, E., Barre-Sinoussi, F., Debre, P., and Theodorou, I. (2006) *Immunogenetics* **58**(7), 533-541

197. Liu, S., Wu, S., and Jiang, S. (2007) *Curr. Pharm. Des.* **13**(2), 143-162

198. Wild, C., Greenwell, T., and Matthews, T. (1993) *AIDS Res. Hum. Retroviruses* **9**(11), 1051-1053

199. Wild, C. T., Shugars, D. C., Greenwell, T. K., McDanal, C. B., and Matthews, T. J. (1994) *Proc. Natl. Acad. Sci. U S A* **91**(21), 9770-9774

200. Root, M. J., Kay, M. S., and Kim, P. S. (2001) *Science* **291**(5505), 884-888

201. Hamburger, A. E., Kim, S., Welch, B. D., and Kay, M. S. (2005) *J. Biol. Chem.* **280**(13), 12567-12572

202. Ji, C., Zhang, J., Dioszegi, M., Chiu, S., Rao, E., Derosier, A., Cammack, N., Brandt, M., and Sankuratri, S. (2007) *Mol. Pharmacol.* **72**(1), 18-28

203. Ketas, T. J., Klasse, P. J., Spenlehauer, C., Nesin, M., Frank, I., Pope, M., Strizki, J. M., Reyes, G. R., Baroudy, B. M., and Moore, J. P. (2003) *AIDS Res. Hum. Retroviruses* **19**(3), 177-186

204. Murga, J. D., Franti, M., Pevear, D. C., Maddon, P. J., and Olson, W. C. (2006) *Antimicrob. Agents. Chemother.* **50**(10), 3289-3296

205. Nagashima, K. A., Thompson, D. A., Rosenfield, S. I., Maddon, P. J., Dragic, T., and Olson, W. C. (2001) *J. Infec. Dis.* **183**(7), 1121-1125

206. Safarian, D., Carnec, X., Tsamis, F., Kajumo, F., and Dragic, T. (2006) *Virology* **352**(2), 477-484

207. Tremblay, C. L., Giguel, F., Kollmann, C., Guan, Y., Chou, T. C., Baroudy, B. M., and Hirsch, M. S. (2002) *Antimicrob. Agents. Chemother.* **46**(5), 1336-1339

208. Tremblay, C. L., Kollmann, C., Giguel, F., Chou, T. C., and Hirsch, M. S. (2000) *J. Acquir. Immune. Defic. Syndr.* **25**(2), 99-102

209. Page, K. A., Landau, N. R., and Littman, D. R. (1990) *J. Virol.* **64**(11), 5270-5276

210. Derdeyn, C. A., Decker, J. M., Sfakianos, J. N., Wu, X., O'Brien, W. A., Ratner, L., Kappes, J. C., Shaw, G. M., and Hunter, E. (2000) *J. Virol.* **74**(18), 8358-8367

211. Platt, E. J., Wehrly, K., Kuhmann, S. E., Chesebro, B., and Kabat, D. (1998) *J. Virol.* **72**(4), 2855-2864

212. Chou, T. C., and Talalay, P. (1984) *Adv. Enzyme. Regul.* **22**, 27-55

213. Farzan, M., Choe, H., Martin, K.A., Sun, Y., Sidelko, M., Mackay, C.R., Gerard, N.P., Sodroski, J. and Gerard, C. (1997) *J. Biol. Chem.* **272**(11), 6854-6857

214. Trkola, A., Gordon, C., Matthews, J., Maxwell, E., Ketas, T., Czaplewski, L., Proudfoot, A. E., and Moore, J. P. (1999) *J. Virol.* **73**(8), 6370-6379

215. Alkhatib, G., Combadiere, C., Broder, C. C., Feng, Y., Kennedy, P. E., Murphy, P. M., and Berger, E. A. (1996) *Science* **272**(5270), 1955-1958

216. Deng, H., Liu, R., Ellmeier, W., Choe, S., Unutmaz, D., Burkhart, M., Di Marzio, P., Marmon, S., Sutton, R. E., Hill, C. M., Davis, C. B., Peiper, S. C., Schall, T. J., Littman, D. R., and Landau, N. R. (1996) *Nature* **381**(6584), 661-666

217. Dragic, T., Litwin, V., Allaway, G. P., Martin, S. R., Huang, Y., Nagashima, K. A., Cayanan, C., Maddon, P. J., Koup, R. A., Moore, J. P., and Paxton, W. A. (1996) *Nature* **381**(6584), 667-673

218. Feng, Y., Broder, C. C., Kennedy, P. E., and Berger, E. A. (1996) *Science* **272**(5263), 872-877

219. Zhou, N., Luo, Z., Hall, J. W., Luo, J., Han, X., and Huang, Z. (2000) *Eur. J. Immunol.* **30**(1), 164-173

220. Wu, L., LaRosa, G., Kassam, N., Gordon, C. J., Heath, H., Ruffing, N., Chen, H., Humblias, J., Samson, M., Parmentier, M., Moore, J. P., and Mackay, C. R. (1997) *J. Exp. Med.* **186**(8), 1373-1381

221. Simmons, G., Reeves, J. D., Hibbitts, S., Stine, J. T., Gray, P. W., Proudfoot, A. E., and Clapham, P. R. (2000) *Immunol. Rev.* **177**, 112-126

222. Viard, M., Parolini, I., Rawat, S. S., Fecchi, K., Sargiacomo, M., Puri, A., and Blumenthal, R. (2004) *Glycoconj. J.* **20**(3), 213-222

223. Rawat, S. S., Eaton, J., Gallo, S. A., Martin, T. D., Ablan, S., Ratnayake, S., Viard, M., KewalRamani, V. N., Wang, J. M., Blumenthal, R., and Puri, A. (2004) *Virology* **318**(1), 55-65

224. Reeves, J. D., Gallo, S. A., Ahmad, N., Miamidian, J. L., Harvey, P. E., Sharron, M., Pohlmann, S., Sfakianos, J. N., Derdeyn, C. A., Blumenthal, R., Hunter, E., and Doms, R. W. (2002) *Proc. Natl. Acad. Sci. USA* **99**(25), 16249-16254

225. Reeves, J. D., Miamidian, J. L., Biscone, M. J., Lee, F. H., Ahmad, N., Pierson, T. C., and Doms, R. W. (2004) *J. Virol.* **78**(10), 5476-5485

226. Heredia, A., Gilliam, B., DeVico, A., Le, N., Bamba, D., Flinko, R., Lewis, G., Gallo, R. C., and Redfield, R. R. (2007) *AIDS* **21**(10), 1317-1322

227. Heredia, A., Gilliam, B., Latinovic, O., Le, N., Bamba, D., Devico, A., Melikyan, G. B., Gallo, R. C., and Redfield, R. R. (2007) *Antimicrob. Agents. Chemother.*

228. Tremblay, C. (2004) *Curr. Pharm. Des.* **10**(15), 1861-1865

229. Tremblay, C., Merrill, D. P., Chou, T. C., and Hirsch, M. S. (1999) *J. Acquir. Immune. Defic. Syndr.* **22**(5), 430-436

VITA

Name: Hongjun Jin

Address: 2-1004 Xiaohuangzhuang District 1, Eastern City, Beijing 100013 China

Email: hongjunjin@yahoo.com

Education: Ph.D., Biochemistry, Texas A&M University, 2007

B.M., Beijing University of Chinese Medicine, 1997

B.Sc., Radiochemistry, Lanzhou University, 1994

Professional Experience:

Graduate Research Assistant 2002-2007

Department of Biochemistry & Biophysics, Texas A&M University, College Station, TX 77843

Research Assistant 2000-2002

College of Dentistry, University of Iowa, Iowa City, 52406

Exchange Scholar 1999-2000

Department of Cardiology, University of Louisville, KY, 42206

Researcher 1997-1999

Department of R&D, GBI Biotech Ltd., Beijing, 100015 China